QUANTUM OPTICAL APPLICATIONS IN SPECTROSCOPY: INVESTIGATIONS OF ENTANGLED TWO-PHOTON ABSORPTION AND ENTANGLED TWO-PHOTON EXCITED FLUORESCENCE IN ORGANIC DENDRITIC SYSTEMS

by

Özgün Süzer

A dissertation submitted in partial fulfillment
of the requirements for the degree of
Doctor of Philosophy
(Applied Physics)
in The University of Michigan
2010

Doctoral Committee:

Professor Theodore G. Goodson III, Chair
Professor Peter F. Green
Professor Raoul Kopelman
Professor Herbert G. Winful

DEDICATION

This dissertation is dedicated to my tirelessly supportive, infinitely patient, and endlessly loving parents, Şefik and Melike Süzer.

ACKNOWLEDGEMENTS

It is a daunting task to attempt to recount and recognize the many people – my family, friends, and colleagues – who have supported, kept, and carried me through the arduous years that, finally, have led to my graduate degree. Also, I fear, neither is it possible to do them any justice in recognition amongst the words of this short, three-page acknowledgement. Nevertheless, with hopes that they are already aware of my deep appreciation for their unwavering support of and vast contributions to my efforts over the years, I will attempt to offer a few futile words of gratitude in return.

First and foremost, I am grateful to my advisor and committee chair, Prof. Theodore G. Goodson, III for his guidance and supervision. Prof. Goodson gave me the opportunity to demonstrate what I am capable of when others wouldn't, allowing me to work in a truly impressive laboratory setting, within which I have learned academically and grown professionally. I have also learned a great deal about the world of academia and the place of an experimentalist in the framework of scientific research from Prof. Goodson, and over the years have come to appreciate his remarkable direction. This thesis would not have been possible without his support and encouragement.

I would also like to thank Professors Duncan G. Steel, Çağlıyan Kurdak, and John L. Gland, whom I have had the distinct privilege of learning from and working with during my graduate education. I have long admired the excellent teaching technique and

vast theoretical insight of Prof. Steel, whose excellent lectures on quantum mechanics and quantum optics were not only inspirational, but also crucial in understanding the theoretical underpinnings of my work. Prof. Kurdak supervised the initial years of my graduate career and has kept a watchful eye on my progress throughout, offering wisdom and support whenever I needed it. Finally, Prof. Emer. Gland has been my primary source of insight into the professional world of scientific research; I have benefited significantly from his immense experience both in academia and industry.

I am truly fortunate to have had the opportunity to collaborate with the other graduate students and post-doctoral researchers in the Goodson Group. Having not come from a background or with any training in optics, my experimental efforts in quantum optics would not have progressed smoothly without the help and significant contributions of Dr. Michael Harpham and Dr. Oleg Varnavski. I am also grateful for the dedicated efforts and dutiful acquiescence of Alica R. Guzman-Smith, who herself is well on her way to becoming an excellent researcher. I would also like to thank Daniel C. Flynn and Jessica E. Donehue for appearing during the most stressful final few years of my long tenure at the University of Michigan, and making this time unbearably bearable, as well as the other former and current members of the Goodson Group for their kind fellowship and support.

The city of Ann Arbor is a quaint and eclectic town that has bestowed me with the pleasure and privilege of the companionship of many friends outside of academic circles. I am grateful for the friendship of Nur S. Lotfi, Krystle E. Weiss, Amina El-Etreby, Sanin and Emina Alic, Daniel and Luciana Aenăşoaie, Nadine and Youmna El-Ayache, Shawn Neal, Corina Kesler, and Michel Samah.

The most stunning gift this town has given me, however, would be the companionship of my beloved and adored Ana Călugăr. If all the hardship I endured for all these years was worth one thing, that would be her coming into my life. Ana might not be aware of or agree with it, but her infectiously optimistic attitude and the enthusiastic approach to every endeavor she undertakes were the paramount influence and inspiration that facilitated the completion of this work. I am grateful for the many wonderful moments we have shared and look forward to our future together.

I would not, of course, have come this far without the loving support of my family; my father, Şefik, my mother, Melike, and my dear sister, Özge. Needless to say, the prevalent inspiration to my scientific endeavors has been the fine standard for quality, diligence, and ingenuity that my father has established as a professor of chemistry over the great span of his career. In addition, the perceptive approach to human relations I have been credited with on many occasions is attributable solely to the keen insights I have gained from my mother and the artful and resourceful manner in which she conducts her dealings. Finally, I believe all of our lives would not be as colorful or exciting without the whimsical offerings of my sister. Throughout the ups and downs of my endeavors, success was only possible through my family's continuous encouragement and selfless sacrifice. It will take me a lifetime to express my gratitude for their support and patience; this thesis, dedicated to them, is a modest beginning.

The work presented here was supported by the Department of Defense, the National Science Foundation, Army Research Office, and the National Geospatial Intelligence Agency.

TABLE OF CONTENTS

LIST OF FIGURES

Figure

LIST OF TABLES

Table

LIST OF APPENDICES

Appendix

ABSTRACT

**Quantum Optical Applications in Spectroscopy:
Investigations of Entangled Two-Photon Absorption and
Entangled Two-Photon Excited Fluorescence
in Organic Dendritic Systems**

by

Özgün Süzer

Chair: Theodore G. Goodson III

Entangled states of light have been utilized successfully in a wide variety of experiments and applications. This dissertation will discuss the application of entangled states of light toward spectroscopy wherein entangled pairs of photons generated via the process of spontaneous parametric down-conversion (SPDC) are utilized to excite entangled two-photon absorption (ETPA) in organic molecules. An enhancement of the brightness of the SPDC entangled photon source under focused pumping conditions is discussed for the purpose of maximizing the entangled-pair flux available in these experiments. The entangled-pair flux utilized in ETPA experiments, however, still constitutes approximately 10 orders of magnitude fewer photons than any classical counterpart requires. Further, the effects of various conditions under which entangled photons are generated via the process of SPDC, specifically the phase-matching conditions and their

resulting impact on the interaction of said photons with matter is presented. It is shown that spatial indistinguishability of entangled photons generated via SPDC is a necessary requirement for ETPA in organic nonlinear optical materials. Investigations of the ETPA response of a wide range of organic dendritic materials with differing geometry, donor-acceptor strength, and charge-transfer character are also presented, where it was observed that materials whose classical TPA cross-section is attributed to a dipole transition, without involvement of an intermediate state, were nearly transparent to entangled photons. In addition, the premiere demonstration of fluorescence from an organic dendrimer subsequent to two-photon excitation by entangled pairs of photons is presented. A novel, high geometric efficiency, spherically-enclosed optical collection system for collection of fluorescence photons is introduced, which is utilized to circumvent any drawbacks related to the weak quantum yield of the organic materials, and it is observed that the dependence of the rate of fluorescence collected from the material on the entangled excitation flux follows that of the ETPA response of the material. This is the first ever demonstration of the ETPEF phenomenon in any kind of material, and these novel results have widespread impact in applications ranging from spectroscopy to chemical and biological sensing, where the demonstration of the ETPEF phenomenon enables advancement in fields such as quantum imaging and microscopy.

CHAPTER I

Introduction

The profound implications of quantum mechanics have produced an archetypal shift in many well-established fields of research such as information theory [1-3], computation and communications technology [4], metrology [5], micro-patterning and lithography [6], spectroscopy [7], and even biology [8]. Resources that are purely quantum in nature, such as superposition and entanglement, are benefiting the quantum counterparts of classical research areas, where they are utilized to shine new light on well-known problems. Utilizing this novel set of "quantum tools," many schemes have been proposed for secure communications [9, 10], overcoming computational limitations for classically intractable problems [11, 12], beating the Rayleigh diffraction limit in imaging [13] and lithography [14], and optical characterization of materials [15]. In the past several decades, the inherently "spooky" phenomenon of quantum entanglement, in particular, has received great interest.

Among all of the physical systems that are currently being considered for quantum entanglement applications, photon entanglement has been singled out as by far the most robust candidate to mediate the realization of these exciting quantum technologies. The convenience of the process of spontaneous parametric down-conversion (SPDC), by which photons in a laser pump incident on a nonlinear optical crystal spontaneously

decay into pairs of photons that can be simultaneously entangled in energy, momentum, and polarization [16], has made it the common method for generation of entangled photon pairs for use in these experimental schemes.

While the general theoretical aspects of the quantum mechanical correlations between the signal and idler photons that constitute a down-converted pair [17, 18], the effects of various parameters that pertain to the interaction that takes place within the crystal to generate entangled photon pairs [19-21], and the various practical considerations that govern the efficient generation and use of such pairs of photons in experimental schemes [9, 22] have been well-studied, there is still a lack of understanding of the fundamental mechanisms governing the interaction of entangled pairs of photons with matter. Specifically, the application of quantum entanglement-based schemes to spectroscopy is a little-explored venue of research. The fundamental knowledge that can be gained about the response of interesting material systems to quantum-entangled state of light would benefit virtually all new avenues of "quantum" research.

In an attempt to gain a better understanding of the underlying mechanisms of interaction of entangled photon pairs with materials, we have focused our efforts on the application of entangled states of light toward spectroscopy wherein entangled pairs of photons that are generated via the process of SPDC are utilized to excite two-photon transitions in various organic molecules. The results of these experimental studies are presented in this dissertation, which can lead to major advancements in the development of tunable sensors of entangled photons, remote sensing, lithography, imaging, and microscopy.

The paramount reason behind the interest in utilizing entangled, rather than classical, photons for spectroscopy applications is the potential benefit gained from entangled two-photon absorption (ETPA) at extremely low excitation photon fluxes [23, 24]. Unlike classical two-photon absorption (TPA), which relies on sequential, and random, absorption of two photons, the high degree of temporal and spatial correlation that is exhibited by entangled photons results in a large enhancement of absorption rate in ETPA [25, 26] that has a linear, rather than quadratic, dependence on the excitation intensity. This linear dependence is dominant in the low-excitation flux regime, within which spectroscopy can be accomplished using an input beam consisting of fewer than 10^7 entangled photons/sec, as opposed to the 10^{20} photons/sec that is required in a classical TPA spectroscopy experiment. Further, ETPA is expected to have a large enhancement in resolution over TPA [27].

Furthermore, this enhanced material response under entangled photon excitation has also been proposed for utilization in various applications that are intractably plagued by specimen photodamage and photobleaching due to excessive excitation intensities, such as quantum lithography, imaging, and biological microscopy. The use of entangled photons offers a unique solution to the practical drawbacks of these applications due to the particular manner in which entangled states of light interact with matter.

The first experimental observation of ETPA was accomplished using a porphyrin dendrimer [23], which exhibited an ETPA cross-section of $\sim 10^{-17}$ cm^2 molecule^{-1} under illumination of $<10^7$ entangled photons/sec. In this dissertation we present systematic investigations of the ETPA response of varying generations and types of organic dendritic materials, as well as potential mechanisms of control of the ETPA process

through the control of the quantum state in which entangled pairs of photons are generated. The results of these studies offer significant insight into the fundamental mechanisms that govern the interaction of entangled photons with matter. Further, we demonstrate the premiere observation of fluorescence emission from an organic dendrimer as a result of excitation by entangled photon pairs. This demonstration of entangled two-photon excited fluorescence (ETPEF) is an enabling discovery for quantum microscopy applications.

This dissertation is organized as follows: We present the results of experimental efforts to maximize the flux of entangled photons available from an SPDC source and an in-depth discussion of the down-conversion efficiency under focused pumping conditions in Chapter II. This chapter also explains the basic theoretical framework for the entangled photon source that we utilize later in our investigations of the interaction of entangled photon pairs with matter. Chapter III details the systematic study of both ETPA and classical TPA cross-sections of a set of thiophene dendrimers, which we have found to follow identical trends with increasing dendrimer generation, demonstrating the ability to do spectroscopy on real materials using extremely low fluxes of entangled photon pairs. We then shift our attention to the control of the ETPA process through the control of the quantum entangled state of the photon pair that is emitted from our down-conversion source, which is addressed in Chapter IV. The characterization of the ETPA response of a variety of types and architectures of organic dendritic systems is presented in Chapter V, where we investigate the underlying mechanisms of ETPA in organic molecules and present findings that could help design better entangled-photon sensor materials. The first-ever demonstration of ETPEF from an organic dendrimer is reported in Chapter VI,

where we introduce a novel, high geometric efficiency optical light collection system that was designed by the author and is utilized to circumvent difficulties associated with the low flux levels at which experiments are carried out. Finally, Chapter VII concludes this dissertation with the summary of contributions and future prospects of the presented work.

I.1. References

1. D. Bouwmeester, J. W. Pan, K. Mattle, M. Eibl, H. Weinfurter, and A. Zeilinger, "Experimental quantum teleportation," Nature **390**, 575-579 (1997).

2. K. S. Choi, H. Deng, J. Laurat, and H. J. Kimble, "Mapping photonic entanglement into and out of a quantum memory," Nature **452**, 67-U64 (2008).

3. W. T. M. Irvine, A. L. Linares, M. J. A. de Dood, and D. Bouwmeester, "Optimal quantum cloning on a beam splitter," Physical Review Letters **92**, 4 (2004).

4. R. Ursin, F. Tiefenbacher, T. Schmitt-Manderbach, H. Weier, T. Scheidl, M. Lindenthal, B. Blauensteiner, T. Jennewein, J. Perdigues, P. Trojek, B. Omer, M. Furst, M. Meyenburg, J. Rarity, Z. Sodnik, C. Barbieri, H. Weinfurter, and A. Zeilinger, "Entanglement-based quantum communication over 144km," Nature Physics **3**, 481-486 (2007).

5. A. F. Abouraddy, K. C. Toussaint, A. V. Sergienko, B. E. A. Saleh, and M. C. Teich, "Entangled-photon ellipsometry," Journal of the Optical Society of America B-Optical Physics **19**, 656-662 (2002).

6. R. W. Boyd, and S. J. Bentley, "Recent progress in quantum and nonlinear optical lithography," Journal of Modern Optics **53**, 713-718 (2006).

7. O. Roslyak, and S. Mukamel, "Multidimensional pump-probe spectroscopy with entangled twin-photon states," Physical Review A **79** (2009).

8. M. Sarovar, A. Ishizaki, G. R. Fleming, and K. B. Whaley, "Quantum entanglement in photosynthetic light-harvesting complexes," Nature Physics **6**, 462-467 (2010).

9. F. A. Bovino, P. Varisco, A. M. Colla, G. Castagnoli, G. Di Giuseppe, and A. V. Sergienko, "Effective fiber-coupling of entangled photons for quantum communication," Optics Communications **227**, 343-348 (2003).

10. W. Tittel, and G. Weihs, "Photonic entanglement for fundamental tests and quantum communication," Quantum Information & Computation **1**, 3-56 (2001).

11. A. Blais, J. Gambetta, A. Wallraff, D. I. Schuster, S. M. Girvin, M. H. Devoret, and R. J. Schoelkopf, "Quantum-information processing with circuit quantum electrodynamics," Physical Review A **75** (2007).

12. P. Walther, K. J. Resch, T. Rudolph, E. Schenck, H. Weinfurter, V. Vedral, M. Aspelmeyer, and A. Zeilinger, "Experimental one-way quantum computing," Nature **434**, 169-176 (2005).

13. M. D'Angelo, A. Valencia, M. H. Rubin, and Y. Shih, "Resolution of quantum and classical ghost imaging," Physical Review A **72** (2005).

14. A. N. Boto, P. Kok, D. S. Abrams, S. L. Braunstein, C. P. Williams, and J. P. Dowling, "Quantum interferometric optical lithography: Exploiting entanglement to beat the diffraction limit," Physical Review Letters **85**, 2733-2736 (2000).

15. A. V. Sergienko, Y. H. Shih, and M. H. Rubin, "Experimental Evaluation Of A 2-Photon Wave-Packet In Type-II Parametric Downconversion," Journal of the Optical Society of America B-Optical Physics **12**, 859-862 (1995).

16. D. N. Klyshko, *Photons and Nonlinear Optics* (Gordon and Breach Science Publishers, New York, 1988).

17. A. Joobeur, B. E. A. Saleh, and M. C. Teich, "Spatiotemporal Coherence Properties Of Entangled Light-Beams Generated By Parametric Down-Conversion," Physical Review A **50**, 3349-3361 (1994).

18. Y. H. Shih, A. V. Sergienko, T. B. Pittman, and M. H. Rubin, "EPR And 2-Photon Interference Experiments Using Type-II Parametric Downconversion," Fundamental Problems in Quantum Theory **755**, 40-60 (1995).

19. W. P. Grice, and I. A. Walmsley, "Spectral information and distinguishability in type-II down-conversion with a broadband pump," Physical Review A **56**, 1627-1634 (1997).

20. S. Carrasco, J. P. Torres, L. Torner, A. Sergienko, and B. E. A. Saleh, "Spatial-to-spectral mapping in spontaneous parametric down-conversion," Physical Review A **70** (2004).

21. R. S. Bennink, Y. Liu, D. D. Earl, and W. P. Grice, "Spatial distinguishability of photons produced by spontaneous parametric down-conversion with a focused pump," Physical Review A **74**, 7 (2006).

22. D. Ljunggren, and M. Tengner, "Optimal focusing for maximal collection of entangled narrow-band photon pairs into single-mode fibers," Physical Review A **72**, 17 (2005).

23. D. I. Lee, and T. Goodson, "Entangled photon absorption in an organic porphyrin dendrimer," Journal of Physical Chemistry B **110**, 25582-25585 (2006).

24. M. R. Harpham, O. Suzer, C.-Q. Ma, P. Bauerle, and T. Goodson, "Thiophene dendrimers as entangled photon sensor materials," J Am Chem Soc **131**, 973-979 (2009).

25. J. Javanainen, and P. L. Gould, "Linear Intensity Dependence Of A 2-Photon Transition Rate," Physical Review A **41**, 5088-5091 (1990).

26. H. B. Fei, B. M. Jost, S. Popescu, B. E. A. Saleh, and M. C. Teich, "Entanglement-induced two-photon transparency," Physical Review Letters **78**, 1679-1682 (1997).

27. P. Kok, A. N. Boto, D. S. Abrams, C. P. Williams, S. L. Braunstein, and J. P. Dowling, "Quantum-interferometric optical lithography: Towards arbitrary two-dimensional patterns," Physical Review A **63** (2001).

CHAPTER II

Does Pump Beam Intensity Affect the Efficiency of SPDC?*

Abstract

We show that, with proper modification of the pump field description from plane-wave to spherical-like, which serves to incorporate geometric effects that were discarded in the plane-wave model, the efficiency of the spontaneous parametric down conversion process exhibits dependence on pump intensity, contrary to previous theoretical predictions. Experimental investigations of this behavior are carried out under focused pumping conditions, where pump divergence is kept constant, and pairs of photons are collected behind an aperture that is large compared to the overall down-conversion profile. The resulting photon yield is found to exhibit a strong dependence on pump intensity, and an enhancement of the down-conversion efficiency is observed. The modified pump field description is also modeled numerically and calculations are presented, which are found to display good accordance with experimental observations. The enhanced yield of spontaneous parametrically down-converted photons will prove beneficial for many practical applications of entangled photon pairs where a high flux is desired.

* The work presented in this chapter has been published as a peer-reviewed journal article with the citation Özgün Süzer and Theodore G. Goodson, III, Optics Express **16**, 20166-20175, (2008).

II.1. Introduction

Spontaneous parametric down-conversion (SPDC) is the process by which photons in a laser pump beam incident on a nonlinear optical crystal (BBO) spontaneously decay into pairs of correlated photons that can be simultaneously entangled in energy, momentum, and polarization (for type-II SPDC) [1]. Entangled states of light such as this have been utilized successfully in a wide variety of experiments ranging from fundamental investigations of the foundations of quantum mechanics [2-4], implementations for quantum information manipulation and applications in communication technology [5-9], absolute calibration of single-photon detectors [10-14], to characterization of optical materials [15]. The convenience of SPDC has made it the common method for generation of entangled pairs for use in these experiments.

The general theoretical aspects of the quantum mechanical correlations between the signal and idler photons that constitute a down-converted pair are well known and thoroughly studied [16-18]. The properties of SPDC photons with respect to various parameters affecting their generation and the interaction that takes place inside the crystal have also been explored. Effects resulting specifically from the spectral properties of the pump beam, on the spatial coherence of the down-converted beams, and the consequences of broadband pulsed pumping have been investigated in [19-21]. In addition, the role of the ***spatial*** properties of the pump, particularly that of focused pumping [22, 23], have been demonstrated to be of crucial importance for applications that require coupling of signal-idler modes into a pair of transmission channels, such as single-mode fibers [24, 25]. Furthermore, the spatial characteristics and evolution of the single-photon SPDC image generated under focused pumping have recently been studied

[26, 27]. It has also been shown that parameters like the pump beam waist and the pump beam wave front affect the "entanglement area" and the "entanglement time" of SPDC photons [28], and consequently have an impact on the interaction of entangled light with matter, where interesting non-classical effects had been predicted theoretically [29], and recently demonstrated experimentally [30].

In general, these studies on the effects of spatial properties of the pump beam on SPDC output state, mentioned above, have concentrated on the consequent changes in the correlations between signal-idler pairs, and particularly, the role of pump divergence has been the main focus of investigation. However, the effect of focused pump intensity, especially under constant pump divergence, on overall SPDC photon ***yield*** (the efficiency of the down conversion process) has not been investigated. This is mainly because of the highly scattering nature of the SPDC process, whose output is governed by the phase-matching conditions, which are a manifestation of momentum and energy conservation; $\mathbf{k}_p=\mathbf{k}_s+\mathbf{k}_i$, $\omega_p=\omega_s+\omega_i$. These conditions stipulate that down-converted photons are emitted with significant probability only when $\Delta k_j L_j=(\mathbf{k}_p-\mathbf{k}_s-\mathbf{k}_i)_j L_j$ is close to zero, where $j=x, y, z$. Here, L_j is the length of the crystal in dimension j, $\mathbf{k}$ denotes wave-vector, and subscripts p, s, i refer to the pump field, signal photon, and idler photon, respectively. It follows that the diversification introduced into the incoming pump wave-vectors due to nonzero pump divergence can affect the SPDC output state, but position of the pump focus with respect to nonlinear crystal surface, cannot. In other words, translating the focal plane of a pump focusing lens via a linear stage, and hence changing the pump intensity, ***is not expected to alter SPDC output yield*** because pump divergence is constant throughout this process

[27]. (Please refer to Appendix A for a detailed discussion of entangled photon pair generation probability and efficiency in SPDC)

While all applications that utilize SPDC as a source of entangled photon pairs can benefit from higher brightness, or increased entangled photon yield of the SPDC process, maximizing this entangled photon flux becomes especially important in practical aspects of experiments that investigate the interaction of entangled photons with matter, mentioned earlier, such as entangled multi-photon absorption.

In this chapter, we present the results of an experimental investigation, in which, ***the SPDC photon yield*** is measured under focused pumping conditions where the pump beam divergence is invariant and down-conversion efficiency is observed to ***exhibit a strong dependence on pump beam intensity.*** We also develop a theoretical model incorporating the geometrical aspects of the pump field for comparison purposes and show by numerical simulations that we have found to agree with our experimental findings. This result is important because the efficiency of the SPDC process is not expected to depend on position of pump beam waist [31, 32] or show enhancement through focusing [33] (Appendix A). The following section describes our experimental conditions. The theory section will summarize our theoretical considerations, which will be followed by the results, discussions and finally concluding remarks.

II.2. Experimental

Our experimental setup, illustrated in Figure II.1, utilizes the second-harmonic of a femtosecond Ti:sapphire laser system as a pump source for the generation of down-converted photons in free space. The laser system (Spectra-Physics MAITAI) delivers

100-fs pulses with a repetition rate of 82 MHz at λ = 800 nm. A neutral-density filter wheel just after the laser system is used to control power admitted into the rest of the setup. The laser output is frequency-doubled by focusing onto a 1-mm thick β-Barium Borate (BBO) nonlinear crystal, which is subsequently collimated into a spot size of ~2-mm diameter. The 400-nm light is then separated from the redundant fundamental by means of a dichroic mirror (DM), followed by a Brewster-angled prism.

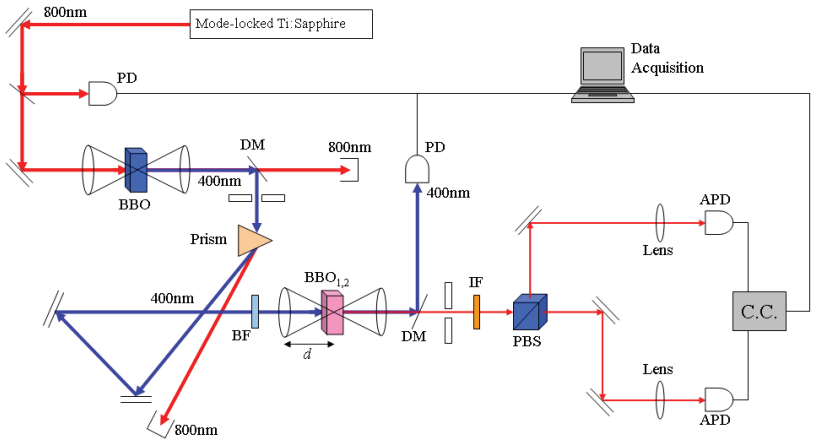

Figure II.1. Schematic representation of our experimental set-up. PD are photodetectors used to monitor fundamental and second harmonic pump power, DM denote dichroic mirrors utilized for spectral selection, PBS is a Glan-laser polarization beam splitter, and IF is a narrow-band interference filter.

A blue filter (BF) is utilized to minimize background intensity before pumping the second BBO crystal for generation of SPDC photons. The 400-nm pump is ***focused onto the input surface of this second BBO crystal via an 8-cm focal length lens*** which is mounted on a translating stage that allows us to vary the distance between the lens and the crystal continuously ranging from 1 cm to 9.5 cm. In our experiments, we have utilized BBO crystals of two different thicknesses for the generation of SPDC photons: one 0.5-mm thick (BBO_1), and the other 2-mm thick (BBO_2), both of which are cut for type-II SPDC at φ=42° with respect to the center pump direction (z). The crystals are tilted slightly to achieve collinear phase-matching. The output surface of the BBO crystal

lies on the focal plane of a successive 6-cm focal length lens that serves to collimate the SPDC photons which are characteristically emitted into two cones. The remaining pump beam is then removed by means of another dichroic mirror, and the SPDC photons are further selected by a spectral filter (IF) with 25-nm bandwidth centered at 800 nm, which also constitutes a ~25-mm spatial aperture that is matched or surpassed by all subsequent optic elements. The reason for the use of such a wide aperture is to guarantee the collection of the whole SPDC pattern.

In order to test for good collection of the whole SPDC profile, we have measured transmitted photon flux through a 1-mm pinhole that was scanned across an image plane perpendicular to the SPDC photons' propagation path after the collimating lens. The measurements were then combined into composite images, given in Figure II.2 below. These scans were repeated for two different separations between the pump focusing lens and BBO down-conversion crystal of d = 10mm and $d = f$ = 80mm, representing both extremes of focusing sharpness for our experimental setup; loose, and sharpest possible focusing, respectively. As is seen from these images, the overall size of the profile is ~13 mm vertically across both rings, with an increase of up to ~3 mm as the focusing lens-BBO separation decreases, which is well within the confines of the aperture, and both focusing schemes depict the whole of the SPDC pattern. Note that the SPDC profile exhibits asymmetric broadening of the signal and idler cones due to non-zero pump divergence. This effect is expected and has been studied in detail in [26] and [27].

Immediately after the spectral selection filter, the signal (*e*-ray plane of BBO) and idler (*o*-ray plane of BBO) modes of SPDC light are separated with a Glan-laser polarization beam-splitter (PBS) before being focused onto free-space single-photon-

sensitive avalanche photodiodes (PerkinElmer Optoelectronics SPCM-AQR-13) by 6-cm focal length collection lenses. The single-photon counting modules have a detection efficiency of ~56% at 800 nm. The output pulses from the photodetectors can then be counted either individually (single-count rate), or fed through a fast coincidence circuit (Ortec NIM7400) with a 10-nsec coincidence window, for coincidence-count rate measurements, through a data acquisition circuit. Since subsequent optic elements after the spectral filter (IF) all match the 25-mm aperture size, and images of the down-converted profile have been verified with the aforementioned pinhole-scans, both photodetectors are able to "see" the whole of their respective signal or idler SPDC patterns under all focusing schemes utilized in our experiments.

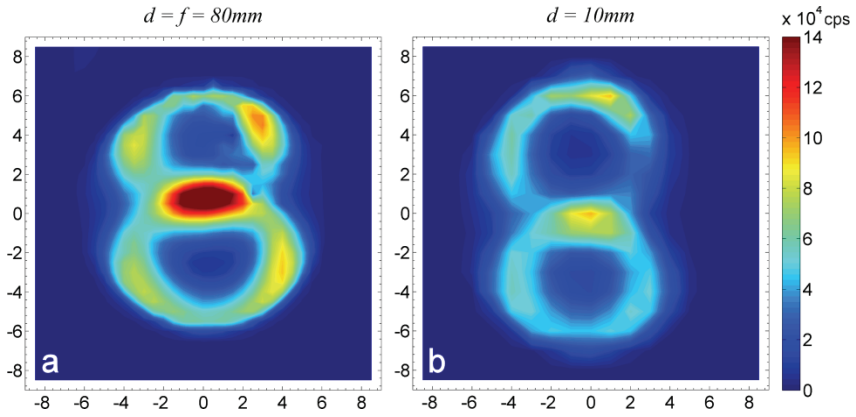

Figure II.2. Image of the SPDC spatial profile in our experimental configuration under (a) sharpest focusing of pump beam ($d = f =$ 80mm), and (b) loose focusing (d = 10mm) condition, generated by measuring transmitted flux through a 1-mm pinhole that is scanned across an image plane normal to the beam path after the collimating lens. Both axes denote position of the pinhole in millimeters. The poor resolution of the image is due to the relatively wide pinhole aperture that was used.

The objective of the experiment is to record single and coincidence count rates as a function of pump power for various separations (d) between the pump focusing lens and BBO crystal. Due to unavoidable imperfection in the experimental alignment, varying the

distance from down-conversion crystal to the focusing lens, via motion of the stage the lens is mounted on, causes the location of the signal and idler collection spots to shift on the focal planes of their respective collection lenses prior to detection. This, combined with the very small active areas (ø175 μm) of the single-photon counting modules, requires that both photodetectors be repositioned to reacquire maximum counts after each adjustment of the focusing lens-BBO distance. To this end, the single-photon counting modules are mounted on free-space, 3-axis motion stages that are controlled electronically, and the collection system is re-optimized after each iteration of the distance *d*.

II.3. Theoretical Background

In this section we present a theoretical analysis of the down-conversion efficiency for photon pairs generated via type-II SPDC under focused pumping conditions. The aim is to express transverse spatial parameters in terms of the separation between down-conversion crystal and pump focusing lens and derive the subsequent SPDC two-photon probability amplitude [34] which will govern the rate of SPDC photons detected in coincidence as a function of input pump intensity.

Pittman et al. [22] have analyzed the spatial correlations of the generated ordinary (idler) and extraordinary (signal) photons under focused CW pumping by describing the transverse-plane pump field profile as a Gaussian intensity distribution and expressing the SPDC two-photon state as having a spherical-like contribution in the momentum phase-matching condition. Following their methodology, we carry out a similar analysis incorporating also the angular frequency envelope for a broadband pulsed pump beam, expressing the classical pump field as

$$\mathbf{E}_p(\mathbf{r};t) = \hat{\mathbf{e}}\, E_p(\mathbf{r}_\perp) \int_0^\infty d\omega_p A(\omega_p) e^{i\mathbf{k}_p(\omega_p)\cdot\mathbf{r}} e^{-i\omega_p t}\,, \tag{II.1}$$

where $\hat{\mathbf{e}}$ is the pump extraordinary polarization direction, $A(\omega_p)$ determines pump spectral width $\Delta\omega_p$, and $E_p(\mathbf{r}\perp)$ is the pump amplitude distribution in the transverse plane, approximated by [35]

$$E_p(\mathbf{r}_\perp) = E_p e^{\mathbf{r}_\perp{}^2/2\sigma_p{}^2}\,, \tag{II.2}$$

with $\sigma_p{}^2 \approx c/\omega_p(d - f - i(\lambda_p^0/\pi w_0{}^2)f^2)$. Here, f is the focal length of the lens, w_0 is the pump beam waist before focusing, $\lambda_p{}^0$ is the pump center wavelength, and d is the variable distance between the lens and input face of the crystal.

Adopting the pump beam center direction as the z-axis in subsequent calculations, it is further required that the dependence on transverse components of pump wave vector be removed from the z-component of the pump wave vector, k_{pz}, by introducing a new pump field quantity, $K_p \equiv (\omega_p/c)n_e(\omega_p)$, which is equal to the magnitude of the pump k vector if it were exactly parallel to the z direction, where $n_{e,o}(\omega)$ respectively are the extraordinary and ordinary refractive indices of the crystal. As a result, the pump field amplitude inside the crystal can now be written as;

$$E_p(\mathbf{r}_\perp, z; t) = E_p' \int_0^\infty d\omega_p A(\omega_p) e^{-i(\omega_p t - K_p z)} \int d^2k_\perp e^{-i(\mathbf{k}_\perp\cdot\mathbf{r}_\perp + \mathbf{k}_\perp^2\sigma_p^2/2)}\,. \tag{II.3}$$

Here, it is assumed that the pump diameter is relatively small compared to the focal length of the lens such that the paraxial approximation [36] can be applied. Further, a thin crystal approximation [37] must also be applied for the above description to be valid, without which the simplification of the pump field into computable terms is extremely complicated. Completing the square in the momentum-space Gaussian integration in Eq. (II.3) yields a ***spherical-like*** description for the pump field, rather than the usual plane-

wave model considered in most treatments of SPDC [22]. It should also be observed that, due to the focal-length dependent term in the denominator of the exponential in Eq. (II.2), the plane-wave model is recovered in the very long focal length ($f \to \infty$) limit, as expected.

The two-photon output state is then calculated to first order in perturbation theory with an interaction Hamiltonian derived from the standard form; [38]

$$\begin{aligned} H_I &= \varepsilon_0 \int_V d^3\mathbf{r}\, \chi\, E_p^{(+)}\, E_s^{(-)}\, E_i^{(-)} \\ &= A_1 \int d\omega_p A(\omega_p) \int d^3\mathbf{k}_s \int d^3\mathbf{k}_i \int_V d^3\mathbf{r}\, \hat{a}^\dagger_{\mathbf{k}_s} \hat{a}^\dagger_{\mathbf{k}_i}\, e^{i(\omega_s+\omega_i-\omega_p)t} \\ &\qquad \times e^{i(k_p-k_{s_z}-k_{i_z})z}\, e^{-i(\mathbf{k}_{s_\perp}-\mathbf{k}_{i_\perp})\cdot\mathbf{r}_\perp}\, e^{i/2\sigma_p^2\mathbf{r}_\perp^2} + \text{H.C.} \end{aligned} \tag{II.4}$$

where V is the volume of interaction for the classical pump field described by Eq. (II.3), H.C. denotes the Hermitian conjugate, $\hat{a}^\dagger_{\mathbf{kj}}$ with j=s, i are the creation operators for the signal and idler modes, respectively, and electric susceptibility χ of the nonlinear crystal, along with all unimportant constants have been absorbed into factor A_1. When the volume integration is broken up into the multiplication of an area integral and integration over the crystal length L, the transverse integration over the $\mathbf{r}_\perp$-dependent terms can be approximated as a Gaussian over an infinite range, provided the crystal cross sectional area is large compared to the pump beam waist. It is then possible to use the technique of first order perturbation theory, and the two-photon state is calculated as [1];

$$\begin{aligned} |\psi\rangle &= A_2 \int d\omega_p A(\omega_p) \int d^3\mathbf{k}_s \int d^3\mathbf{k}_i \delta(\omega_s+\omega_i-\omega_p) \\ &\qquad \times \int_0^L dz e^{i(k_p-k_{s_z}-k_{i_z})z}\, e^{-i\cdot\mathbf{r}_\perp}\, e^{(\sigma_p^2/2)(\mathbf{k}_{s_\perp}+\mathbf{k}_{i_\perp})^2}\, \hat{a}^\dagger_{\mathbf{k}_s} \hat{a}^\dagger_{\mathbf{k}_i} |0\rangle \end{aligned} \tag{II.5}$$

where the new constant factor A_2 has absorbed the constants generated in the transverse integration of (II.4) and A_1.

In the detection scheme utilized for our experiment, the average coincidence-count rate, defined by the Glauber formulation [39], will depend directly on the square of the two-photon probability amplitude;

$$\left|\left\langle\psi\right|E_1^{(-)}E_2^{(-)}E_2^{(+)}E_1^{(+)}\left|\psi\right\rangle\right|^2=\left|\left\langle 0\right|E_2^{(+)}E_1^{(+)}\left|\psi\right\rangle\right|^2, \tag{II.6}$$

where the analytical fields $E^{(+)}_{1,2}$ describe the free-space field operators at detector APD_1 for the ordinary-polarized idler beam, and at detector APD_2 for the extraordinary-polarized signal beam. As such, $E_1^{(+)}$ incorporates the annihilation operator $\hat{a}_{\mathbf{ki}}$ of the idler mode, and $E_2^{(+)}$ contains the annihilation operator $\hat{a}_{\mathbf{ks}}$ for the signal mode. Since the detection scheme utilized in our experiment selects near-degenerate wavelengths before the signal and idler pairs are separated, both fields have identical angular frequency integrations to describe the transmission interval of the interference filter employed. Thus, combining (II.5) and (II.6), we are able to establish a description of the coincidence counting rate of SPDC photons generated in our setup as dependent on the geometry of the focused pump beam, i.e. the separation between pump focusing lens and nonlinear crystal, d.

Note that under conditions where focal-length of the pump-focusing lens is invariant such that pump-beam divergence does not change and average pump power is kept constant, translation of focusing lens to vary d leads only to variation of pump spot size on the input face of the down-conversion crystal and changes the pump intensity distribution. As a result, Eq. (II.5) and (II.6) express, effectively, the coincidence-count rate as a function of input pump intensity.

II.4. Results and Discussion

In Figure II.3 we show, for down-conversion crystals of two different thicknesses, the measured SPDC coincidence-count rates and numerical simulations based on the theoretical model developed in the previous section [Eq. (II.5) and (II.6)] for various focusing lens-BBO separations. The experimental data has been normalized for comparison purposes. Maximum count rates obtained in coincidence under optimized conditions were ~3.60×10^4 cps for BBO_1, and ~1.24×10^5 cps for BBO_2. Due to the complexity of equations (II.4) and (II.5), the theoretical modeling was carried out numerically instead of analytically for near-degenerate wavelengths of the signal and idler photons, detection restricted to the bandwidth of the interference filter (800±12.5 nm), with pump wave vectors defined in terms of measured pump spectral width (<13 nm), at normal incidence to the BBO surface. Note that these simulations are carried out for varying distances between down-conversion crystal and focusing lens, and not for varying focal lengths (pump divergences), where, in the long focal length limit, the theoretical model would represent a plane-wave pump field and all dependencies on pump geometry in SPDC output state would vanish. In this regime, the output yield of the SPDC process would correspond to the dashed plots given in Figure II.3, irrespective of the value of d. Note that while each trace exhibits linear behavior as a function of pump power, the different focusing schemes result in different slopes, or efficiency, of the SPDC process. This is in contrast to previous theoretical predictions [31-33], where SPDC output has been reported to be independent of the position of pump beam waist. The inclusion of the spherical-like geometrical factor in our theoretical model allows for us to calculate the SPDC yield as a function of the separation, d.

The theoretical simulations and experimental results for both cases show good qualitative agreement in their linear dependence on input pump power. The linear character of this dependence is interpreted as evidence that the parametric down-conversion in our experimental configuration is within the spontaneous regime. The quantitative difference between computed theoretical yield and measured SPDC coincidence counting rate for thinner nonlinear crystal BBO_1 [Fig. II.3(a)] is attributed to optical losses not related to aperture size, and alignment imperfections. However, in the case of the thicker crystal BBO_2, the observed coincidence-count rate is slightly higher than the theoretical yield predicted [Fig. II.3(b)]. We suggest that this is due to the larger thickness of nonlinear crystal, which is roughly an order of magnitude thicker than the metric required so that the thin-crystal approximation remains applicable; in this regime,

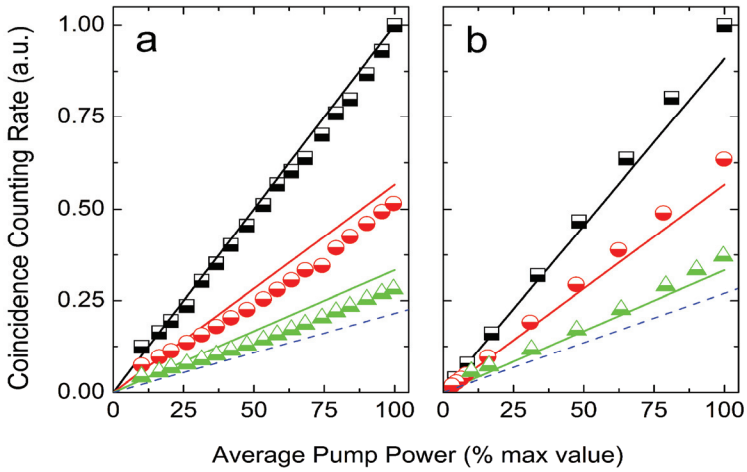

Figure II.3. Normalized coincidence-count rate data from (a) 0.5-mm thick, and (b) 2.0-mm thick BBO crystals measured as a function of percent peak pump power for three focusing conditions of the pump: d = 80mm (squares), d = 38mm (dots), and d = 15mm (triangles). Solid lines represent numerical calculations of each case, and dashed lines show the theoretical prediction for the plane-wave ($f \rightarrow \infty$) limit.

the pump field description given by Eq. (II.3) is no longer sufficient to describe the interaction inside the crystal completely and additive terms that had been dropped for

ease of numerical calculation have a more significant effect compared to the case of the thinner (0.5-mm) crystal.

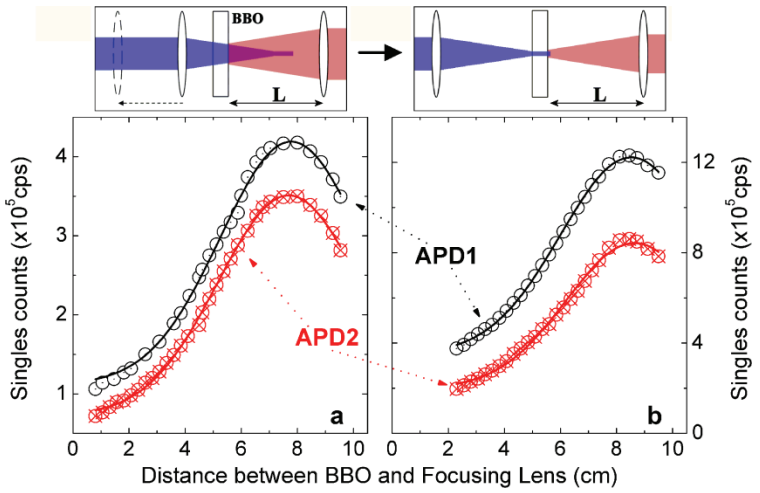

Figure II.4. Intensity dependence of signal and idler single-count rates as a function of focusing lens-BBO separation for (a) 0.5-mm thick, and (b) 2.0-mm thick nonlinear crystals. Note that the scale for the thick crystal is ca. 3 times larger. Solid lines for each trace are fits to a parametrized exponential of a form matching that of the spherical-like envelope of the pump field. The mismatch in signals from the two detectors is due to the presence of extra optical loss along APD2 path which is not present in APD1. The insets illustrate progression from small separations between focusing lens and BBO to where the separation is equal to one focal-length of the pump focusing lens. The distance between the BBO and collimating lens is fixed at L = 60mm. Because pump-beam divergence is constant throughout this translation, the angular spread of the SPDC spatial profile does not change. However, due to the wider cross-sectional area of interaction at small distances, the size of the profile at a constant distance from the BBO output surface gets narrower as one approaches $d = f$ = 80mm limit. A wide aperture is utilized to compensate for this change and ensure collection of the whole down-conversion profile at all d values.

It should be noted here that the presence of "*extra near-infrared fluorescence*" originating from the BBO crystal has previously been reported under focused CW pumping conditions for pump divergence exceeding 32 mrad in [26]. Though the origin and nature of this excess light has not been investigated quantitatively, it is presumed not to be a result of the SPDC process. The pump divergence obtained from the optical setup

employed in our experiment (25±1 mrad) is smaller than this threshold value, excluding the possibility of detecting uncorrelated photons and generating false coincidences. Furthermore, this same communication had reported a decrease in SPDC single-count rate under conditions where entangled pairs were collected through a "bucket" detection scheme which utilizes narrow apertures in front of single-photon counting modules. This decrease, however, is attributed to the inhomogeneous broadening of the SPDC spatial profile, which, combined with the application of narrow apertures for collection, results in diminished collection efficiency of signal-idler pairs. As described previously in the experimental section, our setup utilizes a wide aperture (ø 2.54 cm) in order to circumvent collection drawbacks of this kind.

The phase matching argument, as well as previous theoretical studies [31-33], suggests that change in the pump beam waist at the nonlinear crystal will not have an impact on the SPDC output yield. To test this argument, we have also investigated the dependence of single-count rates of the signal and idler photons on position of pump beam waist under ***fixed*** pump power. In Fig. II.4 we show single-count rates as a function of focusing lens-BBO separation, acquired at peak pump power. As expected, the counting rates for both the signal and idler modes of the SPDC process exhibit an increase toward corresponding maxima as the pump focusing scheme approaches the sharpest configuration, and a decrease after. Note that the data also suggests a symmetry with respect to the $d = f = 80$ mm (sharp) focusing condition, however, collection of counting-rate data for separations $d > 95$ mm was not possible with our current experimental setup due to physical space constraints. Because Eq. (II.5) and (II.6) describe specifically the coincidence-count rate and hence are not directly applicable to

single-count data, we have tested adherence of these plots to a form similar to that of the spherical-like geometrical factor in Eq. (II.3). Solid lines in Fig. II.4 represent analytical fits of the experimental data to such functions. The experimental data is found to show good agreement with this form and suggests that the SPDC output photon yield shows a non-linear dependence on pump beam intensity for both thin and thick BBO crystals.

II.5. Conclusions

Our experimental findings show unambiguously that a pump beam focused into higher intensities enhances the SPDC output yield, despite the constant pump divergence. As opposed to previous publications that had reported no change or even reduced yield under such focused pumping conditions, our experimental setup is designed to collect the entire SPDC pattern, and thus enhancement of output yield is seen to originate from better down-conversion efficiency at higher pump intensity. Accordingly, almost one order of magnitude of enhancement can be achieved under optimized conditions. Furthermore, this enhanced flux of photons is ascribed solely to the SPDC process, because the pump divergence utilized in our experiments is small compared to the divergences at which generation of excess, non-SPDC photons had been reported previously [26].

The comparison of theoretical simulations with our experimental results have shown that adopting a spherical-like description for the pump field, as originally proposed in [22], serves to minimize the discrepancy between theoretical predictions and experimental observations as opposed to a plane-wave model.

II.6. References

1. D. N. Klyshko, *Photons and Nonlinear Optics* (Gordon and Breach Science Publishers, New York, 1988).

2. Z. Y. Ou, and L. Mandel, "Violation of Bells-Inequality and Classical Probability in a 2-Photon Correlation Experiment," Phys. Rev. Lett. **61**, 50-53 (1988).

3. Y. H. Shih, and C. O. Alley, "New Type of Einstein-Podolsky-Rosen-Bohm Experiment Using Pairs of Light Quanta Produced by Optical Parametric Down Conversion," Phys. Rev. Lett. **61**, 2921-2924 (1988).

4. P. G. Kwiat, K. Mattle, H. Weinfurter, A. Zeilinger, A. V. Sergienko, and Y. H. Shih, "New High-Intensity Source of Polarization-Entangled Photon Pairs," Phys. Rev. Lett. **75**, 4337-4341 (1995).

5. D. Bouwmeester, J. W. Pan, K. Mattle, M. Eibl, H. Weinfurter, and A. Zeilinger, "Experimental quantum teleportation," Nature **390**, 575-579 (1997).

6. T. B. Pittman, B. C. Jacobs, and J. D. Franson, "Single photons on pseudodemand from stored parametric down-conversion," Phys. Rev. A **66**, 042303 (2002).

7. P. Walther, K. J. Resch, T. Rudolph, E. Schenck, H. Weinfurter, V. Vedral, M. Aspelmeyer, and A. Zeilinger, "Experimental one-way quantum computing," Nature **434**, 169-176 (2005).

8. W. Tittel, and G. Weihs, "Photonic entanglement for fundamental tests and quantum communication," Quant. Inf. Comput. **1**, 3-56 (2001).

9. W. T. M. Irvine, A. L. Linares, M. J. A. de Dood, and D. Bouwmeester, "Optimal quantum cloning on a beam splitter," Phys. Rev. Lett. **92**, 047902 (2004).

10. A. A. Malygin, A. N. Penin, and A. V. Sergienko, "Absolute Calibration of the Sensitivity of Photodetectors Using a Biphotonic Field," JETP Lett. **33**, 477-480 (1981).

11. J. G. Rarity, K. D. Ridley, and P. R. Tapster, "Absolute Measurement of Detector Quantum Efficiency Using Parametric Downconversion," Appl. Opt. **26**, 4616-4619 (1987).

12. A. N. Penin, and A. V. Sergienko, "Absolute Standardless Calibration of Photodetectors Based on Quantum 2-Photon Fields," Appl. Opt. **30**, 3582-3588 (1991).

13. P. G. Kwiat, A. M. Steinberg, R. Y. Chiao, P. H. Eberhard, and M. D. Petroff, "High-Efficiency Single-Photon Detectors," Phys. Rev. A **48**, R867-R870 (1993).

14. P. G. Kwiat, A. M. Steinberg, R. Y. Chiao, P. H. Eberhard, and M. D. Petroff, "Absolute Efficiency and Time-Response Measurement of Single-Photon Detectors," Appl. Opt. **33**, 1844-1853 (1994).

15. A. V. Sergienko, Y. H. Shih, and M. H. Rubin, "Experimental Evaluation of a 2-Photon Wave-Packet in Type-II Parametric Downconversion," J. Opt. Soc. Am. B **12**, 859-862 (1995).

16. D. C. Burnham, and D. L. Weinberg, "Observation of Simultaneity in Parametric Production of Optical Photon Pairs," Phys. Rev. Lett. **25**, 84-87 (1970).

17. S. Friberg, C. K. Hong, and L. Mandel, "Measurement of Time Delays in the Parametric Production of Photon Pairs," Phys. Rev. Lett. **54**, 2011-2013 (1985).

18. I. Abram, R. K. Raj, J. L. Oudar, and G. Dolique, "Direct Observation of the 2nd-Order Coherence of Parametrically Generated Light," Phys. Rev. Lett. **57**, 2516-2519 (1986).

19. A. Joobeur, B. E. A. Saleh, and M. C. Teich, "Spatiotemporal Coherence Properties of Entangled Light-Beams Generated by Parametric Down-Conversion," Phys. Rev. A **50**, 3349-3361 (1994).

20. T. E. Keller, and M. H. Rubin, "Theory of two-photon entanglement for spontaneous parametric down-conversion driven by a narrow pump pulse," Phys. Rev. A **56**, 1534-1541 (1997).

21. W. P. Grice, and I. A. Walmsley, "Spectral information and distinguishability in type-II down-conversion with a broadband pump," Phys. Rev. A **56**, 1627-1634 (1997).

22. T. B. Pittman, D. V. Strekalov, D. N. Klyshko, M. H. Rubin, A. V. Sergienko, and Y. H. Shih, "Two-photon geometric optics," Phys. Rev. A **53**, 2804-2815 (1996).

23. C. H. Monken, P. H. S. Ribeiro, and S. Padua, "Optimizing the photon pair collection efficiency: A step toward a loophole-free Bell's inequalities experiment," Phys. Rev. A **57**, R2267-R2269 (1998).

24. C. Kurtsiefer, M. Oberparleiter, and H. Weinfurter, "High-efficiency entangled photon pair collection in type-II parametric fluorescence," Phys. Rev. A **64**, 023802 (2001).

25. F. A. Bovino, P. Varisco, A. M. Colla, G. Castagnoli, G. Di Giuseppe, and A. V. Sergienko, "Effective fiber-coupling of entangled photons for quantum communication," Opt. Commun. **227**, 343-348 (2003).

26. P. S. K. Lee, M. P. van Exter, and J. P. Woerdman, "How focused pumping affects type-II spontaneous parametric down-conversion," Phys. Rev. A **72**, 033803 (2005).

27. R. S. Bennink, Y. Liu, D. D. Earl, and W. P. Grice, "Spatial distinguishability of photons produced by spontaneous parametric down-conversion with a focused pump," Phys. Rev. A **74**, 023802 (2006).

28. A. Joobeur, B. E. A. Saleh, T. S. Larchuk, and M. C. Teich, "Coherence properties of entangled light beams generated by parametric down-conversion: Theory and experiment," Phys. Rev. A **53**, 4360-4371 (1996).

29. H. B. Fei, B. M. Jost, S. Popescu, B. E. A. Saleh, and M. C. Teich, "Entanglement-induced two-photon transparency," Phys. Rev. Lett. **78**, 1679-1682 (1997).

30. D. I. Lee, and T. Goodson, "Entangled photon absorption in an organic porphyrin dendrimer," J. Phys. Chem. B **110**, 25582-25585 (2006).

31. E. C. Cheung, K. Koch, G. T. Moore, and J. M. Liu, "Measurements of 2nd-Order Nonlinear-Optical Coefficients from the Spectral Brightness of Parametric Fluorescence," Opt. Lett. **19**, 168-170 (1994).

32. K. Koch, E. C. Cheung, G. T. Moore, S. H. Chakmakjian, and J. M. Liu, "Hot-Spots in Parametric Fluorescence with a Pump Beam of Finite Cross-Section," IEEE J. Quantum Electron. **31**, 769-781 (1995).

33. D. A. Kleinman, "Theory of Optical Parametric Noise," Phys. Rev. **174**, 1027-1041 (1968).

34. Y. Shih, "Two-Photon Entanglement and Quantum Reality," in *Advances in Atomic, Molecular, and Optical Physics*, B. Bederson, and H. Walther, eds. (Academic Press, Cambridge, 1999), pp. 1-42.

35. P. W. Milonni and J. H. Eberly, *Lasers* (John Wiley and Sons, New York, 1988).

36. E. Hecht and A. Zajac, *Optics* (Addison-Wesley Pub. Co., Reading, MA, 1990).

37. This approximation limits the crystal thickness to the order of 10^{-4} m. See Appendix A in [22] for details.

38. M. H. Rubin, D. N. Klyshko, Y. H. Shih, and A. V. Sergienko, "Theory of two-photon entanglement in type-II optical parametric down-conversion," Phys. Rev. A **50**, 5122-5133 (1994).

39. R. J. Glauber, "Quantum Theory of Optical Coherence," Phys. Rev. **130**, 2529-2539 (1963).

CHAPTER III

Thiophene Dendrimers as Entangled Photon Sensor Materials*

Abstract

The ability to do spectroscopy with a small number of entangled photons is an important development in the area of materials and sensing. This chapter investigates the effects of increasing thiophene dendrimer generation on the cross-section for both entangled (σ_E) and random (δ_R) two-photon absorption cross-sections. Nonlinear optical properties of dendrimers are an interesting area of study for potential applications in optical signal processing and remote sensing, and the use of a nonlinear optical material as a sensor for entangled photons offers great possibilities in quantum lithography. Entangled two-photon absorption (ETPA) experiments and two-photon excited fluorescence (TPEF) experiments vary by at least ten orders of magnitude in the photon flux used to probe the material. ETPA cross-sections from liquid samples as well as those of thin film samples are investigated. An increase in σ_E and δ_R with increasing dendrimer generation is observed. The nonlinear spectroscopic features obtained by the TPEF measurements were also obtained by the entangled photon experiments, in which there were ten orders of magnitude fewer photons. All dendrimer generations investigated in this work are found to have great potential for applications in quantum optical devices.

* The work presented in this chapter has been published as a peer-reviewed journal article with the citation Michael R. Harpham, Özgün Süzer, Chang-Qi Ma, Peter Bäuerle, Theodore Goodson, Journal of the American Chemical Society **131**, 973-979 (2009).

III.1. Introduction

Organic conjugated macromolecules have been the subject of intense study for applications such as organic light-emitting diodes [1-5], photovoltaic devices [6], light harvesting [7-12], molecular electronics [13, 14], and optical signal processing [15-18]. Among the many methods of tailoring organic molecules for these applications, chromophores designed in dendritic architectures have been shown [5,10,12,14,19-21] to hold great promise, as dendrimers exhibit efficient intra-molecular energy transfer and energy migration, leading to enhanced nonlinear optical (NLO) properties relative to those of the monomeric architecture. One unexplored application of NLO materials is in detection of entangled photon pairs generated by spontaneous parametric downconversion (SPDC).

The intensity-dependent random nonlinear effect related to the excitation of virtual intermediate states is traditionally explored through two-photon excited fluorescence (TPEF) spectroscopy [22]. As TPEF relies on these random events, a potentially damaging flux of over 10^{20} photons/cm^2/s incident on the sample is required to generate the measurable fluorescence photon count rate necessary to determine a random two-photon absorption (TPA) cross-section. This is particularly damaging for microscopy applications on biological molecules.

Unlike TPEF, which relies on classical photons, correlated photon pairs generated by spontaneous parametric downconversion (SPDC) are used in entangled two-photon absorption spectroscopy (ETPA). Photon pairs produced by SPDC have a high degree of temporal and spatial correlation. This is critical for demonstrating a relatively efficient two-photon absorption event [23]. Theoretical investigations by multiple research groups

have shown [23-26] that the entangled two-photon absorption rate should have a linear rather than quadratic dependence on the intensity of downconverted light. However, experimental demonstrations have been limited [27]. Theoretical estimates of the entangled two-photon absorption cross-sections of hydrogen [24] and sodium [25] are reported as 10^{-12} and 10^{-30} cm^2, respectively. Results from ETPA experiments on a free-standing third-generation porphyrin film, tetraphenylporphyrin within a polyvinylbutyral matrix were recently reported [27]. It was found [27] that the ETPA cross-section for a porphyrin dendrimer film was on the order of 10^{-17} cm^2, which is only an order of magnitude lower than the single-photon absorption (SPA) cross-section of 10^{-16} cm^2 at the linear optical absorption maximum of the dendrimer. Furthermore, a transition from linear (entangled) to quadratic (random) absorption rates with increasing input flux density was observed in these experiments far from any resonances of the porphyrin dendrimer. While these initial results have suggested the possibility of using entangled photons for nonlinear spectroscopy, there has not been a systematic demonstration of the use of entangled photons for this purpose reported in the literature.

In this chapter, a set of thiophene dendrimers (Fig. III.1) synthesized according to reported procedures [28, 29] are systematically investigated as sensors for entangled photons, and the effects of increasing dendrimer generation on two-photon absorption cross-section of these thiophene dendrimers are observed. Previous work on thiophene dendr*ons*, essentially half the dendr*imer* we investigate in this chapter, has shown [20] interesting nonlinear absorption properties. A non-monotonic increase in two-photon absorption cross-section of these dendrons was observed [20], suggesting a cooperative enhancement due to intramolecular interactions between the thiophene branches. While

the overall two-photon absorption cross-section is found to increase with dendron generation, the two-photon absorption cross-section per thiophene unit is found [20] to increase non-monotonically with dendron generation only until the 2nd generation (G2), suggesting a cooperative enhancement of the TPA cross-section. The decrease in TPA cross-section per thiophene in the G3 dendron was attributed [20] to a saturation effect. Here, the two-photon absorption cross-section of thiophene dendrimers is investigated through entangled TPA as well as traditional, TPEF experiments. This is the first report of a comparison between trends in the TPA cross-sections measured by these techniques in a systematic manner for a complete set if dendrimers varying in generation. In addition, thin film, as well as liquid, samples are investigated and compared in this work to determine if either medium is more effective as a sensor for entangled photons.

III.2. Experimental

III.2.1. Materials

The thiophene dendrimers investigated in this work were synthesized by a iterative divergent/convergent method starting from a trimethylsilyl- (TMS) protected branched terthiophene [28,29]. A solvent of tetrahydrofuran (THF, Sigma-Aldrich, 99.9% purity) was used for thiophene dendrimer liquid samples. The optical density for the solutions prepared was controlled by concentration.

Steady-state absorption experiments were performed using an Agilent 8325E UV/Vis spectrometer, and fluorescence measurements with a Jobin Yvon - SPEX Fluoromax-2 spectrometer. Thin film samples were drop-cast in poly-ethylmethacrylate-co-methacrylate (PEMA-MA, Aldrich, $M_w \sim 10^6$ g/mol) with solvent tetrahydrofuran (THF,

Aldrich, 99.98%, inhibitor free) onto a glass substrate. Film thickness and uniformity was assessed using a Dektak surface analyzer. All films studied were prepared to have a uniform thickness between 10 and 80 μm, varied by dendrimer generation to yield a reasonable single-photon absorption spectrum, which matches steady-state spectra in liquid samples and hence shows that there is no aggregation of the thiophene dendrimers within the film.

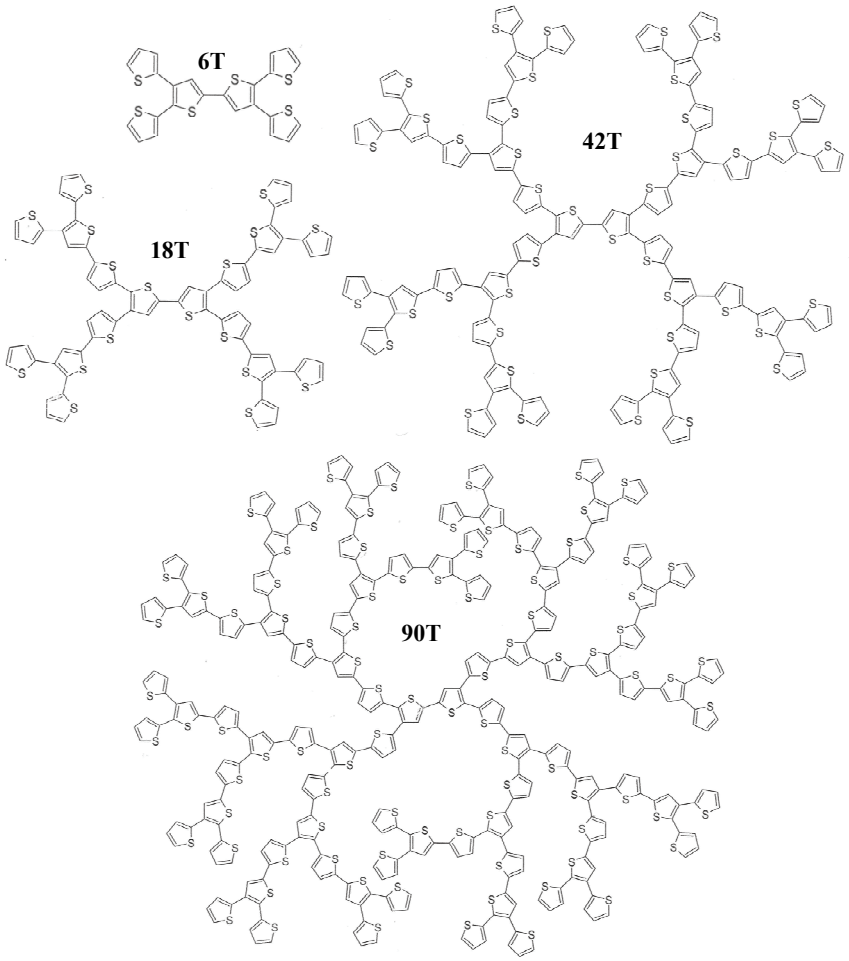

Figure III.1. Thiophene dendrimers **6T** (top left), **18T** (middle left), **42T** (top right) and **90T** (bottom). Dendrimers are named according to the number of the thiophene groups.

III.2.2. Two-Photon Excited Fluorescence

The two-photon excited fluorescence (TPEF) method [22] was employed to evaluate the random two-photon absorption cross-sections (δ_R) of the liquid samples. The random

TPA cross-section δ_R was evaluated over the excitation wavelength range of 700-850 nm using a mode-locked Ti:sapphire laser (Spectra-Physics MaiTai® HP, pulse width < 100 fs, 80 MHz repetition rate). In the TPEF technique, two-photon absorption cross-sections were measured relative to a reference solution of 10^{-4} M Coumarin 307 in methanol.

III.2.3. Entangled Two-Photon Absorption

A significant flux of entangled photon pairs is necessary for observation of the ETPA effect. Our system is designed such that polarization-entangled pairs of photons are generated at a wavelength of 800nm through the SPDC of photons at 400 nm wavelength under the collinear phase-matching conditions illustrated in Figure III.2. The experimental setup is illustrated in Figure III.3. Briefly, sub-100 fs pulses, typically 14 nm FWHM centered at 800 nm with an 82 MHz repetition rate, from a mode-locked Ti:sapphire laser (Spectra-Physics MaiTai®) are frequency-doubled to produce a SHG beam at 400 nm. This SHG beam is then focused onto a 0.5 mm β-barium borate (BBO II in Figure III.2) crystal designed for Type II SPDC to generate entangled pairs of down-converted photons.

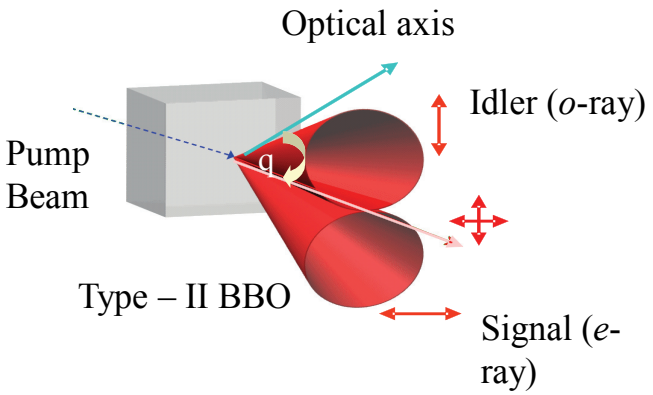

Figure III.2. Illustration of collinear phase-matching condition of Type II SPDC. Idler (vertical polarization) and signal (horizontal polarization) "cones" of photons are overlapped along one line.

Down-converted photons are detected by silicon avalanche photodiode (APD) single photon counting modules (Perkin-Elmer SPCM-AQR-13). Using these APD's individually, the single photon count rate at a given detector is measured. A Glan-Taylor polarization beam splitter is used to direct the idler (*o*-ray) and the signal (*e*-ray) to separate APD's to allow concidence counting by a fast coincidence counting module (Ortec NIM7400, 10 ns coincidence window) connected to the two APD's.

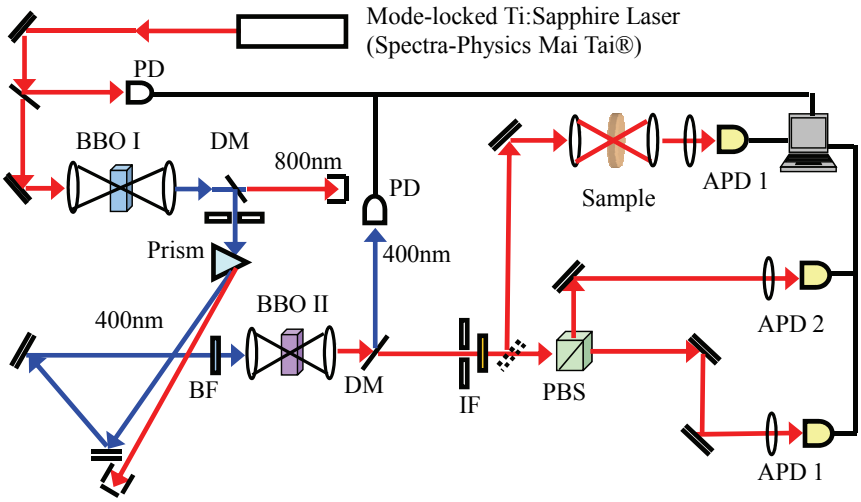

Figure III.3. Experimental setup for ETPA experiments. Dichroic mirrors (DM) are used to separate second-harmonic from fundamental, and entangled photons from second-harmonic. Switching to analysis (coincidence) counting requires addition (removal) of one mirror between the interference filter (IF) and polarization beam splitter (PBS). Photodiodes (PD) are used as a reference for fundamental and second-harmonic power, while avalanche photodiode (APD) single-photon counting modules detect entangled photons.

With this setup, a maximum input photon rate of almost 3×10^7 photons/s for the singles count rate and 2.2×10^5 photons/s for the coincidence count rate is obtained. To vary the input flux, the fundamental beam is attenuated using a continuously variable neutral density filter wheel, with photodiodes (PD's) serving as references for the input power. ETPA measurements are performed based on the transmission method, with

appropriate corrections for background and scatter. Film samples are oriented perpendicular to the incoming SPDC pump, with the film centered at the focal point of the sample telescope. The experimental setup and method used for these experiments have previously been demonstrated [27] effective for ETPA measurements.

III.3. Results and Discussion

III.3.1. Linear Optical Spectroscopy

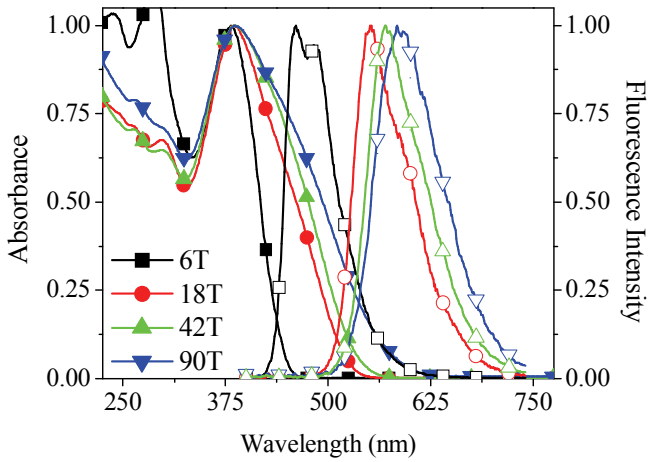

Figure III.4. Normalized absorbance (closed symbols, left axis) and emission (open symbols, right axis) spectra for thiophene dendrimers. Absorbance and emission maxima are red-shifted with increasing dendrimer generation.

Results from steady-state absorption and fluorescence are illustrated in Figure III.4. From these absorption spectra, a red-shift of the absorption maximum and a broadening on the red side of the peak is observed with increasing number of thiophenes. These effects have been observed in thiophene dendrons and ascribed [20,30] to absorption by α-thiophene chains of different lengths within the dendron. The absorption spectrum of the dendron is produced by a linear combination of absorption spectra from individual α-thiophene chains [20,30]. A red-shift of emission maximum with increasing number of thiophenes is observed in the thiophene dendrimers studied in this work. Previous work

on thiophene dendrons has shown [20,30] that this shift in emission maximum can be attributed to emission from the longest α-thiophene chain. With linear spectroscopy alone, the delocalization of excitation and absorption within these dendrimers cannot be explicitly evaluated; a complementary set of nonlinear two-photon absorption measurements is necessary to evaluate delocalization within these dendrimers.

Fluorescence quantum yield Φ_{fl} (Table III.1) is calculated by a known method [31] using Coumarin 307 as a standard. The quantum yield is found to decrease with dendrimer generation, which, based on previous results [20] for thiophene dendrons, may be a result of a decrease in fluorescence lifetime with increasing dendrimer generation. The analysis of fluorescence lifetime of these dendrimers through time-correlated single-photon counting methods will be published [32].

III.3.2. Two-Photon Excited Fluorescence Spectroscopy

The TPA cross-sections were estimated using the two-photon excited fluorescence (TPEF) method [22]. Fluorescence was collected for each dendrimer at the emission maximum determined from steady-state spectroscopy (Fig. III.4, Table III.1). TPA cross-sections of the various dendrimers as a function of excitation wavelength are shown in Figure III.5. A pronounced increase in cross-section with increasing dendrimer generation is observed. At an excitation wavelength of 800 nm, TPA cross-sections for the dendrimers are found to increase from 6 GM to ~1100 GM (1GM = 10^{-50} cm^4 s $photon^{-1}$ $molecule^{-1}$) as the dendrimer generation increases, a trend which has been attributed to delocalization of the excitation over the entire dendrimer [20,33]. The TPA cross-section of the **42T** dendrimer in this work is found to be nearly identical to that of

the **45T** dendron previously reported [20]. Comparing the thiophene dendrimers in this work to nitrogen-centered phenylacetylene dendrimers previously reported [34], the thiophene dendrimer is found to yield a larger TPA cross-section than the phenylacetylene dendrimer does for a given dendrimer generation. Recently, thiophene macrocycles have been reported [33,35] to have TPA cross-sections of 10^4-10^5 GM, with TPA cross-sections per thiophene group of 10^2-10^3 GM. The thiophene dendrimers reported here are found to have a smaller TPA cross-section per subgroup than the macrocycles do. However, the dendrimer architecture may have greater potential in energy transport applications due to the ability of branch-core systems to funnel energy [21].

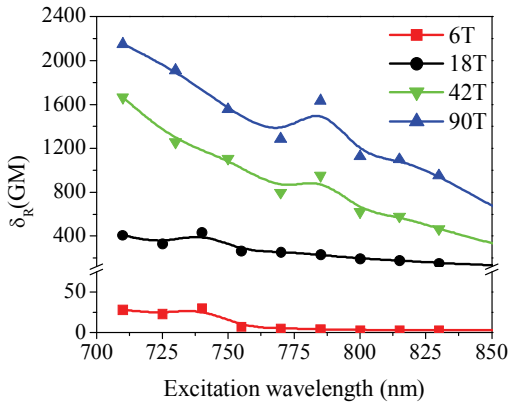

Figure III.5. Two-photon absorption cross section, δ_R, for thiophene dendrimers plotted against excitation wavelength.

Thus, the main spectroscopic trends are that the TPA cross-section increases with increasing dendrimer generation and number of thiophene units, and that the TPA cross-section per thiophene is found to be at a maximum for the **42T** dendrimer. While a larger TPA cross-section is observed in the **90T** dendrimer than is observed in the **42T** dendrimer, a smaller TPA cross-section per thiophene was found. These trends have been explained [20,33] for the case of dendrons by a cooperative enhancement of the TPA

cross-section through an increase in branching, with a saturation effect occurring in the highest dendrimer generation. Time-resolved measurements of energy transfer have also been carried out to show the intramolecular interactions between the thiophene chromophore units, which are in part responsible for the generation dependence of the TPA cross-section in this systematic set of dendrimer materials, and will be reported elsewhere [32].

Dendrimer # Thiophenes	Steady-State λ_{abs} (nm)	Steady-State λ_{em} (nm)	Steady-State Φ_{fl}	Two-Photon Excited Fluorescence at 800nm Random TPA (δ_R) (GM)	Two-Photon Excited Fluorescence at 800nm δ_R/Thiophene (GM)
6	382	483	0.11	6	1.0
18	384	548	0.08	230	12.8
42	387	570	0.07	620	14.8
90	389	596	0.04	1130	12.6

Table III.1. Results from steady-state linear absorption and two-photon excited fluorescence measurements

III.3.3. Entangled Two-Photon Absorption Measurements

The entangled two-photon absorption rate [36], R_E, is derived from time-dependent second-order perturbation theory in terms of the second-order correlation function [37]. Theoretically, the ETPA effect is accompanied by non-entangled or random TPA effect [23]. From this, a bimodal distribution is observed in the flux-dependence of the absorbed photon rate. At low input photon flux density, the ETPA rate dominates and the observed absorption rate is demonstrated [24, 25, 27] as linear with input flux. From this, the TPA rate R_E is expressed as the summation of the linear ETPA rate and the quadratic, random TPA rate [24, 25, 27]:

$$R = \sigma_E \phi + \delta_R \phi^2 \qquad \text{(III.1)}$$

where σ_E is the ETPA cross-section, δ_R is the random TPA cross-section, and ϕ is the input photon flux density of photon pairs. The critical flux ϕ_{crit} is defined [24, 25] as the flux at which the linear and nonlinear absorption rates are equal. ϕ_{crit} is calculated as:

$$\phi_{crit} = \frac{\sigma_E}{\delta_R}. \tag{III.2}$$

Below ϕ_{crit}, the absorption of entangled photons is expected [24, 25] to dominate over random TPA, enabling a clear evaluation of the ETPA cross-section.

There exist two factors critical in an ETPA process – the entanglement time T_E, and the entanglement area A_E. The entanglement area is determined by the angular width of the fourth-order coherence function [24] and depends on the pump beam waist, the pump beam wavefront, and the crystal length. It has been shown that the entanglement area can be increased by decreasing the interaction length of the SPDC process, as well as by decreasing the spot size through focusing [38]. The entanglement area is related [24, 25, 27] to the entangled and random two-photon absorption cross-sections, and the entanglement time by:

$$A_E = \frac{\delta_R}{2\sigma_E T_E} \tag{III.3}$$

where the entanglement time, T_E, is equivalent to the difference between the transit times of the correlated photon pair through the nonlinear crystal [39].

An interference filter was employed to obtain a SPDC pump wavelength of 800 nm for these entangled two-photon absorption experiments. Entangled two-photon absorption was observed in all generations of dendrimer investigated in this work. Shown in Figure III.6 is the plot of normalized absorbed photon rate against input photon flux for the **90T**

dendrimer prepared in solution and in thin film. Both linear and quadratic character is observed, which, from equation III.1, is due to ETPA and random TPA, respectively. From these plots, it is shown that entangled two-photon absorption for these thiophene dendrimers is measurable with an input flux of 10^{12} photons/cm^2/s in both types of samples.

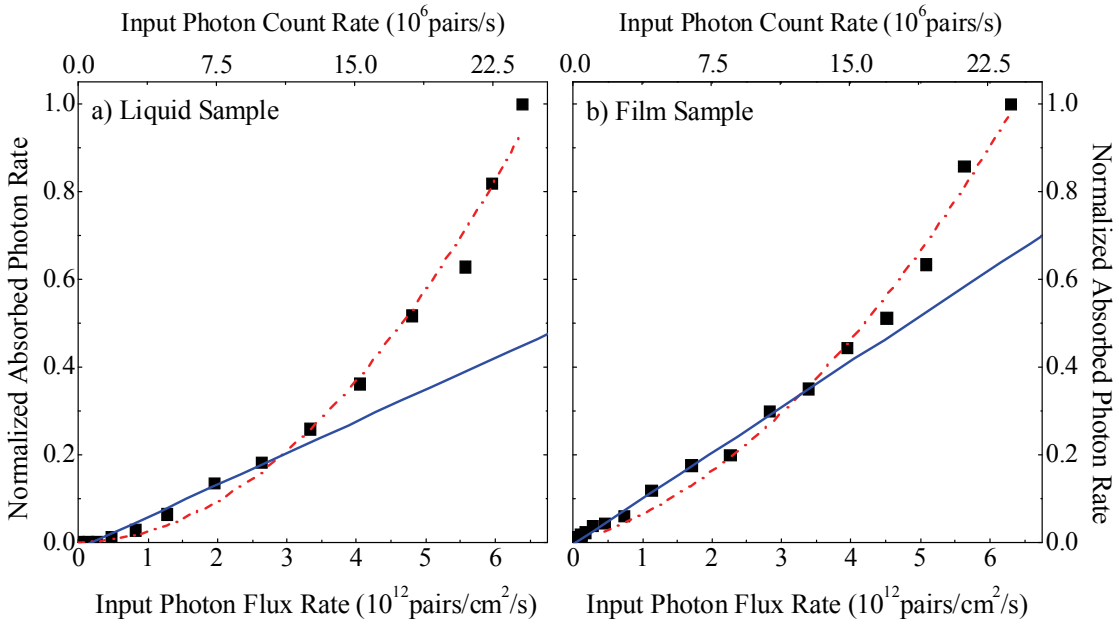

Figure III.6. Normalized absorbed photon rate for **90T** dendrimer / THF liquid samples (a) and **90T** dendrimer film sample (b) plotted against input flux (bottom axis) and photon count rate (top axis). The linear component of the absorbed photon rate is shown with a solid blue line, while the quadratic component is shown with a dashed red line.

ETPA cross-sections were extracted from the linear component of the absorption and are summarized in Table III.2. These ETPA cross-sections are on the order of 10^{-18} cm^2/molecule for liquid samples, and 10^{-17} cm^2 molecule^{-1} for film samples. The ETPA cross-sections are nearly on the order of single-photon absorption cross-sections of these dendrimers. The magnitude of these ETPA cross-sections compares well to that obtained from ETPA experiments performed [27] on porphyrin dendrimers. A linear dependence of ETPA cross-section on generation is observed in these thiophene dendrimers, as seen

in other reports of thiophene macrocycles [33, 35] and *dendrons* [20]. From this, ETPA experiments are found to be sensitive to the cooperative interaction of the thiophene units within the dendrimers. For a given film sample, σ_E is 5-25 times that of the corresponding liquid sample is obtained. It is found that the ratio $\sigma_{E,film}/\sigma_{E,liquid}$ decreases exponentially with the number of thiophenes in the dendrimer. The number density of the dendrimer films was on the order of 10^{20} molecules/cm^3, one or two orders of magnitude greater than that of equivalent liquid samples, so there may be a greater degree of inter-molecular coupling in the thin film sample than in the liquid sample.

Dendrimer # Thiophenes	Entangled TPA cross-section (σ_E)			
	Absolute (cm^2 $molecule^{-1}$)		Relative to 90T	
	Liquid x 10^{-18}	Film x 10^{-17}	Liquid	Film
6	0.13	0.33	0.10	0.22
18	0.71	0.98	0.26	0.32
42	2.6	2.0	0.67	0.74
90	5.9	3.7	1.0	1.0

Table III.2. Entangled two-photon absorption (ETPA) cross-sections

A higher-order nonlinear absorption (HoNLA) cross-section on the order of 10^{-30} cm^4 s photon^{-1} (10^{20} GM) was determined from the quadratic component of the absorbed photon rate. Although the possibility of random TPA is suggested by equation III.1, the incredible difference in order of magnitude between this HoNLA cross-section and the rTPA cross-section obtained from TPEF experiments makes the underlying cause of this higher-order nonlinear absorption uncertain. The HoNLA cross-section is found to increase with dendrimer generation, while being independent of sample type. The dependence of the HoNLA cross-sections on the number of thiophene units is found to be

nearly identical to that observed in TPEF and ETPA cross-sections. While this HoNLA cross-section has not been proven in this study to be a result of random TPA of these thiophene dendrimers, the HoNLA cross-section follows the same trend as that of ETPA cross-sections, as well as that of random TPA from TPEF experiments. Based on this result, it is suggested that this nonlinear absorption is due to non-entangled, but correlated, photons generated by the SPDC process.

The entanglement time was calculated from the difference in transit times between signal and idler photons produced by the down-conversion crystal [40]. In this experimental setup, T_E is determined to be 96 fs. Using this entanglement time and the results from the ETPA measurements, an entanglement area was calculated from equation III.3. Entanglement areas of 4 cm^2 for liquid samples and 0.6 cm^2 for film samples are obtained, and A_E does not appear to vary by dendrimer generation within a given sample type. Several factors may contribute to these macroscopic results for A_E. First, under focused pumping conditions, the divergence of the pump beam used for SPDC contributes to the uncertainty in the entanglement area. As this experiment relies on a mode-locked source rather than a continuous wave source, creation of correlated photons is expected [41] to be localized rather than random, which may contribute to a further increase in entanglement area over that calculated based on continuous wave sources [24]. A larger entanglement area is observed in thiophene dendrimers than in previous experimental investigations [27] of porphyrin dendrimers, in which an A_E on the order of 10^{-2} cm^2 was observed. In the case of thiophene dendrimers, which are known to be space-filling structures [28, 29], there may be additional effects from the cooperative interaction between the thiophene units. Previous results for thiophene *dendrons* have

shown [20] that excitation is delocalized across the entire dendrimer. A_E is known [24] to have implications in the critical flux ϕ_{crit}. Using equations III.2 and III.3, it is found that ϕ_{crit} is inversely proportional to A_E, suggesting that a large A_E allows evaluation of both entangled and random two-photon absorption at low input flux. While the ETPA cross-section is also shown [24] to be inversely proportional to A_E, the negative effect of a large entanglement area on σ_E can be compensated for by decreasing the entanglement time T_E by addition of quartz plates to decrease the delay between signal and idler photons.

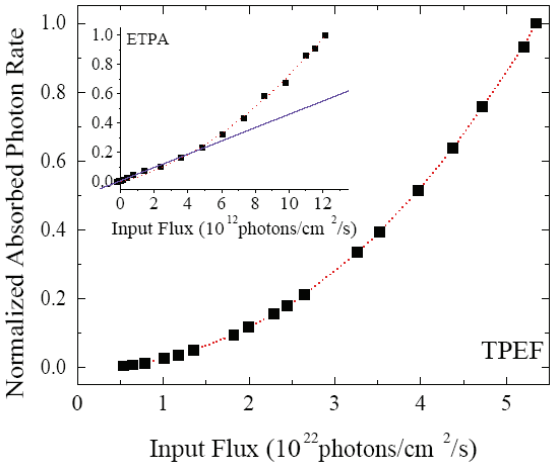

Figure III.7. Normalized absorbed photon rate for **42T** liquid samples plotted against input flux rate for ETPA experiments (squares, inset) and traditional TPEF experiments (squares). Solid blue and dashed red lines denote fits of the data to linear and quadratic functions, respectively. Note that the TPEF horizontal axis has units 10^{22} photons/cm^2/s, while inset ETPA horizontal axis has units of 10^{12} photons/cm^2/s.

For comparison to traditional methods, the absorption rates of **42T** liquid samples against the input flux density for both TPEF and ETPA experiments are plotted in Figure III.7. Results from traditional TPEF experiments are shown to be perfectly quadratic. Both linear and quadratic terms, suggesting entangled and random TPA, respectively, are observed in ETPA results. From this, the nonlinear two-photon absorption of these thiophene dendrimers can be detected through ETPA measurements using ten orders of

magnitude fewer photons than that necessary for TPEF measurements. The ability to evaluate the nonlinear absorption of a material using a very low flux of photons is desired for imaging applications involving biological materials.

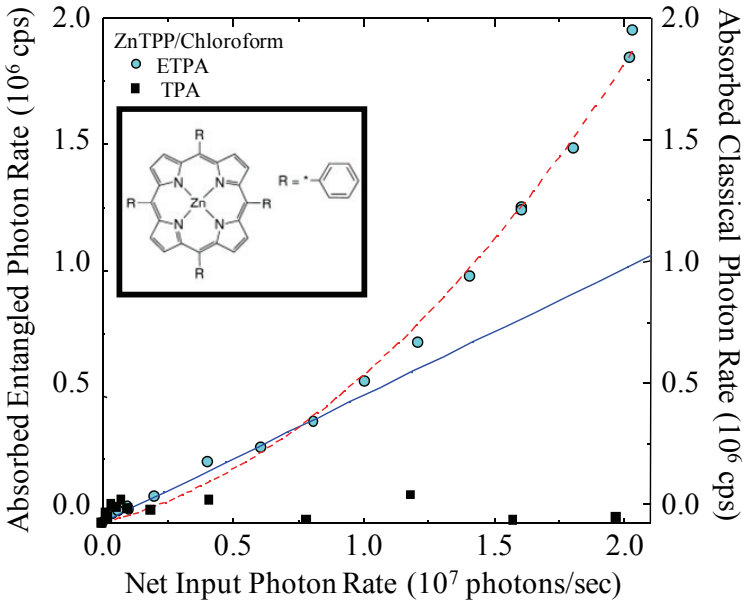

Figure III.8. Comparison of classical and entangled two-photon absorption characteristics measured at very low flux of excitation photons. Absorbed photon rate is plotted against net excitation photon rate for both ETPA (round symbols, left axis) and classical TPA (square symbols, right axis) measurements performed on a ZnTPP chromophore (inset) solution. Classical TPA measurements were carried out in the same transmission configuration as ETPA experiments, with the coherent output of the Spectra-Physics MAITAI® laser system used directly as the excitation source, after being heavily attenuated to obtain an excitation photon flux that is comparable to that utilized in ETPA measurements. The best fit to a second order polynomial (dashed red line), and the extracted linear contribution (solid blue line) are shown for the ETPA response. No discernable classical TPA response was observed.

In order to verify the 10-order of magnitude enhancement that is observed in ETPA measurements compared to results obtained by classical TPA methods (TPEF), we have compared the ETPA and classical TPA response of a 3rd generation ZnTPP dendrimer in a control experiment that utilizes both entangled and classical photons as the excitation source in the low-flux regime. The results of these measurements are presented in Fig.

III.8. The ZnTPP material was chosen for its structural similarity to the H_2TPP dendrimer system that had previously been shown to exhibit good ETPA and classical TPA response [27], and to further generalize the enhancement presented in Fig. III.7 to materials that are dissimilar to any of the oligothiophene systems studied in this chapter. ETPA response experiments were carried out with the same methodology that was discussed earlier in this chapter. Classical TPA measurements were carried out using the fundamental coherent output of the Spectra-Physics MAITAI® ultrafast laser system, which was heavily attenuated to achieve a classical excitation flux of photons that is comparable to those utilized in our ETPA experiments. The attenuated classical excitation beam path was matched to that of the entangled excitation, and absorption measurements were again performed in the transmission regime, using the same sample telescope and detection scheme that is utilized for ETPA measurements. As can be seen clearly in Fig. III.8, the ZnTPP material exhibits the expected linear- and quadratic-dependencies on excitation flux under entangled photon-pair excitation, while no discernable absorption characteristics were observed for the classical excitation at these low flux ranges.

Two-photon absorption cross-sections of the dendrimers, relative to that of **90T**, are plotted in Figure III.9 against the number of thiophene units. The relative ETPA cross-sections obtained for dendrimer samples are found to match the trends obtained by TPEF measurements on dendrimers presented in this chapter, as well as previously published TPEF results for thiophene dendrons [20]. The fact that random TPA trends have been reproduced with ETPA measurements gives additional confidence in the ETPA method. From the results presented in Fig. III.9, it is shown that nonlinear absorption, and more

importantly, trends in nonlinear absorption cross-section, can be observed by entangled photon pairs using ten orders of magnitude fewer photons than are required by traditional methods.

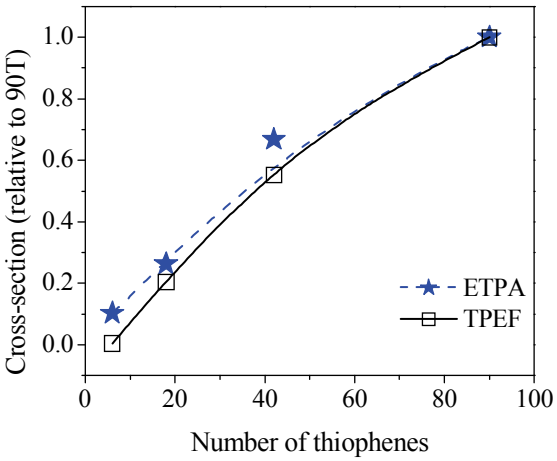

Figure III.9. ETPA (stars) and rTPA (open squares) cross-sections relative to those of 90T for dendrimer liquid samples. rTPA cross-sections are obtained from traditional TPEF experiments.

III.4. Conclusions

Thiophene dendrimers systematically explored in this work are demonstrated to be effective sensors for entangled photons at very low flux, which has applications in imaging of biological systems, remote sensing, and quantum optical applications. A linear dependence on input flux, which is a signature of entangled two-photon absorption, is observed in ETPA measurements for all thiophene dendrimers in this study. ETPA effects are observed regardless of whether the sample is prepared as a thin film or liquid. ETPA cross-sections of these dendrimers are measured to be on the order of 10^{-19}-10^{-17} cm^2, only one or two orders of magnitude smaller than their linear optical absorption cross-sections. The ETPA cross-sections are found to be an order of magnitude greater in the thin film samples than in the liquid samples, suggesting that the dendrimer thin films exhibit better performance than dendrimer solutions as detectors for entangled photons.

This enhancement due to sample medium is found to be most pronounced in the lower generation dendrimers, where concentration and number density are the highest. Despite differences in the sample medium, nearly identical nonlinear absorption cross-section dependence on the number of the thiophene units in the dendrimer is obtained. Trends in nonlinear absorption cross-section measured by ETPA are found to match those measured by TPEF experiments, despite the fact that ten orders of magnitude *fewer* photons are used in the ETPA measurements. The ability to measure nonlinear optical properties of materials with a very low flux of photons has extraordinary implications in nonlinear spectroscopy and quantum optical applications.

III.5. References

1. Giebeler, C.; Antoniadis, H.; Bradley, D. D. C.; Shirota, Y. *J. Appl. Phys.* **1999**, *85*, 608-615.
2. Halim, M.; Samuel, I. D. W.; Pillow, J. N. G.; Monkman, A. P.; Burn, P. L. *Synth. Met.* **1999**, *102*, 1571-1574.
3. Wang, P. W.; Liu, Y. J.; Devadoss, C.; Bharathi, P.; Moore, J. S. *Adv. Mater.* **1996**, *8*, 237-241.
4. Burn, P. L.; Lo, S. C.; Samuel, I. D. W. *Adv. Mater.* **2007**, *19*, 1675-1688.
5. Kwon, T. W.; Alam, M. M.; Jenekhe, S. A. *Chem. Mater.* **2004**, *16*, 4657-4666.
6. Hagfeldt, A.; Gratzel, M. *Acc. Chem. Res.* **2000**, *33*, 269-277.
7. Adronov, A.; Frechet, J. M. J. *Chem. Commun.* **2000**, 1701-1710.
8. Balzani, V.; Campagna, S.; Denti, G.; Juris, A.; Serroni, S.; Venturi, M. *Acc. Chem. Res.* **1998**, *31*, 26-34.
9. Gust, D.; Moore, T. A.; Moore, A. L. *Acc. Chem. Res.* **2001**, *34*, 40-48.
10. Gilat, S. L.; Adronov, A.; Frechet, J. M. J. *Angew. Chem. Int. Ed.* **1999**, *38*, 1422-1427.
11. Prathapan, S.; Johnson, T. E.; Lindsey, J. S. *J. Am. Chem. Soc.* **1993**, *115*, 7519-7520.

12. Andrews, D. L.; Bradshaw, D. S. *J. Chem. Phys.* **2004**, *121*, 2445-2454.

13. Hoeben, F. J. M.; Jonkheijm, P.; Meijer, E. W.; Schenning, A. *Chem. Rev.* **2005**, *105*, 1491-1546.

14. Cifuentes, M. P.; Powell, C. E.; Morrall, J. P.; McDonagh, A. M.; Lucas, N. T.; Humphrey, M. G.; Samoc, M.; Houbrechts, S.; Asselberghs, I.; Clays, K.; Persoons, A.; Isoshima, T. *J. Am. Chem. Soc.* **2006**, *128*, 10819-10832.

15. Kaino, T. *J. Opt. A* **2000**, *2*, R1-R7.

16. Ledoux, I.; Zyss, J. *Int. J. Nonlin. Opt. Phys.* **1994**, *3*, 287-316.

17. Tatsuura, S.; Matsubara, T.; Tian, M. Q.; Mitsu, H.; Iwasa, I.; Sato, Y.; Furuki, M. *Appl. Phys. Lett.* **2004**, *85*, 540-542.

18. Wada, O. *New J. Phys.* **2004**, *6*.

19. Devadoss, C.; Bharathi, P.; Moore, J. S. *J. Am. Chem. Soc.* **1996**, *118*, 9635-9644.

20. Ramakrishna, G.; Bhaskar, A.; Bauerle, P.; Goodson, T. *J. Phys. Chem. A* **2008**, *112*, 2018-2026.

21. Kopelman, R.; Shortreed, M.; Shi, Z. Y.; Tan, W. H.; Xu, Z. F.; Moore, J. S.; BarHaim, A.; Klafter, J. *Phys. Rev. Lett.* **1997**, *78*, 1239-1242.

22. Xu, C.; Webb, W. W. *J. Opt. Soc. Am. B-Opt. Phys.* **1996**, *13*, 481-491.

23. Javanainen, J.; Gould, P. L. *Phys. Rev. A: At. Mol. Opt. Phys.* **1990**, *41*, 5088-5091.

24. Fei, H. B.; Jost, B. M.; Popescu, S.; Saleh, B. E. A.; Teich, M. C. *Phys. Rev. Lett.* **1997**, *78*, 1679-1682.

25. Lissandrin, F.; Saleh, B. E. A.; Sergienko, A. V.; Teich, M. C. *Phys. Rev. B: Condens. Matter* **2004**, *69*.

26. Agarwal, A.; Chung, S.; Balkan, N.; Hill, G. *J. Appl. Phys.* **2007**, *101*.

27. Lee, D. I.; Goodson, T. *J. Phys. Chem. B* **2006**, *110*, 25582-25585.

28. Ma, C. Q.; Mena-Osteritz, E.; Debaerdemaeker, T.; Wienk, M. M.; Janssen, R. A. J.; Bäuerle, P. *Angew. Chem. Int. Ed.* **2007**, *46*, 1679-1683.

29. Ma, C. Q.; Wunderlin, M.; Mena-Osteritz, E.; Bäuerle, P. *Chem. Eur. J., submitted* **2008**.

30. Bäuerle, P.; Fischer, T.; Bidlingmeier, B.; Stabel, A.; Rabe, J. P. *Angew. Chem. Int. Ed. Engl.* **1995**, *34*, 303-307.

31. Maciejewski, A.; Steer, R. P. *J. Photochem.* **1986**, *35*, 59-69.

32. Ramakrishna, G.; Harpham, M. R.; Suzer, O.; Ma, C. Q.; Bauerle, P.; Goodson, T. *to be published* **2010**.

33. Bhaskar, A.; Ramakrishna, G.; Hagedorn, K.; Varnavski, O.; Mena-Osteritz, E.; Bauerle, P.; Goodson, T. *J. Phys. Chem. B* **2007**, *111*, 946-954.

34. Varnavski, O.; Yan, X. Z.; Mongin, O.; Blanchard-Desce, M.; Goodson, T. *J. Phys. Chem. C* **2007**, *111*, 149-162.

35. Williams-Harry, M.; Bhaskar, A.; Rarnakrishna, G.; Goodson, T.; Imamura, M.; Mawatari, A.; Nakao, K.; Enozawa, H.; Nishinaga, T.; Iyoda, M. *J. Am. Chem. Soc.* **2008**, *130*, 3252-3253.

36. Geabanacloche, J. *Phys. Rev. Lett.* **1989**, *62*, 1603-1606.

37. Mollow, B. R. *Phys. Rev.* **1968**, *175*, 1555-1563.

38. Joobeur, A.; Saleh, B. E. A.; Larchuk, T. S.; Teich, M. C. *Phys. Rev. A: At. Mol. Opt. Phys.* **1996**, *53*, 4360-4371.

39. Sergienko, A. V.; Shih, Y. H.; Rubin, M. H. *J. Opt. Soc. Am. B-Opt. Phys.* **1995**, *12*, 859-862.

40. Rubin, M. H.; Klyshko, D. N.; Shih, Y. H.; Sergienko, A. V. *Phys. Rev. A: At. Mol. Opt. Phys.* **1994**, *50*, 5122-5133.

41. Kim, Y. H.; Chekhova, M. V.; Kulik, S. P.; Rubin, M. H.; Shih, Y. H. *Phys. Rev. A* **2001**, *6306*.

CHAPTER IV

Spatial Control of ETPA with Organic Chromophores[*]

Abstract

Entangled photons generated by spontaneous parametric down-conversion (SPDC) are used to investigate entangled two-photon absorption (ETPA) in multi-annulene systems. ETPA characteristics are shown to depend on the spatial orientation of the SPDC emission pattern. The expected dependence of absorption rate on input flux is seen for emission patterns which exhibit spatial indistinguishability between the signal and idler photons, while no absorption is observed for a spatially distinguishable emission pattern. The amount of absorption of entangled photons is also seen to depend on the degree of overlap of the entangled photons for the indistinguishable conditions. A tunability of the entangled photon absorption can thus be achieved by utilizing the spatial characteristics of the entangled photon pairs.

[*] The work presented in this chapter has been published as a peer-reviewed journal article with the citation Alica Guzman, Michael R. Harpham, Özgün Süzer, Michael M. Haley, and Theodore Goodson III, Journal of the American Chemical Society **132**, 7840-7841 (2010).

IV.1. Introduction

Organic conjugated nonlinear optical (NLO) macromolecules have been used in a variety of important optical applications [1]. One relatively unexplored area for organic NLO materials is the absorption and detection of entangled photons generated by spontaneous parametric down-conversion (SPDC). Entangled two-photon absorption (ETPA) in real materials may be very useful for applications in quantum sensing and communication, as well as new methods of spectroscopy at extremely low input photon flux [2, 3]. ETPA has been successfully performed for a variety of organic two-photon absorbing materials with a very small number of photons [4, 5]. However, there have not been any reports of the control of the ETPA process through different quantum entangled states of the photons. The SPDC in BBO crystals results in signal and idler daughter photons governed by the so-called phase-matching conditions of $\omega_p = \omega_s + \omega_i$ and $k_p = k_s + k_i$, where subscripts p, s, i denote pump, signal, and idler photons, respectively. Phase-matching also dictates the spatio-temporal characteristics of the SPDC emission [7]. Three distinct spatial orientations of the resulting emission pattern are found and in this chapter it is shown that these patterns also allow a method to either enhance or limit the degree of entangled photon absorption in an organic material. The particular mechanism and cause for varying amounts of ETPA is also discussed in reference to controlling the entangled photon absorption process.

IV.2. Results and Discussion

Figure IV.1 shows the structures of the two-photon absorbing macromolecules used in this investigation [8]. The bis-annulene system and similar structures have shown very

impressive two-photon absorption (TPA) cross-sections with classical photons [9, 10]. Our investigation shows an unprecedented enhancement due to delocalized excitons for the tri- and tetra-annulene systems (see Table IV.1).

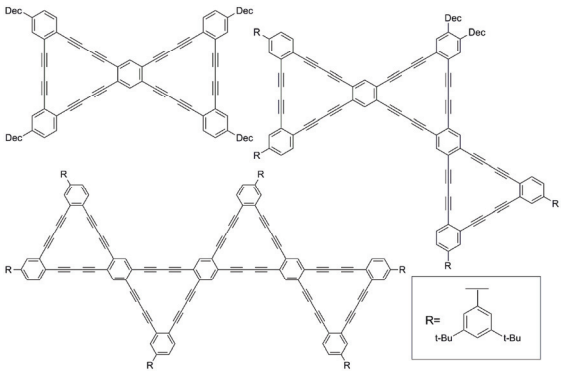

Figure IV.1. Annulene systems: bis[18]annulene (top left), tri[18]annulene (top right), and "linear" tetra[18]annulene (bottom).

Measurement of classical TPA cross-sections follows that of references 9, 10, and is detailed in the Supporting Information section.

sample	TPA δ (GM)	phase-matching condition	ETPA σ ($\times 10^{-17}$ cm^2)
bis-annulene	150	non-collinear	3.2
		collinear	3.0
		separated	0
tri-annulene	1650	non-collinear	8.1
		collinear	2.4
		separated	0
tetra-annulene	2960	non-collinear	9.9
		collinear	6.7
		separated	0

Table IV.1. Two-photon and entangled two-photon cross-sections of annulene systems. Cross-sections are calculated at 800nm excitation wavelength. 1 GM = 1×10^{-50} cm^4 s photon^{-1}.

ETPA is a process involving entangled photon pairs which populate excited (or virtual) states of a molecule with a finite interaction time (entanglement time) and area (entanglement area). Shown in Table IV.1 is the entangled photon absorption cross-section for the annulene materials, tabulated for different phase-matching conditions. A

description of the experimental setup for ETPA can be found in the Supporting Information section [4, 5]. These cross-sections are calculated utilizing a simplified theory for ETPA [11]. The total absorption rate is expressed as [11]

$$R = \sigma_e \varphi + \delta_r \varphi^2 \tag{IV.1}$$

where σ_e denotes ETPA cross-section, giving a linear dependence on input photon flux, and δ denotes classical (or random) TPA cross-section, giving a quadratic dependence on input flux.

We have found a way to control the ETPA process through use of the phase-matching conditions from SPDC. Shown in Figure IV.2 are three images obtained from the different controlled phase-matching conditions. Images of the SPDC spatial profile were obtained with an intensified ICCD camera (PI-MAX2: 1003), which has 27.5% quantum efficiency at 800 nm. The ICCD was positioned after the sample telescope and before the NPBS, with no sample in place. The images confirm the phase-matching condition (non-collinear, collinear, or spatially separated) under which the SPDC process occurs, and also confirm that the entire profile is being collected without clipping of the pattern. The resulting signal and idler fluxes propagate as a pair of polychromatic cones, from which frequency selection yields a pair of rings in the transverse plane, whose angular distribution depends on the angle of the crystal optical axis relative to the pump beam. The three distinct spatial orientations of the rings are: non-collinear, in which the rings overlap in two areas; collinear, in which the rings are tangential, or overlap in one area; and spatially separated, in which there is no spatial overlap. In type-II SPDC, the signal and idler fluxes also carry orthogonal polarizations, making it useful for observation of polarization entanglement [12].

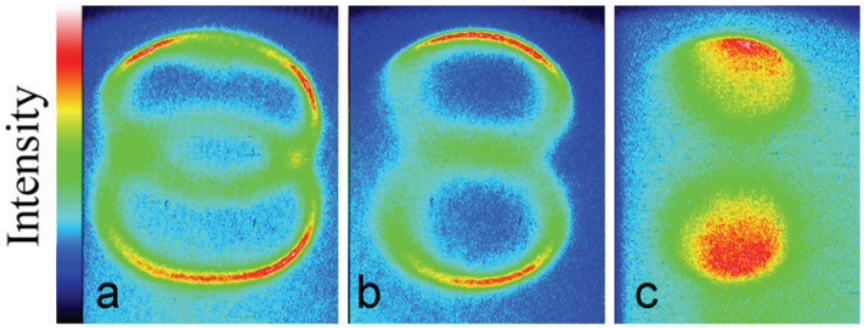

Figure IV.2. SPDC spatial profiles for (a) non-collinear, (b) collinear, and (c) spatially separated phase-matching conditions.

We have carried out ETPA experiments with all three phase-matching conditions for these novel, highly nonlinear two-photon materials. The ETPA collection data are shown in Figure IV.3, grouped by phase-matching condition. From the ETPA cross-sections in Table IV.1, a downward trend is observed when going from non-collinear, to collinear, to spatially separated phase-matching condition. In addition, ETPA data for the spatially separated condition show no significant absorption for any of the samples.

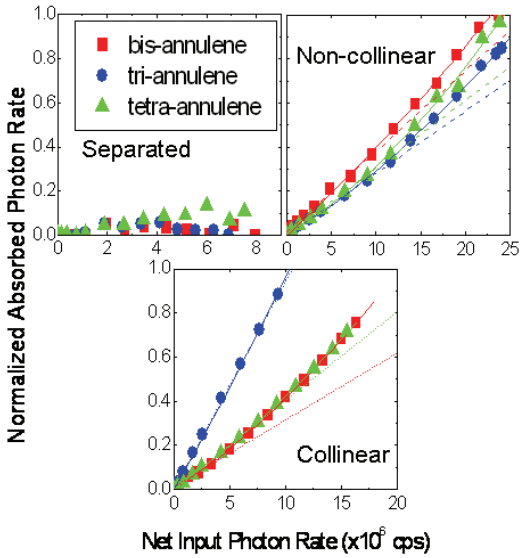

Figure IV.3. Results from ETPA measurements grouped by phase-matching condition: spatially separated (top left), collinear (top right), non-collinear (bottom). The normalized absorption rates are plotted against the input photon rate. The dashed lines show the linear fits and solid curves show quadratic fits.

The dependence of ETPA cross-section on the entanglement area, A_e, and entanglement time, T_e, were investigated as a cause for the variation in absorption characteristics between the phase-matching conditions. The temporal- and spatial-widths of the fourth order coherence function, given by T_e and A_e, affect the ETPA cross-section according to the expression [2]:

$$\sigma_e\left(T_e,\tau\right)=\frac{\pi\omega_p^2}{16A_eT_e}\delta\left(\varepsilon_f-\varepsilon_i-\omega_p\right)s\left(T_e,\tau\right) \tag{IV.2}$$

under degenerate pumping, where

$$s\left(T_e,\tau\right)=\left|\sum_j\frac{D_j}{\Delta_j}\left\{2-\exp\left[-i\Delta_j\left(T_e-\tau\right)\right]-\exp\left[-i\Delta_j\left(T_e+\tau\right)\right]\right\}\right|^2 \tag{IV.3}$$

for signal-idler path delay τ, pump frequency ω_p, energy mismatch Δ_j and transition matrix elements D_j. A_e has been shown to depend on the beam waist and is not expected to vary with phase-matching condition [13]. The difference in entanglement time between the different phase-matching conditions is 8×10^{-2} fs (see the Supporting Information section for calculation). This small change in T_e cannot account for the difference in ETPA characteristics between the spatially separated case and the other two conditions.

Visibility also offers no explanation for the absence of entangled photon absorption. There is no indication that visibility for the spatially separated condition should be drastically lower than for the collinear or noncollinear conditions. The spatially separated case (which showed no ETPA) has previously been shown to exhibit high visibility for SPDC [14]. Our polarization visibility measurements yielded a maximum visibility of 85% which did not vary significantly between the phase-matching conditions.

In attempts to determine the cause of the dissimilarity in absorption characteristics for the spatially separated condition, it was found that the polarization visibilities,

entanglement time, and entanglement area do not vary significantly with SPDC phase-matching condition. Instead, we suggest that "distinguishability" between the signal and idler fluxes is a significant difference which may give rise to the change in ETPA behavior with different phase-matching conditions. The entangled photons are said to be spatially indistinguishable in the regions of overlap of the signal and idler emission cones, where it is impossible to distinguish which photon is the idler and which the signal in the pair [15]. The non-collinear condition contains two regions of overlap, the collinear condition one region, and the spatially separated condition produces no spatial indistinguishability.

IV.3. Supporting Information

IV.3.1. Materials

The annulene molecules were synthesized by intramolecular macrocyclization of α,ω-polyyne precursors via oxidative homocoupling [8]. Liquid samples were prepared with tetrahydrofuran (THF, Sigma-Aldrich, 99.9% purity) as the solvent. Thin film samples were prepared with poly(ethyl methacrylate-*co*-methyl acrylate) (PEMA-co-MA, Aldrich, $M_w \approx 10^6$ g/mol) in chloroform and were drop-cast onto a glass substrate. The drop-cast films were heated overnight in a vacuum oven at 313 K evacuated to a pressure difference of 20 inHg. A Dektak surface analyzer was used to assess film thickness and uniformity. Steady-state absorption and fluorescence emission spectra were obtained using an Agilent 8453 UV-Visible Spectrophotometer and a Jobin Yvon - SPEX Fluoromax-2 spectrometer and were found to match previous results [8, 16]. The spectra are shown in Figure IV.4.

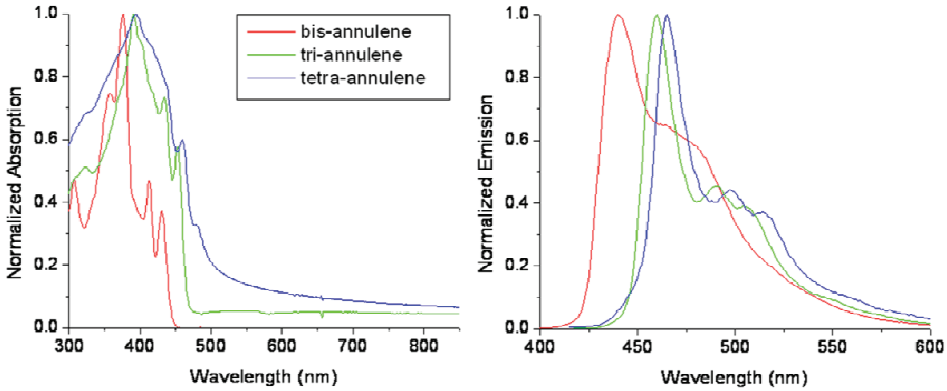

Figure IV.4. Steady-state absorption (left) and emission (right) spectra for annulene molecules.

The one-photon cross-section at 800 nm of the annulene samples have been estimated from the UV-Vis absorption measurements to be on the order of 10^{-19} cm^2. This is a full two orders of magnitude smaller than the entangled two-photon cross-sections at the same wavelength. Furthermore, absorption experiments that exactly follow the methodology of our ETPA measurements have been performed where classical fundamental light from our laser source was utilized as the excitation instead of the entangled SPDC source. In these measurements, the laser source was heavily attenuated such that the flux of classical photons will match the entangled photon flux in our ETPA measurements. At such low excitation flux, no absorption of the classical photons by the samples was observed. Based on this evidence, we are confident that the linear portions of our submitted ETPA plots can predominantly be attributed to the entangled photon contribution.

IV.3.2. Two-Photon Excited Fluorescence

Random two-photon absorption cross-sections, δ_R, for liquid samples were determined by the two-photon excited fluorescence (TPEF) method [17]. We have investigated a number of multi-chromophore systems with enhanced cross-sections due to

strong intra-molecular coupling [9, 18-20]. In the present investigation, cross-sections were determined for excitation wavelengths in the range 770-830 nm using a mode-locked Ti:Sapphire laser (KMLabs mini Ti:Sapphire, pulse width < 30 fs, 80 MHz repetition rate).

The excitation beam is passed through a circular aperture to ensure a circular beam, and the intensity is controlled through the use of a neutral-density filter wheel placed after this aperture. The beam is then focused onto the sample cell (quartz cuvette, 0.5 cm path length). The fluorescence is collected at an angle perpendicular to the excitation beam. This fluorescence passes through a circular aperture and a collection lens, which directs it into a monochromator (Cornerstone 130^{TM}, Oriel Instruments). The monochromator output is coupled to a photomultiplier tube, and photons are converted into counts by a photon counting unit (M8485 counting board, C3866 counting circuit). The fluorescence intensity is monitored as the excitation intensity is varied. The cross section is calculated from the equation for the TPEF signal, *F(t)*:

$$F(t) = \frac{1}{2}\eta\delta cn\frac{g_p}{\pi\lambda f\tau}\phi\langle P(t)\rangle^2, \qquad \text{(IV.4)}$$

where η is the fluorescence quantum yield, δ denotes TPA cross section, c is the concentration of chromophore, n is the refractive index of solvent, g_p is a shape factor (0.664 for a Gaussian pulse), λ denotes wavelength, f is the frequency of pulses from the laser source, τ is pulse duration, ϕ is collection efficiency, and $\langle P(t)\rangle$ denotes the average input intensity of excitation.

The terms $\frac{g_p}{\pi\lambda f\tau}$ are all known laser parameters. The terms $\frac{1}{2}\eta\delta cn$ are all related to the sample. The collection efficiency, which is related to the optical setup, is determined from a standard. In this case, the standard was a solution of 10^{-4} M Coumarin 307 in methanol. Taking the logarithm of each side of the above equation gives:

$$\log(F(t)) = 2\log\langle P(t)\rangle + \log\left(\frac{1}{2}\eta\delta cn\frac{g_p}{\pi\lambda f\tau}\phi\right) \quad \text{(IV.5)}$$

Thus, a log-log plot of fluorescence intensity versus input intensity is linear with a slope of two and an intercept equal to $\log\left(\frac{1}{2}\eta\delta cn\frac{g_p}{\pi\lambda f\tau}\phi\right)$. Since all of these terms except ϕ are known for the standard, the collection efficiency may be calculated. The TPA cross section can then be calculated for the sample using this collection efficiency.

IV.3.3. Optical Configuration

The experimental setup (Figure IV.5) is pumped by a mode-locked Ti:Sapphire laser (Spectra-Physics MaiTai®, pulse width < 100 fs, 80 MHz repetition rate) with emission centered at 800 nm with 12 nm bandwidth. References for input power are monitored by photodetectors (PD). The 800nm output is frequency doubled in a 1-mm thick β-barium borate crystal (BBO I) cut for type-I configuration. Residual fundamental light is discarded by a dichroic mirror (DM) and Brewster-angled prism followed by a blue filter (BF) to minimize background intensity. The second-harmonic is passed through a 0.5-mm thick BBO crystal (BBO II) cut for type-II SPDC with an angle φ=42° relative to the pump direction. The phase-matching condition under which the SPDC process occurs is selected by changing the angle of the BBO II crystal with respect to the central pump

direction. A dichroic mirror is used to remove the remaining fundamental and near-degenerate entangled photon pairs are selected via an interference filter (IF) with 25-nm bandwidth centered at 800 nm.

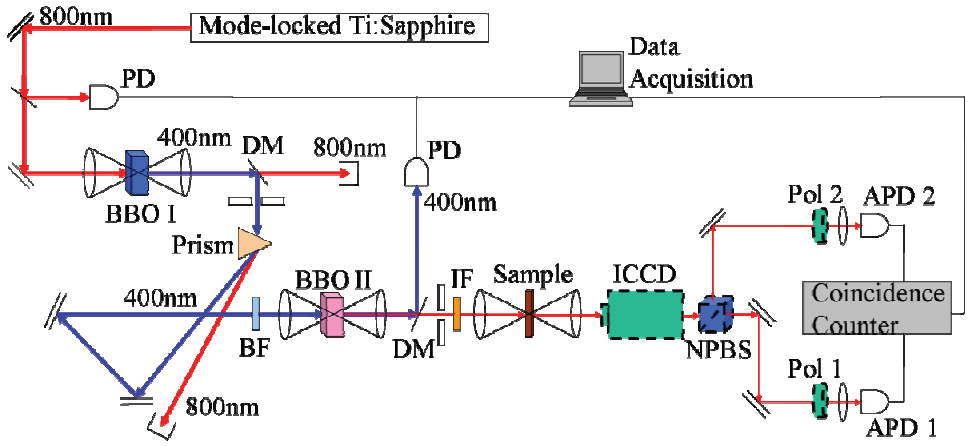

Figure IV.5. Experimental setup. Dichroic mirrors (DM) separate SHG from fundamental and entangled photons from SHG. Entangled photons are detected by avalanche photodiode (APD) single photon counting modules. Power references are provided by photodetectors (PD). Spatial profile images are obtained with an intensified ICCD camera (ICCD). A 50/50 nonpolarizing beam splitter (NPBS) is removed (replaced) for ETPA (polarization visibility) measurements. For visibility measurements, two polarizers (Pol) are inserted into the optical paths of each APD.

Photon count rates are measured using silicon avalanche photodiode (APD) single-photon counting modules (Perkin-Elmer SPCM-AQR-13). Single-photon count rates are measured by using the APD detectors individually. Coincidence count rates are measured by directing the signal and idler to separate APDs using a 50/50 nonpolarizing beam splitter (NPBS) cube. Coincidence counting is accomplished by a fast coincidence counting module (Ortec NIM7400, 10 ns coincidence window) connected to the two APDs.

IV.3.4. Entangled Two-Photon Absorption

ETPA measurements are based on the transmission-difference method. The excitation photon flux is varied by attenuating the fundamental with a continuously variable neutral-density filter wheel. Film samples are centered in the focal plane of the sample telescope and are oriented perpendicular to the SPDC pump. A PEMA-co-MA film of comparable thickness to the sample films is placed in the sample holder and used as a blank to determine proper correction factors for background intensity and non-absorptive scattering in the film. The single count rates are measured as a function of pump power. The method for the ETPA experiments has been previously established [4, 5, 22].

IV.3.5. Polarization Visibility

Polarization visibility measurements to confirm entanglement quality are performed with a 50/50 non-polarizing beam splitter and two polarization analyzers (Pol) placed in the individual APD optical paths. Coincidence count-rates are recorded as a function of varying polarizer angle of Pol 2, while Pol 1 is fixed at 0° or 45° for H/V or A/D bases, respectively. Figure IV.6 shows the results of visibility measurements under H/V basis for the three phase-matching conditions.

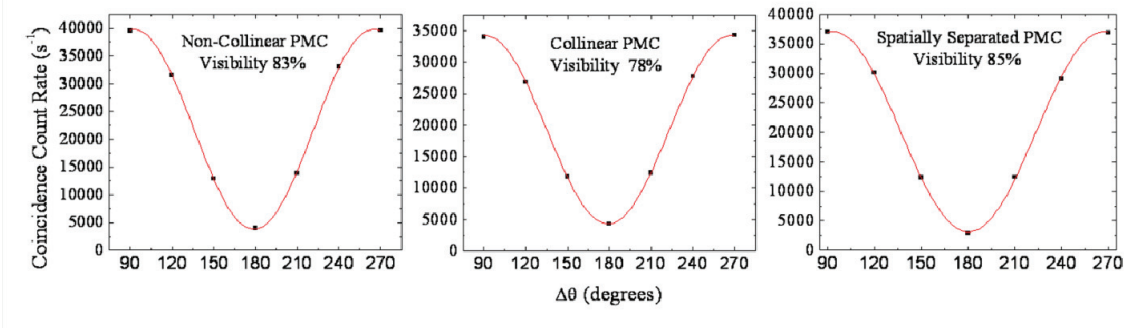

Figure IV.6. Visibility Measurements under H/V basis for non-collinear, collinear, and spatially separated phase-matching conditions.

IV.3.6. Calculation of Approximate Change in Entanglement Time

The travel time through the crystal is given by T_e = DL, where D is the inverse group velocity and L is the crystal length. Relating T_e to the difference in travel times for the signal and idler photons, the range of T_e for the three phase-matching conditions may be calculated from the change in effective crystal length. The latter is calculated from the crystal angles for the spatially separated and non-collinear cases (27 mrad and 25 mrad, respectively) and is approximately 0.4 μm. Using a typical value for D in BBO (0.2 ps/mm) [23], the range of T_e is calculated as approximately 8×10^{-2} fs.

IV.4. Conclusions

These ETPA experiments demonstrate a way to control the amount of absorption of entangled photons by changing the spatial orientation of the SPDC emission pattern. We have shown that the ETPA cross-section of organic conjugated molecules decreases as the overlap of the signal and idler photons decreases, with an absence of absorption in the case where there is no overlap. Such a tunable absorption has the possibility for utilization in applications such as quantum imaging, sensing and communication.

IV.5. References

1. a) Goodson, T. III; *Accts. of Chem. Res.* **2005**, *38*, 99. b) Goodson III, T.; *Annu. Rev. Phys. Chem.* **2005**, *56*, 581.
2. Saleh, B.E.A.; Jost, B.M.; Fei, H.-B.; Teich, M.C. *Phys. Rev. Lett.* **1998**, *80*, 3483.
3. Kojima, J.; Nguyen, Q.-V. *Chem. Phys. Lett.* **2004**, *396*, 323.
4. Lee, D.I.; Goodson, T. *J. Phys. Chem. B* **2006**, *110*, 25582.

5. Harpham, M.R.; Süzer, Ö.; Ma, C.-Q.; Bäuerle, P.; Goodson, T. *J. Am. Chem. Soc.* **2009**, *131*, 973.

6. Saleh, B.E.A.; Abouraddy, A.F.; Sergienko, A.V.; Teich, M.C. *Phys. Rev. A* **2000**, *62*, 043816.

7. Kiess, T.E.; Shih, Y.H.; Sergienko, A.V.; Alley, C.O. *Phys. Rev. Lett.* **1993**, *71*, 3893.

8. Marsden, J.A.; Haley, M.M. *J. Org. Chem.* **2005**, *70*, 10213.

9. Bhaskar, A.; Ramakrishna, G.; Haley, M.M.; Goodson III, T. *J. Am. Chem. Soc.* **2006**, *128*, 13972.

10. Anand, S.; Varnavski, O.; Marsden, J.A.; Haley, M.M.; Schlegel, H.B.; Goodson III, T. *J. Phys. Chem. A* **2006**, *110*, 1305.

11. Fei, H.-B.; Jost, B.M.; Popescu, S.; Saleh, B.E.A.; Teich, M.C. *Phys. Rev. Lett*. **1997**, *78*, 1679.

12. a) Kwiat, P.G.; Mattle, K.; Weinfurter, H.; Zeilinger, A.; Sergienko, A.V.; Shih, Y.H. *Phys. Rev. Lett.* **1995**, *75*, 4337. b) Ou, Z.Y.; Mandel, L. *Phys. Rev. Lett.* **1988**, *61*, 50. c) Hong, C.K.; Mandel, L. *Phys. Rev. A* **1985**, *31*, 2409.

13. Joobeur, A.; Saleh, B.E.A.; Larchuk, T.S.; Teich, M.C. *Phys. Rev. A* **1996**, *53*, 4360.

14. Niu, X.L.; Huang, Y.F. ; Xiang, G.Y.; Guo, G.C.; Ou, Z.Y. *Opt. Let.* **2008**, *33*, 968.

15. Bennink, R.S.; Liu, Y.; Earl, D.; Grice, W.P. *Phys. Rev. A* **2006**, *74*, 023802.

16. Wan, W.B.; Brand, S.C.; Pak, J.J.; Haley, M.M. *Chem. Eur. J.* **2006**, *6*, 2044.

17. Xu, C.; Webb, W.W.; *J. Opt. Soc. Am. B: Opt. Phys.* **1996**, *13*, 481.

18. Raymond, J.E.; Bhaskar, A.; Goodson, T. *J. Am. Chem. Soc.* **2008**, *130*, 17212.

19. Williams-Harry, M.; Bhaskar, A.; Ramakrishna, G.; Goodson, T.; Imamura, M.; Mawatari, A.; Nakao, K.; Enozawa, H.; Nishinaga, T.; Iyoda, M. *J. Am. Chem. Soc.* **2008**, *130*, 3252.

20. Ramakrishna, G.; Bhaskar, A.; Bauerle, P.; Goodson, T. *J. Phys. Chem. A* **2008**, *112*, 2018.

21. Bhaskar, A.; Ramakrishna, G.; Lu, Z.; Twieg, R.; Hales, J.M.; Hagan, D.J.; Van Stryland, E.; Goodson, T. *J. Am. Chem. Soc.* **2006**, *128*, 11840.

22. Süzer, Ö; Goodson, T. *Opt. Express* **2008**, *16*, 20166.

23. Rubin, M.H.; Kylshko, D.N.; Shih, Y.H.; Sergienko, A.V. *Phys. Rev. A* **1994**, *50*, 5122.

CHAPTER V

Virtual States, Entangled Photons, and Organic Nonlinear Optical Sensors*

Abstract

The use of entangled light for the purposes of spectroscopy as well as applications such as sensing, quantum microscopy, and quantum lithography has been of great interest in recent years. The entangled two-photon absorption (ETPA) cross-section of a set of nonlinear optical materials, with known, and large, classical two-photon absorption (TPA) cross-sections, but of differing geometry, donor-acceptor strength, and charge-transfer character, is evaluated in this work. Materials with classical TPA cross-sections attributed to virtual transitions involving an intermediate state are found to have measurable, and large, ETPA cross-sections. However, it is found that the materials whose (large) classical TPA cross-section is attributed to a dipole transition, without involvement of an intermediate state, are nearly transparent to entangled photons. From these results, it is shown that entangled photons are highly sensitive to the intermediate states of a nonlinear optical material. This result has great impact in applications involving quantum entanglement.

* The work presented in this chapter has been submitted for publication as a peer-reviewed journal article with the citation Michael R. Harpham, Özgün Süzer, Alica R. Guzman, Theodore Goodson III, Science (submitted, 2010).

V.1. Introduction

Recently, there has been great interest in the potential benefits of using entangled rather than classical photons for spectroscopy as well as for quantum microscopy and quantum lithography applications. Entangled light is known to possess numerous advantages over classical light. Entangled two-photon absorption (ETPA) is known [1-3] to show a large advantage in absorption efficiency over classical two-photon absorption (TPA); spectroscopy can be accomplished using 10^7 entangled photons/s, as compared to 10^{20} classical photons/s. ETPA is predicted [4, 5] to have a large enhancement in resolution over TPA.

Unlike classical TPA, which relies on sequential, and random, absorption of two photons, photon pairs generated by spontaneous parametric downconversion (SPDC) are used in entangled two-photon absorption experiments. Photon pairs created by SPDC are known [6, 7] to have a high degree of temporal and spatial correlation, manifested [8] in the temporal and spatial widths of the fourth-order coherence function, which are described by the entanglement time T_E and entanglement area A_E, respectively. The absorption rate of the material was shown [1, 2, 9, 10] to be linearly proportional to the input photon flux, as it depends on the probability of entangled photons generated within T_E and A_E arriving within the virtual state lifetime τ and one photon absorption cross-section σ.

Theoretical investigations of ETPA have been performed [11-13] on a number of relatively simple systems. Lissandrin et al. had conducted [12] investigations of the ETPA effect using sodium and K_2CsSb. The ETPA cross-sections of these materials were found to be on the order of 10^{-30} cm^2 and 10^{-25} cm^2, respectively. The discrepancy

between these results and earlier results for atomic hydrogen [11] had been explained by the fact that, in the former case, the transition was not in resonance with the entangled photons. Kojima and Nguyen had demonstrated [13] the possibility of virtual state spectroscopy in their investigation of an OH radical system. They had calculated the energy spectrum as a function of detuning energy, allowing determination of the transitions that contribute to the ETPA cross-section of the material.

The first experimental observation of ETPA was made using a porphyrin dendrimer [1], in which an ETPA cross-section of $\sim 10^{-17}$ cm^2 was obtained using $<10^7$ photons s^{-1}. We had estimated the virtual state energy of the dendrimer by assuming the functional form given by Fei et al. [11] Since then, we have conducted [2] a systematic investigation of both entangled and classical TPA cross-sections of a set of thiophene dendrimers. We have found that the ETPA and TPA cross-sections followed identical trends with increasing dendrimer generation, demonstrating that, using entangled photons, spectroscopy could be performed on real materials using ten orders of magnitude fewer photons than conventional TPA methods.

In the current work, we investigate the ETPA cross-sections of materials of varying architecture and donor-acceptor strength to further investigate the nature of the ETPA process. We find that certain materials do not absorb entangled photons, despite having large classical TPA cross-sections at the entangled photon wavelength. The common characteristic [14, 15] of the materials which do not exhibit ETPA is excited state charge transfer, in which the dominant absorption mechanism is a dipole transition which does not involve intermediate states of the material.

V.2. Results and Discussion

The entangled two-photon absorption rate, R_E, is derived [9] from time-dependent second-order perturbation theory in terms of the second-order correlation function [16]. In theory, the ETPA effect is accompanied by a non-entangled or random TPA effect [10]. The overall TPA rate R_E is thus expressed [1, 2, 11, 12] as the summation of the linear ETPA rate and the quadratic, random TPA rate:

$$R_E = \sigma_E \phi + \delta_R \phi^2 , \tag{V.1}$$

where σ_E is the ETPA cross-section, δ_R is the random TPA cross-section, and ϕ is the input photon flux density of photon pairs. The ETPA cross-section is reported to have dependence on the detuning energy between the entangled photon and the intermediate state, as well as on the intermediate state linewidth, and the transition matrix elements. For a system with ground, virtual, and excited state wavefunctions Ψ_i, Ψ_j, and Ψ_k, and under a simplified case of a monochromatic pump, Fei et al. [11] have shown that σ_E can be expanded as:

$$\sigma_e = \frac{2\pi}{\hbar^2 \varepsilon_0^2 c^2 A_e T_e} \omega_1^0 \omega_2^0 \delta(\varepsilon_f - \varepsilon_i - \omega_1^0 - \omega_2^0)$$
$$\times \left| \left\{ \sum_j D_{21}^{(j)} \frac{1 - \exp[-iT_e \Delta_1^{(j)} - T_e \kappa_j / 2]}{\Delta_1^{(j)} - i\kappa_j / 2} + D_{12}^{(j)} \frac{1 - \exp[-iT_e \Delta_2^{(j)} - T_e \kappa_j / 2]}{\Delta_2^{(j)} - i\kappa_j / 2} \right\} \right|^2 , \tag{V.2}$$

where A_E and T_E are entanglement area and entanglement time, respectively, ω_k^0 is the energy of the signal or idler photon, ε_i and ε_f are the energy of the initial and excited state, respectively, $D_{k,l}^{(j)}$ are the transition matrix elements, κ_j is the virtual state linewidth, and $\Delta_k^{(j)}$ is the detuning energy. The transition matrix element is defined as:

$$D_{k,l}^{(j)} = \langle \Psi_f | d_k | \Psi_j \rangle \langle \Psi_j | d_l | \Psi_i \rangle , \tag{V.3}$$

where d_k and d_l are the material electric-dipole moment components and $k,l = 1,2$ for signal and idler photons, with the detuning energy $\Delta_k^{(j)}$ is defined as:

$$\Delta_k^{(j)} = \varepsilon_j - \varepsilon_i - \omega_k^0 . \tag{V.4}$$

From Eq. (V.2), it can be expected that either a large detuning energy or small coupling to the intermediate states is undesirable for the purposes of ETPA.

We had shown [1] previously that a G3 porphyrin dendrimer was capable of absorbing entangled photons, and by varying the entanglement time T_E, we were able to evaluate the virtual state energy by assuming the functional form given in Eq. (V.2). This virtual state energy was found [1] to be approximately 2000 cm^{-1} below that of an 800 nm photon (12,500 cm^{-1}), which itself is ~2000 cm^{-1} below the ^1B_u Q_x state within the Q-band [17]. From quantum chemistry calculations performed [17] on the porphyrin H_2TPP, it is known that a two-photon transition through the ^1B_u Q_x state is parity allowed, supporting

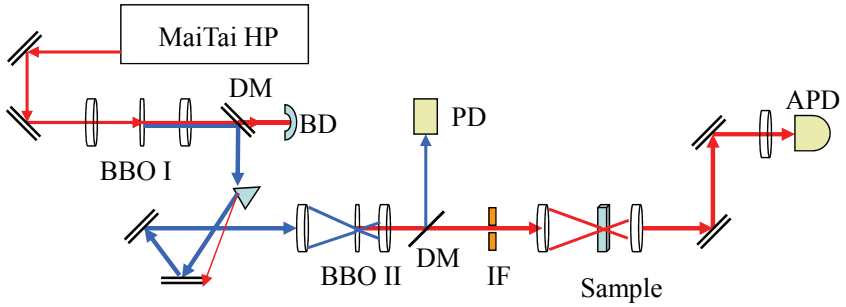

Figure V.1. Depiction of entangled two-photon absorption experimental setup. Dichroic mirrors (DM) are used to separate second-harmonic from fundamental beam, and entangled photons from second-harmonic beam. Photodetectors (PD) are used as a reference for fundamental and second-harmonic power, while an avalanche photodiode (APD) single-photon counting module detects entangled photons. An interference filter (IF) is used to select nearly-degenerate photons centered at 800 nm (20 nm FWHM).

the theory advanced by Fei et al. [11] and Kojima and Nguyen [13] that ETPA requires involvement of the intermediate states.

ETPA experiments were performed using the experimental configuration given in Figure V.1, which is discussed in greater detail within the Materials and Methods section of this chapter. Results of the ETPA measurements are shown in Figure V.2. From Eq. (V.1), it is expected that a plot of absorbed photon rate against input photon rate (which is proportional to flux) should have a linear contribution from ETPA, as well as a quadratic contribution from non-entangled photon absorption. In a previous experimental study [2], we had found that the cross-section calculated from the coefficient on the quadratic term exceeds the classical TPA cross-section by approximately 20 orders of magnitude, suggesting a non-classical effect, but scales with material in the same manner. This linear/quadratic character is observed in **90T**, ZnTPP, *bis*-[18]annulene, 30-*mer*, and OM82C. Among the materials studied, T161 series as well as the stilbene derivative I, are found to not absorb entangled photons, despite their substantial classical TPACS. Initial solutions for T161 series, and the stilbene derivative I were initially prepared at approximately 40 μM concentration, however, no decrease in transmitted photon count rate (increase in absorbed photon count rate) was observed, even at very high (> 300 μM) concentration. In contrast to this, ZnTPP, with a ~20 GM classical TPA cross-section, exhibits strong ETPA at a ~200 μM concentration. ETPA cross-sections obtained from these data, as well as TPACS from the respective works, are reported in Table V.1.

To interpret why some materials with a large classical TPACS do not appear to absorb entangled photons, the origin of the TPACS is explored. For a non-centro-symmetric molecule, one can consider a three-level system involving ground state *g*,

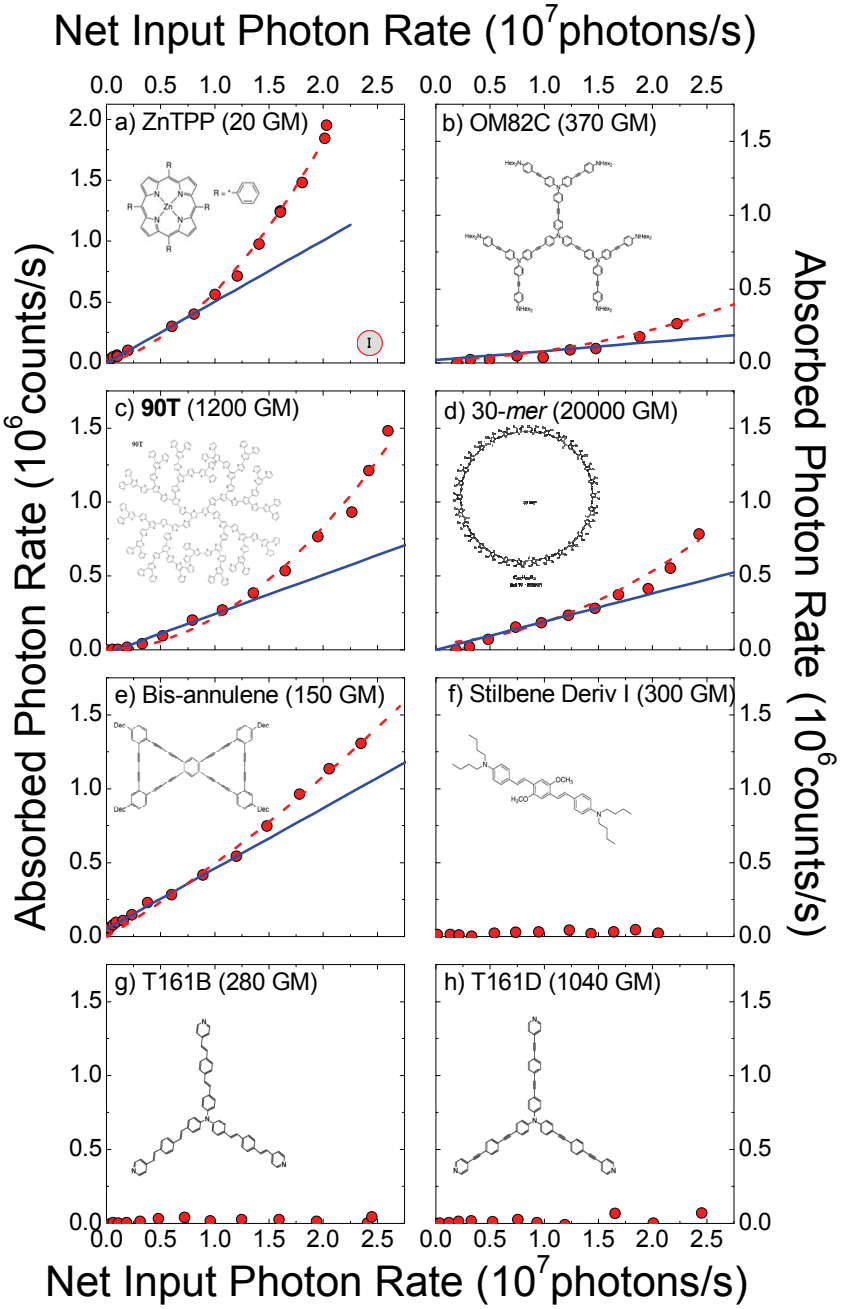

Figure V.2. Entangled two-photon absorption properties of nonlinear optical materials. The entangled two-photon absorption (ETPA) rate for solutions of a) ZnTPP, b) OM82C, c) **90T**, d) 30-*mer*, e) bis-[18]annulene, f) stilbene derivative I, g) T161B, h) T161D, plotted against input photon rate. Standard deviation is depicted in the bottom right corner of a). For the materials showing ETPA, a linear fit of the initial points of absorbed photon rate is shown with a solid blue line to demonstrate a non-zero derivative at zero i.e. the presence of linear component, while the best fit to Eq. (V.1) is shown with a dashed red line. Numbers in parentheses correspond to classical TPA cross-sections.

Material	TPA cross-section δ_R (GM)	ETPA cross-section σ_E (10^{-18} cm^2)
90T thiophene dendrimer	1200	5.9
bis-[18]annulene	150	5.4
30-*mer* thiophene macrocycle	20000	40
Tetraphenylporphine, Zinc	20	8.0
OM82C	370	2.6
T161B	280	--
T161D	1040	--
Stilbene derivative I	300	--

Table V.1. Two-photon absorption cross-sections of materials investigated. TPA cross-sections reported are for 800 nm excitation, with 1 GM = 10^{-50} cm^2 photon^{-1} s^{-1} molecule^{-1}.

intermediate state *j*, and final state *f*. From second-order perturbation theory, the two-photon absorption cross-section (TPACS) δ_R is given by [18]:

$$\delta_R = A\left\langle \left| \left(\mathbf{e}\bullet\mu_{fj}\right)\left(\mathbf{e}\bullet\mu_{jg}\right)\frac{\nu}{\nu_{jg}-\nu} + \left(\mathbf{e}\bullet\mu_{fg}\right)\left(\mathbf{e}\bullet\Delta\mu_{fg}\right) \right|^2 \right\rangle g\left(2\upsilon\right), \qquad \text{(V.5)}$$

where μ_{ab} refers to the transition dipole moment between states *a* and *b*, **e** refers to the unit field polarization vector, ν is the laser excitation frequency (Hz), ν_{ab} are the transition frequencies, $\Delta\mu_{fg}$ is the difference in permanent dipole moment between final and ground states *f* and *g*, and $g\left(2\upsilon\right)$ is the normalized TPA lineshape function (Hz^{-1}). TPA results are typically interpreted [19-25] by one of two mechanisms, depending on the material, with the TPA rate increasing quadratically with photon flux [18], regardless of the mechanism. Two potential pathways for TPA are observed in the two terms within Equation V.5 and illustrated in Figure V.3. In the virtual pathway, given by the first term, an intermediate state (close to resonance with the photon) is involved, and the transition

dipole moments μ_{fj} and μ_{jg}, as well as the detuning between the laser frequency and the intermediate state, are known to play an important role. Materials with moderate donor acceptor character, and without charge-transfer character, are described [23, 26-28] as absorbing through the virtual pathway. In the so-called dipole pathway, given by the second term, the intermediate state is bypassed entirely; ground and excited states are connected directly, and resonance between intermediate states and the laser is not a necessary condition for TPA. In the case of charge transfer materials, the contribution to the TPACS from the intermediate state terms is overshadowed by that occurring based on the difference between permanent dipole moments of the ground and excited states; the second term of Equation V.5 dominates, and the TPACS is explained [14, 19-25, 29-32] by the dipole pathway. This is known to occur when the intermediate states of the material are very far from resonance with the photons.

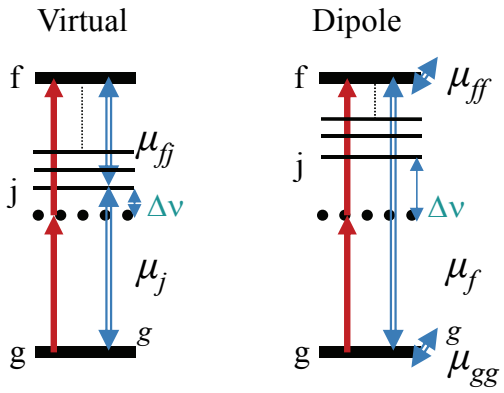

Figure V.3. Simplified depiction of two-photon absorption pathways. Illustration of the virtual (left) and dipole (right) pathways of classical two-photon absorption. Final, intermediate, and ground states are denoted by *f*, *j*, and *g*, respectively. The transition dipole moment is represented as μ. Photon energies and transition dipole moments are represented by filled and hollow arrows, respectively.

All materials in which we have observed ETPA were previously described [17, 26, 28, 33-35] as having a classical two-photon excitation through the virtual pathway, in

which an intermediate state *is* involved in the transition. Theoretical investigations have indicated [11-13, 36-38] an enhancement of the ETPA cross-section under conditions of near-resonance between entangled photons and an intermediate state. We have found that T161 series as well as the stilbene derivative I do not absorb entangled photons. Previous literature has suggested [14, 15] that these materials undergo a two-photon transition by the dipole mechanism, in which the substantial change in permanent dipole moment between ground and excited states allows a direct transition; coupling of the virtual or real intermediate states to the ground and final states, in part due to a large detuning energy between the photon and the intermediate state, is significantly less efficient than the dipole pathway. The stilbene derivative I was shown15 to have a $1B_u$ band at 20,600 cm^{-1}, which is approximately 8,000 cm^{-1} higher in energy than the entangled photons used in our experiment. From Equation V.2, the combination of a large detuning energy between the entangled photon and the $1B_u$ band of stilbene derivative I and a weak coupling to the intermediate state is expected to have a negative impact on the ETPA cross-section of this material, which leads to no measurable ETPA with our current source of entangled photons.

V.3. Conclusions

Entangled two-photon absorption (ETPA) experiments, with nearly-degenerate entangled photons of 800 nm wavelength, have been performed on a set of nonlinear optical materials including thiophene dendrimers, thiophene macrocycles, [18]annulenes, porphyrins, phenylamine-centered alkene and alkyne dendrimers, stilbenes, and nitrogen-centered tolane dendrimers. Each of these materials is known [2, 3, 14, 17, 26, 29, 33, 35,

39, 40] to possess a moderate (10s of GM) to large (20,000 GM) classical TPACS. This current investigation has found that several materials, including stilbene derivative I, and the phenylamine-centered T161B and T161D, appear to *not* absorb entangled photons, despite having relatively large (130 GM to 1000 GM) classical TPACS for an 800nm excitation [14, 15]. According to previous publications, these materials undergo TPA through a direct transition [14, 15, 23], based on the large change in permanent dipole moment between ground and excited states. This mechanism does not require that virtual states be close to resonance with the photons. Indeed, in the case of bis(styryl) benzene derivative, the lowest energy intermediate state was calculated [15] to be approximately 8000 cm^{-1} *higher* in energy than a single photon with 800 nm wavelength. Other materials, such as ZnTPP, have been reported [35] to possess classical TPACS on the order of 20 GM, and yet *do* absorb entangled photons. In addition to this, the ETPA cross-sections, while scaling with TPA cross-sections for a given system, do not correlate when comparing different systems. That is, in the case of thiophene dendrimers **6T** – **90T**, the ETPA cross-section has been shown [2] to scale with the TPA cross-section, however, the ETPA cross-section of ZnTPP is a factor of 1.4 *larger* than that of **90T**, despite the TPA cross-section of ZnTPP being a factor of 60 *smaller* than that of **90T**. While information regarding the intermediate states of ZnTPP has not been published, quantum chemistry calculations [17] have shown that H_2TPP has a real intermediate state relatively close to the entangled photon energy, which is desirable for ETPA, as the detuning energy can be relatively small. Theoretical investigations [11-13] have predicted that intermediate states far from resonance with the entangled photon are not expected to contribute to the entangled two-photon absorption cross-section of a material. Our

investigation has provided experimental proof that intermediate states have an important role in the ETPA process.

Our experiments were performed with nearly-degenerate photons at a wavelength centered at 800 nm, however, it may be possible to shift the entangled photon wavelength such that a real intermediate state *is* near resonance with these photons, and the material shifts from transparent to absorbing. This could have implications in imaging or lithography applications involving multiple types of absorbing materials. Alternatively, the ability of a NLO material to absorb non-entangled photons while being transparent to entangled photons could be useful for filtering applications.

V.4. Materials and Methods

The chromophore zinc tetraphenylporphine (ZnTPP) was obtained from Aldrich and used without further purification. Other NLO materials were obtained from collaborators, with details of synthesis and properties reported as follows : thiophene dendrimer **90T** from reference 2, *bis*-[18]Annulene from references 3, 28, 41, 42, 30-*mer* thiophene macrocycle from reference 33, OM82C from references 26, 40, T161B and T161D from reference 14, and 4,4'-bis(N,N-di-*n*-butylamino)-*E*-stilbene (stilbene derivative I) from reference 29. All of these materials are known to have significant one-photon absorption around 400 nm, and negligible absorption at 800 nm. Solutions for ETPA measurements were prepared at concentrations between 20 and 300 μM, depending on their reported classical TPA cross-sections. T161 series, as well as 4,4'-bis(N,N-di-*n*-butylamino)-*E*-stilbene, were initially prepared at a concentration of 40 μM, but the chromophore concentration was increased to nearly 400 μM based on negative experimental results.

ETPA measurements were performed using an equipment configuration previously published [1, 2] by our group. Briefly, sub-100 fs pulses, typically 14 nm FWHM centered at 800 nm with an 80 MHz repetition rate, from a mode-locked Ti:sapphire laser (Spectra-Physics MaiTai®) are frequency-doubled to produce a SHG beam at 400 nm. This SHG beam is then focused onto a 0.5 mm thickness β-barium borate (BBO II in Figure V.1) crystal designed for Type II SPDC. Within Type II SPDC, signal (*o*-ray) and idler (*e*-ray) photons are generated at orthogonal polarization. Down-converted photons are detected by silicon avalanche photodiode (APD) single photon counting modules (Perkin-Elmer SPCM-AQR-13). To vary the input flux, the fundamental beam is attenuated using a continuously variable neutral density filter wheel, with photodetectors (PD's) serving as references for the input power. ETPA measurements are performed based on the transmission method, with appropriate corrections for background and scatter. Quartz cells, 0.4 cm path length, are used in liquid sample ETPA measurements. Using a polarizer set at *H*- or *V*-polarization, which blocks signal or idler photon, respectively, was found to result in zero absorption by the material.

Two-photon absorbing materials investigated in this work were chosen based on chromophore, architecture, one-photon absorption wavelength, classical TPACS, and previous ETPA results. As we have reported [1] ETPA results for a G3 porphyrin dendrimer, the porphyrin ZnTPP is investigated to determine the effect of a non-dendrimeric structure on ETPA. Similarly, we have previously investigated [2] thiophene dendrimers, so a 30-*mer* thiophene macrocycle is investigated as an alternate structure based on the thiophene chromophore. As [18]annulenes have also shown [3] evidence of ETPA, materials which have alternating alkyne and phenyl groups are investigated, in the

form of T161D and OM82C, which are both nitrogen-centered dendrimers. T161D is known [14] to have excited state charge transfer, while OM82C does not [26]. T161B and 4,4'-bis(N,N-di-*n*-butylamino)-*E*-stilbene have alternating phenyl and alkene (rather than alkyne) groups, but are otherwise similar in structure to T161D, and also are known [14, 15] to have excited state charge transfer.

V.5. References

1. Lee, D.I. & Goodson, T., Entangled photon absorption in an organic porphyrin dendrimer. *J. Phys. Chem. B* 110 (51), 25582-25585 (2006).

2. Harpham, M.R., Suzer, O., Ma, C.-Q., Bauerle, P., & Goodson, T., Thiophene Dendrimers as Entangled Photon Sensor Materials. *J. Am. Chem. Soc.* 131 (3), 973-979 (2009).

3. Guzman, A.R., Suzer, O., Harpham, M.R., Haley, M., & Goodson, T., Spatial control of entangled two-photon absorption with organic chromophores. *J. Am. Chem. Soc.* 132(23), 7840-7842 (2009).

4. Saleh, B.E.A., Teich, M.C., & Sergienko, A.V., Wolf equations for two-photon light. *Phys. Rev. Lett.* 94 (22) (2005).

5. Boto, A.N. *et al.*, Quantum interferometric optical lithography: Exploiting entanglement to beat the diffraction limit. *Phys. Rev. Lett.* 85 (13), 2733-2736 (2000).

6. Hong, C.K. & Mandel, L., Theory of Parametric Frequency down Conversion of Light. *Phys. Rev. A: At. Mol. Opt. Phys.* 31 (4), 2409-2418 (1985).

7. Mollow, B.R., Photon Correlations in Parametric Frequency Splitting of Light. *Phys. Rev. A: At. Mol. Opt. Phys.* 8 (5), 2684-2694 (1973).

8. Joobeur, A., Saleh, B.E.A., Larchuk, T.S., & Teich, M.C., Coherence properties of entangled light beams generated by parametric down-conversion: Theory and experiment. *Phys. Rev. A: At. Mol. Opt. Phys.* 53 (6), 4360-4371 (1996).

9. Geabanacloche, J., 2-Photon Absorption of Nonclassical Light. *Phys. Rev. Lett.* 62 (14), 1603-1606 (1989).

10. Javanainen, J. & Gould, P.L., Linear Intensity Dependence of a 2-Photon Transition Rate. *Phys. Rev. A: At. Mol. Opt. Phys.* 41 (9), 5088-5091 (1990).

11. Fei, H.B., Jost, B.M., Popescu, S., Saleh, B.E.A., & Teich, M.C., Entanglement-induced two-photon transparency. *Phys. Rev. Lett.* 78 (9), 1679-1682 (1997).

12. Lissandrin, F., Saleh, B.E.A., Sergienko, A.V., & Teich, M.C., Quantum theory of entangled-photon photoemission. *Phys. Rev. B: Condens. Matter* 69 (16) (2004).

13. Kojima, J. & Nguyen, Q.V., Entangled biphoton virtual-state spectroscopy of the A(2)Sigma(+)-X-2 pi system of OH. *Chem. Phys. Lett.* 396 (4-6), 323-328 (2004).

14. Bhaskar, A. *et al.*, Investigation of two-photon absorption properties in branched alkene and alkyne chromophores. *J. Am. Chem. Soc.* 128 (36), 11840-11849 (2006).

15. Albota, M. *et al.*, Design of organic molecules with large two-photon absorption cross sections. *Science* 281 (5383), 1653-1656 (1998).

16. Mollow, B.R., 2-Photon Absorption and Field Correlation Functions. *Phys. Rev.* 175 (5), 1555-1563 (1968).

17. Kruk, M. *et al.*, Two-photon absorption of tetraphenylporphin free base. *J. Lumin.* 105 (1), 45-55 (2003).

18. McClain, W.M. & Harris, R.A., Two-photon molecular spectroscopy in liquids and gases in *Excited States*, edited by E.C. Lim (Academic, New York, 1977), pp. 1-56.

19. Drobizhev, M., Karotki, A., Kruk, M., Mamardashvili, N.Z., & Rebane, A., Drastic enhancement of two-photon absorption in porphyrins associated with symmetrical electron-accepting substitution. *Chem. Phys. Lett.* 361 (5-6), 504-512 (2002).

20. Jagatap, B.N. & Meath, W.J., On the competition between permanent dipole and virtual state two-photon excitation mechanisms, and two-photon optical excitation pathways, in molecular excitation. *Chem. Phys. Lett.* 258 (1-2), 293-300 (1996).

21. Karotki, A. *et al.*, Enhancement of two-photon absorption in tetrapyrrolic compounds. *J. Opt. Soc. Am. B-Opt. Phys.* 20 (2), 321-332 (2003).

22. Lukaszewicz, A. *et al.*, Photophysical processes in electronic states of zinc tetraphenyl porphyrin accessed on one- and two-photon excitation in the soret region. *Chem. Phys.* 331 (2-3), 359-372 (2007).

23. Macak, P., Luo, Y., Norman, P., & Agren, H., Electronic and vibronic contributions to two-photon absorption of molecules with multi-branched structures. *J. Chem. Phys.* 113 (17), 7055-7061 (2000).

24. McIlroy, S.P. *et al.*, Two-photon photosensitized production of singlet oxygen: Sensitizers with phenylene-ethynylene-based chromophores. *J. Org. Chem.* 70 (4), 1134-1146 (2005).

25. Drobizhev, M. *et al.*, Strong two-photon absorption in new asymmetrically substituted porphyrins: Interference between charge-transfer and intermediate-resonance pathways. *J. Phys. Chem. B* 110 (20), 9802-9814 (2006).

26. Varnavski, O., Yan, X.Z., Mongin, O., Blanchard-Desce, M., & Goodson, T., Strongly interacting organic conjugated dendrimers with enhanced two-photon absorption. *J. Phys. Chem. C* 111 (1), 149-162 (2007).

27. Zhao, M.T., Singh, B.P., & Prasad, P.N., A Systematic Study of Polarizability and Microscopic 3rd-Order Optical Nonlinearity in Thiophene Oligomers. *J. Chem. Phys.* 89 (9), 5535-5541 (1988).

28. Bhaskar, A., Guda, R., Haley, M., & Goodson, T., Building symmetric two-dimensional two-photon materials. *J. Am. Chem. Soc.* 128 (43), 13972-13973 (2006).

29. Cumpston, B.H. *et al.*, Two-photon polymerization initiators for three-dimensional optical data storage and microfabrication. *Nature* 398 (6722), 51-54 (1999).

30. Rubio-Pons, O., Luo, Y., & Agren, H., Effects of conjugation length, electron donor and acceptor strengths on two-photon absorption cross sections of asymmetric zinc-porphyrin derivatives. *J. Chem. Phys.* 124 (9) (2006).

31. Guo, J.D., Wang, C.K., Luo, Y., & Agren, H., Influence of electron-acceptor strength on the resonant two-photon absorption cross sections of diphenylaminofluorene-based chromophores. *PCCP* 5 (18), 3869-3873 (2003).

32. Lee, J.Y., Kim, K.S., & Mhin, B.J., Intramolecular charge transfer of pi-conjugated push-pull systems in terms of polarizability and electronegativity. *J. Chem. Phys.* 115 (20), 9484-9489 (2001).

33. Williams-Harry, M. *et al.*, Giant thienylene-acetylene-ethylene macrocycles with large two-photon absorption cross section and semishape-persistence. *J. Am. Chem. Soc.* 130 (11), 3252-3253 (2008).

34. Ramakrishna, G., Bhaskar, A., Bauerle, P., & Goodson, T., Oligothiophene dendrimers as new building blocks for optical applications. *J. Phys. Chem. A* 112, 2018-2026 (2008).

35. Drobizhev, M., Karotki, A., Kruk, M., & Rebane, A., Resonance enhancement of two-photon absorption in porphyrins. *Chem. Phys. Lett.* 355 (1-2), 175-182 (2002).

36. Perina, J., Saleh, B.E.A., & Teich, M.C., Multiphoton absorption cross section and virtual-state spectroscopy for the entangled n-photon state. *Phys. Rev. A: At. Mol. Opt. Phys.* 57 (5), 3972-3986 (1998).

37. Saleh, B.E.A., Jost, B.M., Fei, H.B., & Teich, M.C., Entangled-photon virtual-state spectroscopy. *Phys. Rev. Lett.* 80 (16), 3483-3486 (1998).

38. Roslyak, O. & Mukamel, S., Multidimensional pump-probe spectroscopy with entangled twin-photon states. *Physical Review A (Atomic, Molecular, and Optical Physics)* 79 (6), 063409 (2009).

39. Narayanan, A. *et al.*, Detection of TNT using a sensitive two-photon organic dendrimer for remote sensing. *Nanotechnology* 19 (11), 6 (2008).

40. Goodson, T.G., Optical excitations in organic dendrimers investigated by time-resolved and nonlinear optical spectroscopy. *Acc. Chem. Res.* 38 (2), 99-107 (2005).

41. Marsden, J.A. & Haley, M.M., Carbon networks based on dehydrobenzoannulenes. 5. Extension of two-dimensional conjugation in graphdiyne nanoarchitectures. *J. Org. Chem.* 70 (25), 10213-10226 (2005).

42. Wan, W.B., Brand, S.C., Pak, J.J., & Haley, M.M., Synthesis of expanded graphdiyne substructures. *Chem.-Eur. J.* 6 (11), 2044-2052 (2000).

CHAPTER VI

Entangled Two-Photon Excited Fluorescence from an Organic Dendrimer

Abstract

We report the observation of fluorescence emission from an organic dendrimer subsequent to two-photon excitation by entangled pairs of photons. The entangled-pair flux utilized to excite two-photon transitions in our experiments constitutes approximately 10 orders of magnitude fewer photons than any classical counterpart requires. A novel, high geometric efficiency, spherically-enclosed optical collection system for collection of the resulting fluorescence photons is utilized to circumvent any drawbacks related to the low flux conditions under which experiments are carried out. These results have widespread impact in applications ranging from spectroscopy to chemical and biological sensing, imaging, and microscopy.

VI.1. Introduction

Quantum entanglement has received a great deal of interest over the past several decades for a wide variety of applications and investigations ranging from the foundations of quantum mechanics [1-5] to implementations for quantum computation [6, 7], information technology and communications [8, 9], and even biology [10]. Furthermore, entangled-state illumination is at the heart of several quantum imaging implementations [11-14], such as quantum optical coherence tomography [15] and quantum holography [16]. Applications such as background-free quantum ghost imaging have been both proposed theoretically and demonstrated experimentally [17-23]. These implementations offer performance advantages over their conventional optical counterparts that employ coherent light sources, which have traditionally been ascribed to the inherent quantum mechanical correlations between the photons that constitute a quantum entangled pair.

The interaction of entangled states of light with matter has also received interest for applications such as quantum lithography [24], where fabrication of micro- and nano-scale structures below the diffraction limit have been proposed [25-28], as well as for more fundamental investigations for spectroscopic purposes [29-33] and the development of remote sensing [34, 35]. The phenomenon of entangled two-photon absorption (ETPA), which had been theoretically predicted to exhibit interesting non-classical effects [36, 37], has been experimentally demonstrated in both atomic systems and small molecules [32], as well as a variety of macromolecular systems [38-42] using entangled pairs of photons that are generated via the process of spontaneous parametric down-conversion (SPDC). The use of quantum entangled pairs of photons as the excitation

source for two-photon absorption in matter offers a unique advantage compared to its classical counterpart due to the linear, rather than quadratic, dependence of the absorption rate on the excitation intensity, which is dominant in the low excitation flux-density regime [36, 37]. This, in turn, enables spectroscopy to be done at extremely low excitation flux levels [41].

A particularly important field of research into which entangled states of light have been proposed could bring significant improvement is microscopy. Following the conception of the confocal microscope [43] and its combination with fluorescence imaging [44, 45], confocal laser scanning fluorescence microscopy (CLSM) has become a powerful tool of experimental research in a wide variety of fields, ranging from biological science disciplines including genetics and microbiology to clinical medicine [46]. However, CLSM is limited in its use of excitation photons because it relies on near-resonant excitation of fluorophores in a sample, which leads to absorption throughout a specimen of interest but "useful" light is obtained only from a thin slice around the focal plane of the objective lens. Further, the detector aperture utilized in CLSM rejects all out-of-focus light, which means only a small portion of the fluorescence photons – those that exit the specimen without undergoing any scattering – can contribute to the signal. As a result, a high flux of excitation photons is generally necessary in CLSM to compensate for signal loss, which limits the practical operation of this technique due to photobleaching and photodynamic damage to the specimen of interest [45, 47]. These drawbacks of CLSM are partially overcome by the use of multiphoton absorption to mediate excitation in laser scanning microscopy. In two-photon laser scanning fluorescence microscopy (TPLSM), two photons that coincidentally arrive at a

fluorophore are absorbed simultaneously and the resulting emission of a fluorescence photon is detected [46]. Because the two-photon absorption process (TPA) is dependent on the accidental coincidence of two excitation photons, the absorption rate, and hence the resulting rate of fluorescence emission, exhibits a strong quadratic dependence on the excitation photon-flux and excitation is highly confined to the focal point of the objective lens, where the intensity is highest [46, 48, 49]. This, in turn, limits the emission of out-of-focus fluorescence photons, reducing background intensity and enhancing transverse resolution [46, 50]. However, due to the purely random arrival times of photons and the low probability of TPA events [51], TPLSM requires a relatively high flux of excitation photons to generate a viable signal, which often necessitates the use of mode-locked laser sources to provide a sufficiently large peak excitation photon-flux density. This requirement further exacerbates photodamage and photobleaching in the specimen [52, 53].

In order to overcome these limitations of TPLSM, several schemes of entangled-photon fluorescence microscopy (EPM) have been proposed and patented [50, 54-56] in recent years, all of which aim to take advantage of the particular manner in which entangled states of light interact with matter, as discussed above. Utilizing entangled pairs of photons for excitation in microscopy applications like TPLSM offers a unique solution to the high excitation flux requirement due to the extremely low flux levels at which ETPA can be achieved in organic systems [41]. Further, because the ETPA process still requires the simultaneous absorption of a pair of entangled photons, the resolution enhancements of TPLSM that are attributed to confinement of the excitation photons are preserved. However, despite the operational advantages and the proposition

of many conceptual and theoretical prospects for such application of entangled photon pair excitation in microscopy, experimental implementations of this concept have yet to be realized. The primary obstacle in the way of the realization of practical entangled photon fluorescence microscopy is the absence of a successful proof-of-concept experiment wherein fluorescence emission from a sample due to two-photon excitation by entangled pairs of photons is observed. The difficulty of this demonstration stems from the low flux levels at which the entangled two-photon excited fluorescence experiments (ETPEF) are carried out, where traditional fluorescence detection schemes fall short due to the prohibitively low number of fluorescence photons that are expected to be emitted from a useful sample such as an organic chromophore. To the authors' knowledge, ETPEF from any material has not been demonstrated to date.

In this chapter, we present the results of an experimental investigation where we have observed fluorescence emission from an organic dendrimer subsequent to excitation by entangled pairs of photons that are generated via the process of spontaneous parametric down-conversion (SPDC). This first demonstration of ETPEF from an organic dendrimer is realized by utilizing a high geometric efficiency optical light collection assembly that was designed specifically to overcome difficulties associated with the low flux levels at which experiments are carried out, allowing the collection of fluorescence photons for detection with maximum efficiency. We present fluorescence quantum yield information about the organic dendrimer that is extracted from the fluorescence emission and ETPA rates in the sample, which we have found to agree well with values that have previously been published in literature. This experimental demonstration of ETPEF from an organic dendrimer is an enabling discovery for the realization of quantum microscopy

schemes such as EPM, and has widespread impact on a wide range of applications ranging from spectroscopy to chemical and biological sensing, as well as imaging and microscopy. The following section describes our experimental conditions, which will be followed by a detailed discussion of the design criteria of the optical collection assembly that is utilized in ETPEF experiments, followed by a discussion of our experimental findings, and finally concluding remarks.

VI.2. Experimental Methodology

ETPA measurements are carried out using an experimental configuration that has previously been developed by our group [38, 41, 42]. As illustrated in Figure VI.1, after modification to include a custom-designed high geometric efficiency optical collection assembly (OCA), ETPA and ETPEF measurements are carried out simultaneously in this experimental setup.

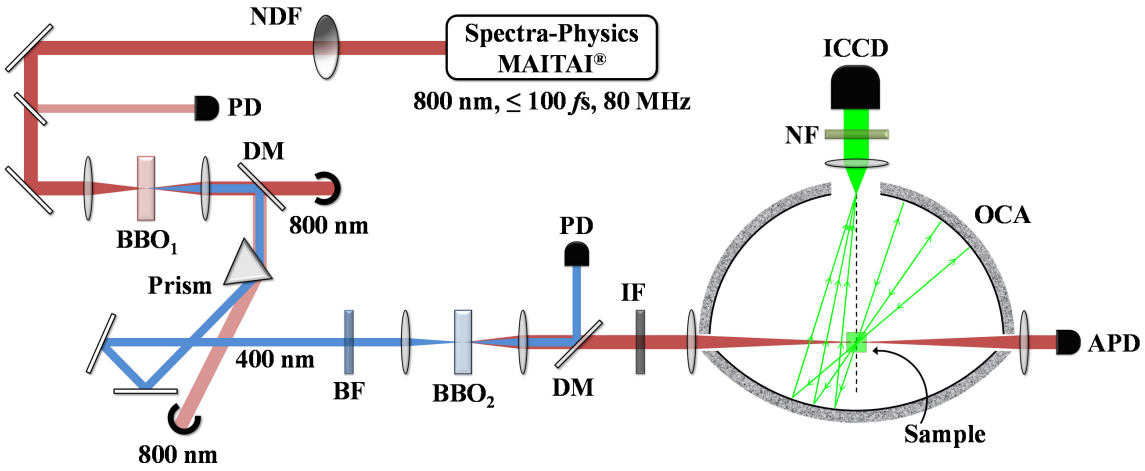

Figure VI.1. Schematic representation of our experimental set-up. PD are photodetectors used to monitor fundamental and second harmonic pump power, DM denote dichroic mirrors utilized for spectral selection, IF is a narrow-band interference filter, and OCA is a high geometric efficiency optical collection assembly.

Briefly, the second-harmonic of a femtosecond Ti:sapphire laser system is utilized as a pump source for the generation of entangled pairs of photons in free space via the process of spontaneous parametric down-conversion, which are utilized as the entangled two-photon excitation source for ETPA and ETPEF measurements. The Spectra-Physics MAITAI® laser system delivers a fundamental beam in sub-100 fs pulses with a repetition rate of 80 MHz centered at 800 nm wavelength, which are frequency-doubled by focusing onto a 1-mm thick β-Barium Borate (BBO_1) nonlinear crystal. The 400-nm light is subsequently collimated into a spot size of ~2-mm diameter and separated from the redundant fundamental by means of a dichroic mirror (DM), followed by a Brewster-angled prism. After passing through a blue filter (BF) to minimize background intensity, the 400-nm pump is focused onto the input surface of a second BBO crystal for generation of SPDC photons. In our experiments, we utilize a BBO crystal of 0.5-mm thickness (BBO_2) that is cut for type-II SPDC at $\varphi=42°$ with respect to the center pump direction, and is capable of generating $\sim 1.5\times10^7$ down-converted pairs per second under optimized conditions. The crystal is tilted slightly to achieve collinear phase-matching. The entangled photon pairs generated via the SPDC process are characteristically emitted into two cones, which are collimated into a parallel beam by a subsequent 6-cm focal length lens. The remaining pump beam is then removed by means of another dichroic mirror (DM), and the SPDC photons are further selected around the degenerate wavelength by a narrow band-pass spectral filter (IF) with 25-nm bandwidth centered at 800 nm. Down-converted photons are then focused onto and detected by a silicon avalanche photodiode (APD) single-photon counting module (Perkin-Elmer SPCM-AQR-13), which has a detection efficiency of ~ 56%, at 800 nm. A neutral-density filter

wheel with variable transmittance (NDF) just after the laser system is used to vary power admitted into the rest of the setup, which controls the entangled excitation flux utilized in experiments, and photodetectors (PD) serve as references for the input power.

ETPA experiments are performed based on the transmission method, wherein transmitted count-rates are measured as a function of varying excitation flux through a "blank" solvent and a solution of the sample of interest within the same solvent, which are positioned perpendicular to the excitation path at the focal plane of a focusing-collimating lens-pair telescope. Quartz cells of 1.0-cm path-length are used to contain the liquid samples. The calculated difference between the transmitted count-rates through the blank and the sample constitutes the absorption rate of the material of interest. With application of appropriate corrections for background and scatter, this experimental method has previously been shown to be an effective technique in evaluating the ETPA cross-section of materials [38, 41, 42].

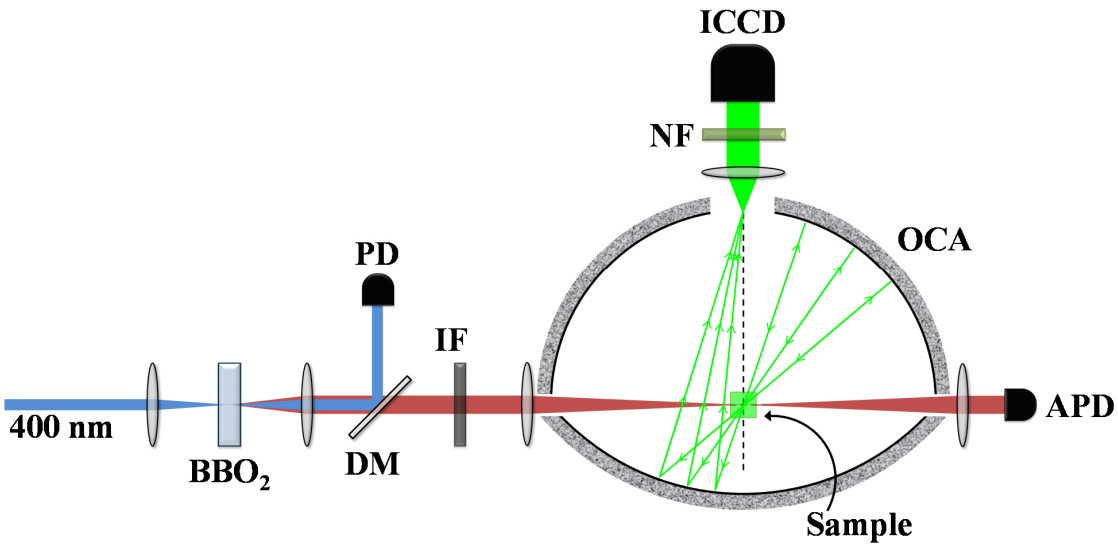

Figure VI.2. Detail view of the ETPEF experimental scheme, illustrating the operational principle of the optical collection assembly. $Mirror_1$ denotes the hemispherical mirror and the spherical cap mirror is designated as $Mirror_2$.

ETPEF measurements are carried out in tandem with ETPA measurements through the use of an optical collection assembly (OCA) that was designed and manufactured by single-point diamond turning specifically for high geometric efficiency collection of fluorescent light from a sample that is placed at the assembly center. The detail schematic given in Figure VI.2 illustrates the operating principle of the OCA. The assembly consists of a hemispherical mirror and a spherical cap mirror whose optical apertures are matched such that the assembly forms a spherically-enclosed reflecting surface with ports that have been cut open to allow entry and exit of the entangled excitation light, insertion of the quartz cell containing the blank or the solution of the sample of interest, and finally a port to output light that is collected within the assembly. The hemispherical surface is centered on the sample of interest such that all light that is emitted within the assembly will originate from or near the center of curvature of this mirror. The radius of curvature of the spherical cap mirror has been chosen such that light originating from the center of the hemispherical mirror is reflected toward the output port by the spherical cap. The reflective surfaces of the assembly have a protected Ag coating to maximize reflectivity in the visible spectrum. In this arrangement, the overall geometric collection efficiency of the OCA exceeds 75% and the assembly has a magnification factor approximately equal to -2.34. Please refer to the Design Criteria section of this chapter for a detailed discussion of the design of the OCA. Also, Appendix B illustrates the full specifications and technical drawings that were used in the manufacture of the OCA. A collimating lens that is positioned one focal length away from the output port of the assembly directs collected light toward an intensified CCD camera (Princeton Instruments PI-MAX2:1003UNIGEN2), which acts as a large area detector with a detection efficiency

~ 15% in the visible spectrum. An optical "notch" filter (NF) with a transparency window of 350-600 nm is placed in the path of the detector to avoid false detections due to scattered excitation light. In performing ETPEF measurements, we take advantage of the math functions built into the software that controls the CCD camera to apply appropriate corrections for background intensity and multiple exposures of collected fluorescent light are allowed to accumulate for each image acquisition at varying input fluxes of the entangled excitation beam. The images are then integrated and processed individually to extract fluorescence count-rates as a function of entangled excitation flux. Figure VI.3 below illustrates several such raw images that were acquired at low-, intermediate-, and high-flux levels for a typical fluorescence collection experiment.

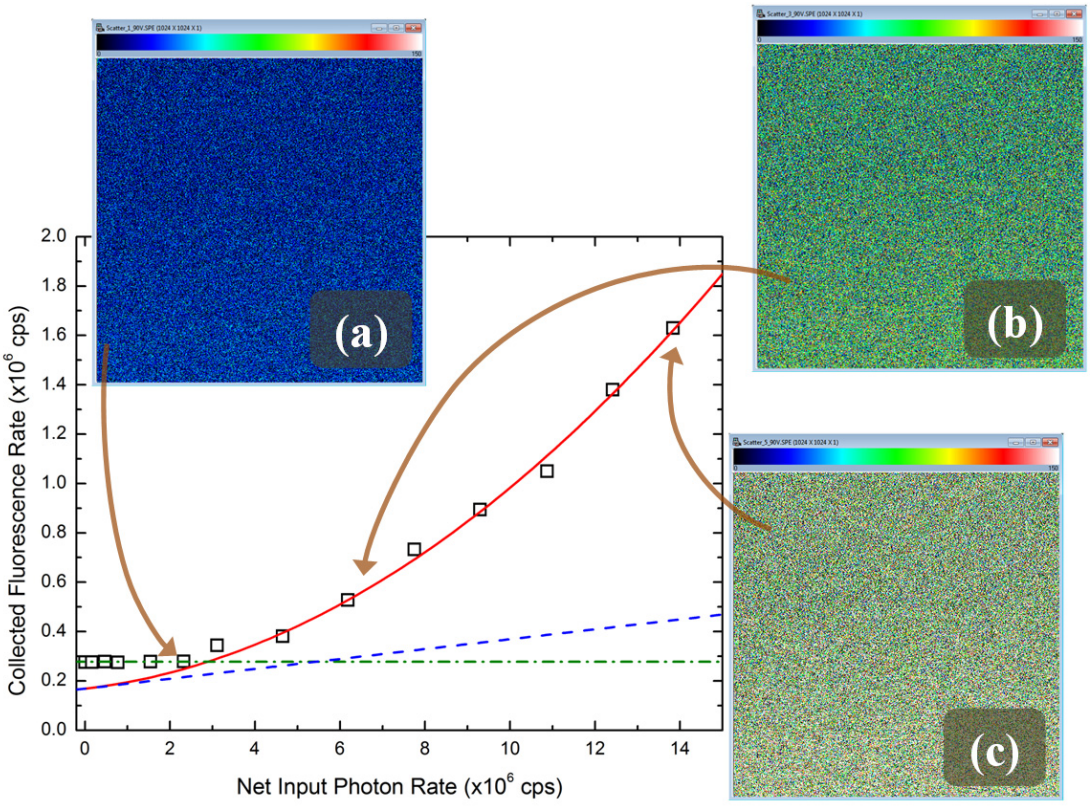

Figure VI.3. Raw image acquisitions for a typical ETPEF experiment. Images shown were acquired at net entangled excitation incidence rates of 2.326×10^{6} photons·sec^{-1} for the low-flux (a), 6.185×10^{6} photons·sec^{-1} for the intermediate-flux (b), and 1.383×10^{7} photons·sec^{-1} for the high-flux (c) images.

VI.3. Design Criteria for Optical Collection Assembly

In this section, we will discuss in further detail the optical techniques utilized in collection of fluorescent light and emphasize the distinctions of the custom-designed optical apparatus that is utilized in entangled two-photon excited fluorescence characterization experiments. The sub-section below will introduce the fundamental shortcomings of conventional collection methodology for fluorescence collection, followed by a detailed description and derivation of how the custom-designed OCA we utilize overcomes these drawbacks.

VI.3.1. Conventional Fluorescence Collection Methodology

A typical experimental setup for collection and characterization of fluorescent light from a sample is illustrated in Fig. VI.4 below.

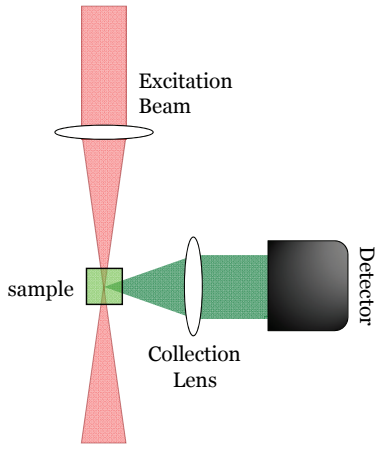

Figure VI.4. Optical schematic of a conventional fluorescence collection system.

Because fluorescent light from the sample is emitted with equal probability in every direction along the solid angle, the efficiency of light collection depends solely on the geometric and electronic parameters of the optical and detection equipment utilized. The geometric efficiency can be calculated by considering the total area over which

fluorescent light is collected, compared to the complete solid angle over which it is emitted. Fig VI.5 below illustrates these geometrical concerns.

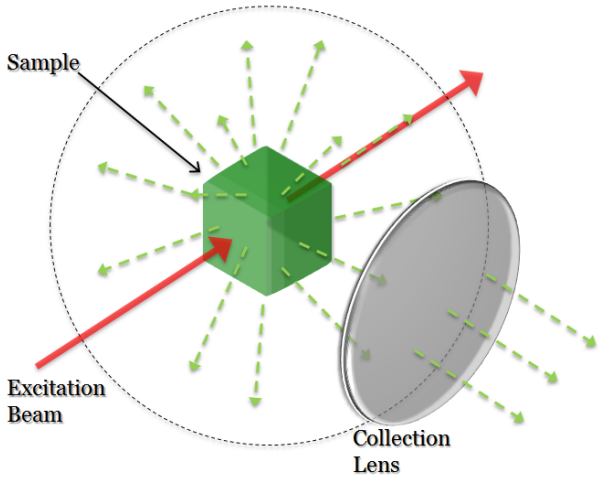

Figure VI.5. Schematic diagram depicting fluorescent light that is optically collected by a conventional detection scheme. Only a small portion of the available fluorescence is directed to the detector.

Using commercially available optical components of 2" optical aperture and 25 mm focal length, the highest geometric efficiency that can be achieved with such a setup is,

$$g = \frac{\pi r^2}{4\pi f^2} = \frac{d^2}{16 f^2} \qquad \text{(VI.1)}$$

where r is the radius of the optical aperture of the lens and f denotes the focal length. With the specifications given above, the best geometric collection efficiency that can be achieved with commercially available optical components is ~ 25%. Note that this is a purely geometric calculation; a real system will further suffer from optical losses due to surface reflections. A realistic estimate for the real collection of such a system is ~ 15%.

VI.3.2. Optical Collection Assembly

In order to increase the geometric efficiency of light collection, it is necessary to increase the solid angle over which light is collected. The ideal solution would redirect all light emitted from a sample of interest in all directions toward a detecting surface.

The fluorescence collection optical assembly consists of two hemispherical mirrors whose openings cross-sectional areas are matched such that the assembly forms a spherically-enclosed reflecting surface. Under these conditions, the only geometric losses are due to ports that need to be cut into the reflecting surface in order to allow entry and exit of excitation light and a port for insertion of a sample of interest. Fig. VI.6 below illustrates the operating principle of this assembly.

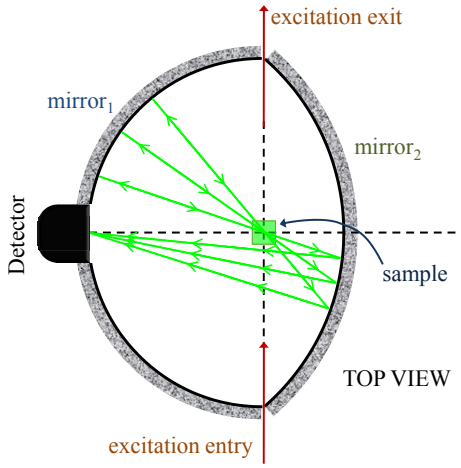

Figure VI.6. Schematic depiction of the operational principles of the optical collection assembly.

The complete hemispherical surface, labeled mirror_1, is centered on the sample of interest such that all light that is emitted within the assembly will originate from or near the center of curvature of this mirror. The second half of the assembly, designated mirror_2, is less than a complete hemisphere; a spherical cap spanning a cross-sectional angle of 2θ, which has a longer radius of curvature than mirror_1. In this arrangement, the sole purpose of mirror_1 is to reflect all light that originates near its center back to the same region, where the sample of interest lies. Due to the offset arrangement of the mirrors, the image formed from light that is incident upon the surface of mirror_2 from the center of mirror_1 will be located again on the surface of mirror_1, where a port is cut open and a detector is positioned.

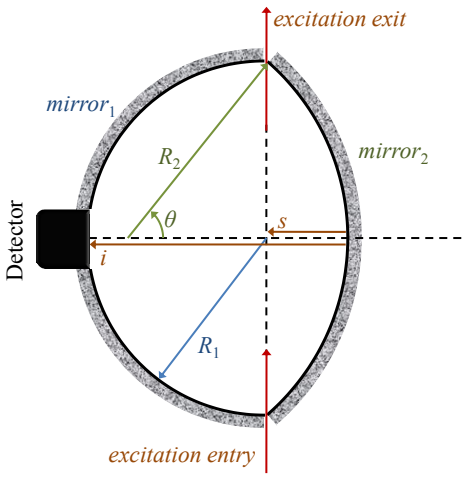

Figure VI.7. Schematic diagram of the optical collection assembly.

The general physical constraints for the OCA are illustrated in Fig. VI.7. Following the illustration, we write the object distance to mirror$_2$ as

$$s = R_2 - R_2 \cos\theta\,, \tag{VI.2}$$

where R_2 is the radius of curvature of mirror$_2$ and θ is the cross-sectional half-angle of span. We require that the image formed lie on the surface of mirror$_1$, such that the image distance is given by

$$i = s + R_1 = R_1 + R_2 - R_2 \cos\theta\,, \tag{VI.3}$$

where R_1 is the radius of curvature of mirror$_1$. It is also required that the cross-sectional areas of the mirror faces match each other exactly, which allows the relation of the radii of curvature of the two mirrors;

$$R_1 = R_2 \sin\theta\,. \tag{VI.4}$$

Using this relationship, the object and image distances to mirror$_2$ can be re-written as

$$s = \frac{R_1}{\sin\theta} - \frac{R_1}{\sin\theta}\cos\theta = \frac{R_1}{\sin\theta}\left(1 - \cos\theta\right), \tag{VI.5}$$

and

$$i = R_1\left(1+\frac{1}{\sin\theta}-\frac{\cos\theta}{\sin\theta}\right). \tag{VI.6}$$

The object and image distances need to satisfy the Gaussian mirror equation;

$$\frac{1}{s}+\frac{1}{i}=\frac{1}{f}, \tag{VI.7}$$

where f is the focal length of mirror$_2$, and is equal to half of it radius of curvature,

$$f=\frac{R_2}{2}=\frac{R_1}{2\sin\theta}. \tag{VI.8}$$

The Gaussian mirror equation for the optical fluorescence collection assembly thus becomes

$$\frac{1}{R_1\left(\frac{1}{\sin\theta}-\frac{\cos\theta}{\sin\theta}\right)}+\frac{1}{R_1\left(1+\frac{1}{\sin\theta}-\frac{\cos\theta}{\sin\theta}\right)}=\frac{2\sin\theta}{R_1}. \tag{VI.9}$$

At this point, it is interesting to note that because the cross-sectional areas of the mirror faces were constrained to match each other exactly, the dependence on the radii of curvature of either of the mirrors vanishes completely from the Gaussian mirror equation. The resulting equation is a function of only one variable, θ, the cross-sectional solid angle spanned by mirror$_2$. Thus, Eq. VI.9 can be re-written as

$$\frac{1}{1-\cos\theta}+\frac{1}{1+\sin\theta-\cos\theta}=2. \tag{VI.10}$$

Expanding the denominators of both terms in Eq. VI.10 and simplifying, we obtain

$$2\cos^2\theta-2\cos\theta+\sin\theta-2\sin\theta\cos\theta=0. \tag{VI.11}$$

Eq. VI.11 has only one real and positive root at $\theta=1.28013\,\text{rad}=73.34605^\circ$, and the overall magnification of the assembly is given by,

$$m = -\frac{i}{s} = -\frac{R_2\left(\sin\theta - \cos\theta + 1\right)}{R_2\left(1 - \cos\theta\right)} \cong -2.343$$

As a result of the negative magnification, the image that is formed on the detector plane is inverted with respect to the fluorescent source, and magnified to more than twice its original size. This design constraint necessitates the use of a large-area detector such as the intensified CCD array utilized in our experiments.

VI.4. Results and Discussion

The two-photon absorbing material investigated in this report, illustrated in Figure VI.8(a), is a large conjugated dendrimer based on rigid tolane linear building blocks connected through nitrogen branching centers, and is designated OM82C [57]. The classical and entangled two-photon response of this material was investigated previously by our group, which was found to be satisfactory. The classical TPA cross-section was reported as 370 GM (1 GM = 10^{-50} cm^2 $photon^{-1}$ sec^{-1} $molecule^{-1}$), and the ETPA cross-section was found to be 2.6×10^{-18} cm^2 $molecule^{-1}$. The details of this experiment were presented in chapter V and will be published elsewhere [58]. In addition to its favorable ETPA response, the OM82C dendrimer was chosen based on its high fluorescence quantum yield, reported to be ~ 74% [57]. The steady-state absorption spectrum of the OM82C dendrimer is given in Figure VI.8(b). Note that the 800 nm wavelength of the entangled photon pairs used to excite the dendrimer is far from any one-photon resonances. As can be seen from the steady-state emission spectrum of OM82C, given in Figure VI.8(c), the main emission peak lies at 427 nm, which is well within the transparency window of the notch filter that is utilized in our ETPEF experiments.

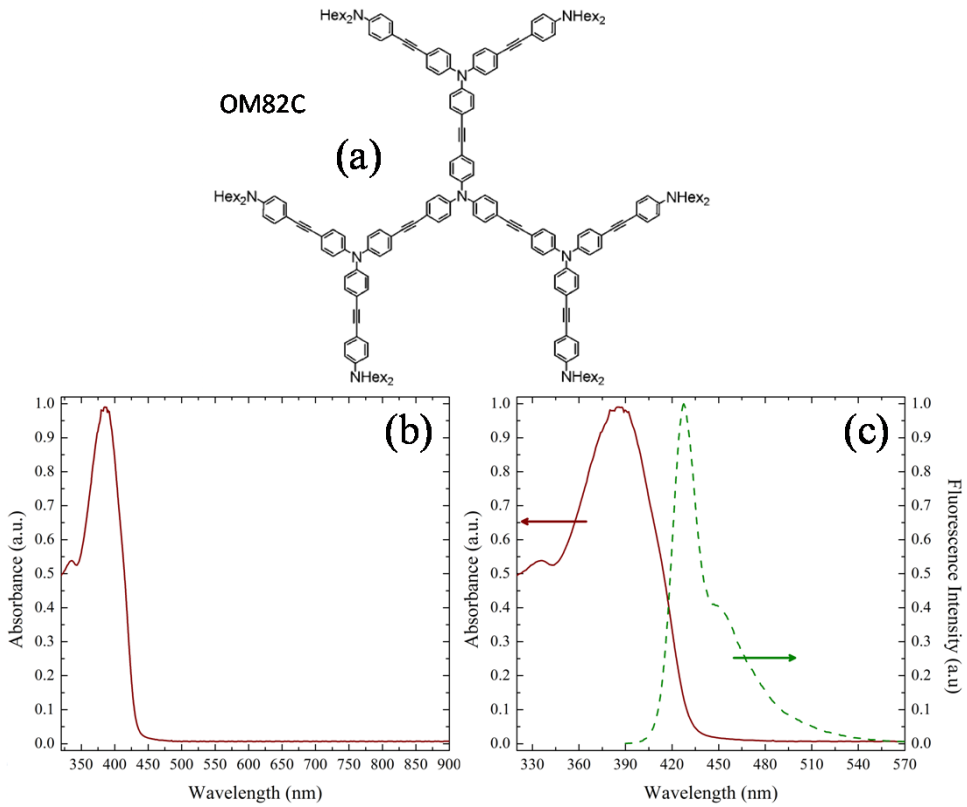

Figure VI.8. Molecular structure (a) of the OM82C dendrimer that is investigated in ETPA and ETPEF experiments. The normalized steady-state absorption spectrum of OM82C is plotted against an extended wavelength range in (b) to illustrate the negligible one-photon response of the material at the entangled excitation wavelength of 800 nm. Both normalized steady-state absorption (solid line, left axis), and emission spectra (dashed line, right axis) are plotted in panel (c).

In order to verify that the OM82C dendrimer is a suitable entangled two-photon absorber for use in ETPEF measurements, ETPA measurements were carried out under conditions described in the Experimental Methodology section. An approximately 11.08 μM solution of the dendrimer was prepared in a 1-cm quartz cell, which exhibited an absorbance of ~ 1.537 near the absorption maximum wavelength of 387 nm, and ~ 1.058×10^{-3} at the entangled excitation wavelength of 800 nm. The one-photon linear absorption cross-sections of the dendrimer at the absorption peak and at 800 nm are calculated as ~5.762×10^{-6} cm^2 $molecule^{-1}$ and ~3.965×10^{-22} cm^2 $molecule^{-1}$, respectively.

Shown in Figure VI.9 is the plot of normalized absorbed photon rate as a function of net excitation photon rate for the OM82C dendrimer, which illustrates a typical trace that is obtained from ETPA measurements on the OM82C dendrimer solution under the experimental conditions that were described earlier. The dependence of the absorption rate on the excitation photon flux-density clearly exhibits the bi-modal behavior that is expected [37] for entangled-pair excitation, where a linear dependence that is ascribed to the ETPA process is observed for low flux-densities, and a quadratic dependence becomes dominant after a critical flux-density of ~ 2.26×10^{6} cps. The ETPA cross-section of the OM82C dendrimer was extracted from the linear component of the absorption rate and was found to be ~ 2.03×10^{-18} cm^{2} $molecule^{-1}$, which agrees well with our previous findings [58]. The ETPA cross-section is two orders of magnitude lower than the peak one-photon linear absorption cross-section of the molecule.

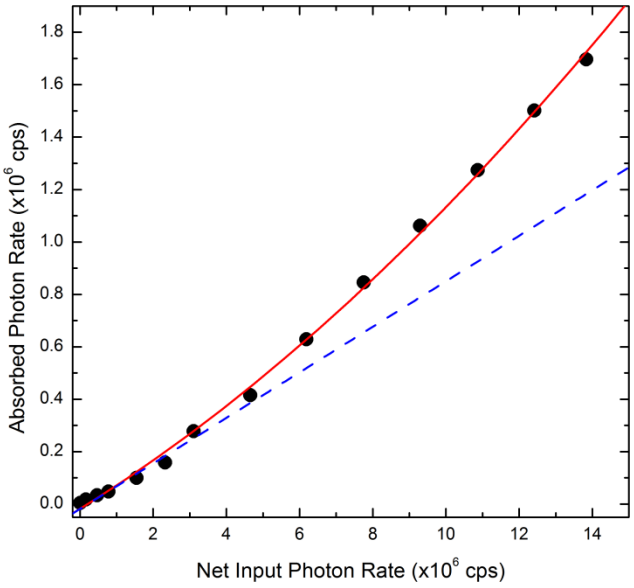

Figure VI.9. Entangled two-photon absorption properties of OM82C dendrimer solution. The entangled two-photon absorption (ETPA) rate is plotted against input photon rate. The linear fit of the initial data points of absorbed photon rate is shown with a dashed blue line to demonstrate the presence of the linear component, while the best fit to a second order polynomial function is shown with a solid red line.

ETPEF experiments were carried out by allowing the intensified CCD camera to capture 25 accumulations of 2 sec each while the sample was exposed to various excitation flux levels, resulting in a 50-sec exposure time per data point. The resulting images were first integrated to obtain the total number of photons that were detected for each acquisition, and then compared to a "dark" image that was captured in the absence of excitation flux. The differences between exposed images and the dark image were then corrected for the detection efficiency of the intensified CCD camera at 427 nm, the transmittance of the collection lens, and notch filter to give the collected fluorescence rate as a function of entangled excitation rate. Figure VI.10 shows the results of these experiments. Note that the dependence of the fluorescence count-rate on the excitation rate parallels that of the absorption rate given in Figure VI.9.

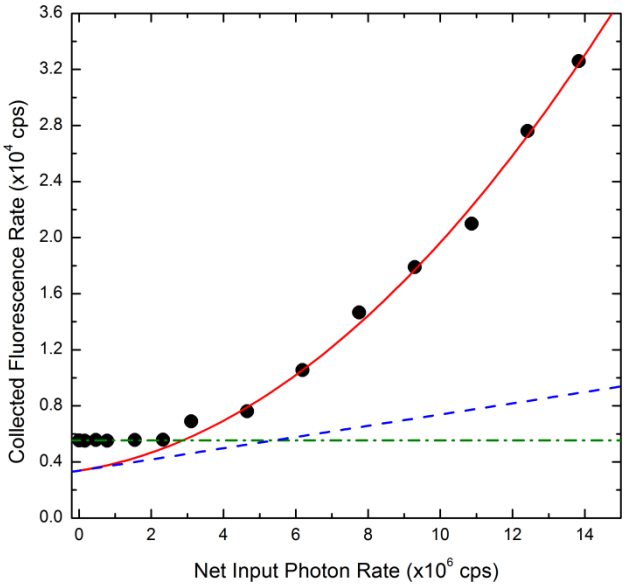

Figure VI.10. Entangled two-photon excited fluorescence properties of OM82C dendrimer solution. The collected fluorescence photon rate is plotted against input photon rate. The best fit to a second order polynomial function is shown with a solid red line and the linear component of the best fit function is plotted in a dashed blue line. The low-flux regime where the fluorescence rate is expected to depend linearly on the excitation flux cannot be resolved due to the constant background intensity, depicted as a green dash-dot line.

In order to test the effectiveness of the notch filter and to ensure that the results obtained from ETPEF experiments are not mired by false detections due to scattered excitation photons, control experiments were carried out wherein a strong scattering sample was exposed to varying levels of entangled excitation flux and count-rates of photons collected by the OCA, both with and without the notch filter in place, were measured using a procedure that is identical to the ETPEF measurements. The purely scattering sample solution was prepared by dispersing chalk dust into DI-water, which resulted in an optical density of ~ 1.203 in a 1-cm quartz cell. We observed that in the absence of the notch filter, the photon count-rates collected by the OCA exhibited a purely linear dependence on the excitation flux, as is expected for a scattering medium. Upon insertion of the notch filter in the photon collection path, the linear dependence was observed to diminish completely, and a constant "background" level of photon count-rates were measured at ~ 6×10^3 photons·sec^{-1}, which was found to be independent of the excitation flux. This level of background intensity is higher than that measured for the APD single-photon counting modules (~ 500 photons·sec^{-1}), but is consistent with the larger detection area, wider dynamic range, and sensitivity of the intensified CCD camera that is used for detection of photons collected by the OCA, and the control experiments confirm that scattering events do not affect the collection and accurate measurement of fluorescence count-rates in our experimental setup. As a trade-off, however, the constant level of background noise obscures the low range of excitation flux-densities in our setup.

As a measure of confidence for the results obtained from ETPEF experiments, the fluorescence quantum yield of the OM82C dendrimer was extracted from the ETPEF and ETPA measurement results. After application of appropriate corrections for the collection

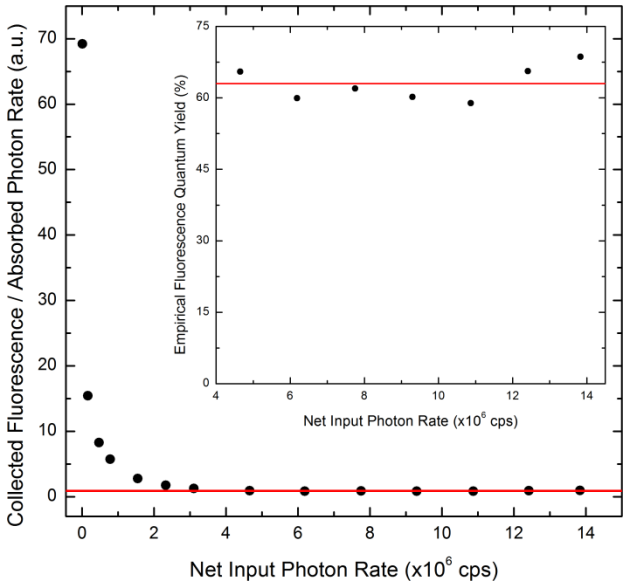

Figure VI.11. Empirical fluorescence quantum yield calculation for the OM82C dendrimer that is extracted from ETPA and ETPEF data. The ratio of collected fluorescence count-rate to absorption rate is plotted as a function of excitation flux, which yields the empirical fluorescence quantum yield of the sample after application of appropriate corrections, depicted in the inset. The best fit to a constant value of the high excitation flux data points are plotted as solid red lines. The fluorescence quantum yield of the OM82C dendrimer is calculated to be ~ 63%.

efficiency and surface reflectivity of the OCA, the ratio of fluorescence count-rate to absorption rate as a function of entangled excitation rate was calculated. Shown in Figure VI.11 is a plot of this ratio at varying excitation rates, where the inset isolates data points in the higher-flux range that are less affected by measurement noise compared to the low-flux range data. As can be seen from the inset of Figure VI.11, the empirical value of the fluorescence quantum yield of the OM82C dendrimer, extracted from ETPEF measurements is ~ 63%, while the value reported in literature is 74% [57]. This is a good agreement between the empirical value calculated here and the published value of the fluorescence quantum yield, considering the various sources of experimental error that could have contributed to the difference, such as optical losses due to aperture size and alignment imperfections. The strongest contribution to the error in the empirical value is

attributable to re-absorption of fluorescence light in the sample; as illustrated in Figures VI.8(b) and VI.8(c), there is appreciable overlap between the steady-state absorption and emission spectra of the OM82C dendrimer which, combined with the fact that the hemispherical portion of the OCA reflects emitted fluorescence photons back toward the sample, results in a small portion of fluorescence photons that are emitted from the sample being re-absorbed.

As a consequence of the observed agreement between the empirically calculated fluorescence quantum yield of the OM82C dendrimer with values previously published in literature, the similar excitation flux-density dependences of the ETPA measurement results and fluorescence collection experiments, and the exclusion of scattering effects, we ascribe the fluorescence count-rate that is observed in ETPEF experiments to emission subsequent to excitation by entangled pairs of photons. Further, it is important to note that the data presented in Figure VI.10 has not been corrected for the geometric collection efficiency of the OCA, and that the maximum collected fluorescence count-rate is on the order of 10^4 cps, despite the use of a relatively high quantum yield material such as OM82C. The practical acquisition of these results would not have been possible without the use of the OCA.

VI.5. Conclusions

We have accomplished the first ever demonstration of fluorescence emission from an organic dendrimer subsequent to excitation by entangled pairs of photons. Processes related to scattering of excitation photons were expressly eliminated as a possible source of the observed emission, and the entangled two-photon excited fluorescence was

observed to exhibit similar excitation flux-rate dependence to entangled two-photon absorption in the dendrimer material. Furthermore, an empirical value for the fluorescence quantum yield of the dendrimer system that is extracted from the ETPEF experiments was found to agree well with values reported in literature.

Accordingly, under optimized experimental conditions wherein a maximum entangled excitation rate on the order of 1.4×10^{7} photons·sec^{-1} is utilized, using an approximately 11 μM solution of the OM82C dendrimer that exhibits an absorbance of 1.537 at 387 nm in a 0.4-cm path-length quartz cell, with individual image acquisitions configured to accumulate 25 exposures of 2 seconds each, we were able to observe a maximum fluorescence rate of 3.26×10^{4} photons·sec^{-1} from the sample of interest.

In addition, the experimental demonstration of ETPEF was carried out using an excitation flux that is on the order of 10^{12} photons·cm^{-2}, which is approximately 10 orders of magnitude lower than the flux levels required for any classical counterpart of this experiment. The ability to characterize fluorescence from a fluorophore at such low levels of excitation flux and utilizing a two-photon process has significant impact on the field of fluorescence microscopy because the demonstration of ETPEF from an organic dendrimer system is an enabling discovery for applications that improve upon two-photon laser scanning fluorescence microscopy, such as entangled photon fluorescence microscopy.

VI.6. References

1. R. Horodecki, P. Horodecki, M. Horodecki, and K. Horodecki, "Quantum entanglement," Reviews of Modern Physics **81**, 865-942 (2009).

2. M. P. Almeida, F. de Melo, M. Hor-Meyll, A. Salles, S. P. Walborn, P. H. S. Ribeiro, and L. Davidovich, "Environment-induced sudden death of entanglement," Science **316**, 579-582 (2007).

3. A. F. Abouraddy, T. Yarnall, B. E. A. Saleh, and M. C. Teich, "Violation of Bell's inequality with continuous spatial variables," Physical Review A **75** (2007).

4. Z. Y. Ou, and L. Mandel, "Violation Of Bells-Inequality And Classical Probability In A 2-Photon Correlation Experiment," Physical Review Letters **61**, 50-53 (1988).

5. J. C. Howell, R. S. Bennink, S. J. Bentley, and R. W. Boyd, "Realization of the Einstein-Podolsky-Rosen paradox using momentum- and position-entangled photons from spontaneous parametric down conversion," Physical Review Letters **92** (2004).

6. P. Walther, K. J. Resch, T. Rudolph, E. Schenck, H. Weinfurter, V. Vedral, M. Aspelmeyer, and A. Zeilinger, "Experimental one-way quantum computing," Nature **434**, 169-176 (2005).

7. D. F. V. James, P. G. Kwiat, W. J. Munro, and A. G. White, "Measurement of qubits," Physical Review A **64** (2001).

8. R. Ursin, F. Tiefenbacher, T. Schmitt-Manderbach, H. Weier, T. Scheidl, M. Lindenthal, B. Blauensteiner, T. Jennewein, J. Perdigues, P. Trojek, B. Omer, M. Furst, M. Meyenburg, J. Rarity, Z. Sodnik, C. Barbieri, H. Weinfurter, and A. Zeilinger, "Entanglement-based quantum communication over 144km," Nature Physics **3**, 481-486 (2007).

9. A. Blais, J. Gambetta, A. Wallraff, D. I. Schuster, S. M. Girvin, M. H. Devoret, and R. J. Schoelkopf, "Quantum-information processing with circuit quantum electrodynamics," Physical Review A **75** (2007).

10. M. Sarovar, A. Ishizaki, G. R. Fleming, and K. B. Whaley, "Quantum entanglement in photosynthetic light-harvesting complexes," Nature Physics **6**, 462-467 (2010).

11. A. Gatti, E. Brambilla, and L. Lugiato, "Quantum imaging," in *Progress in Optics, Vol 51*(2008), pp. 251-348.

12. S. Carrasco, J. P. Torres, L. Torner, A. Sergienko, and B. E. A. Saleh, "Spatial-to-spectral mapping in spontaneous parametric down-conversion," Physical Review A **70** (2004).

13. Y. H. Shih, "Quantum imaging," Ieee Journal of Selected Topics in Quantum Electronics **13**, 1016-1030 (2007).

14. M. D'Angelo, and Y. H. Shih, "Quantum imaging," Laser Physics Letters **2**, 567-596 (2005).

15. A. F. Abouraddy, M. B. Nasr, B. E. A. Saleh, A. V. Sergienko, and M. C. Teich, "Quantum-optical coherence tomography with dispersion cancellation," Physical Review A **65** (2002).

16. A. F. Abouraddy, B. E. A. Saleh, A. V. Sergienko, and M. C. Teich, "Quantum holography," Optics Express **9**, 498-505 (2001).

17. T. B. Pittman, Y. H. Shih, D. V. Strekalov, and A. V. Sergienko, "Optical Imaging By Means Of 2-Photon Quantum Entanglement," Physical Review A **52**, R3429-R3432 (1995).

18. Y. H. Shih, A. V. Sergienko, T. B. Pittman, and M. H. Rubin, "EPR And 2-Photon Interference Experiments Using Type-II Parametric Downconversion," Fundamental Problems in Quantum Theory **755**, 40-60 (1995).

19. B. I. Erkmen, and J. H. Shapiro, "Unified theory of ghost imaging with Gaussian-state light," Physical Review A **77** (2008).

20. R. S. Bennink, S. J. Bentley, R. W. Boyd, and J. C. Howell, "Quantum and classical coincidence imaging," Physical Review Letters **92** (2004).

21. M. D'Angelo, A. Valencia, M. H. Rubin, and Y. Shih, "Resolution of quantum and classical ghost imaging," Physical Review A **72** (2005).

22. M. Malik, H. Shin, M. O'Sullivan, P. Zerom, and R. W. Boyd, "Quantum Ghost Image Identification with Correlated Photon Pairs," Physical Review Letters **104** (2010).

23. M. D'Angelo, Y. H. Kim, S. P. Kulik, and Y. Shih, "Identifying entanglement using quantum ghost interference and imaging," Physical Review Letters **92** (2004).

24. M. D'Angelo, M. V. Chekhova, and Y. Shih, "Two-photon diffraction and quantum lithography," Physical Review Letters **87** (2001).

25. V. Giovannetti, S. Lloyd, and L. Maccone, "Quantum-enhanced measurements: Beating the standard quantum limit," Science **306**, 1330-1336 (2004).

26. A. N. Boto, P. Kok, D. S. Abrams, S. L. Braunstein, C. P. Williams, and J. P. Dowling, "Quantum interferometric optical lithography: Exploiting entanglement to beat the diffraction limit," Physical Review Letters **85**, 2733-2736 (2000).

27. P. Kok, A. N. Boto, D. S. Abrams, C. P. Williams, S. L. Braunstein, and J. P. Dowling, "Quantum-interferometric optical lithography: Towards arbitrary two-dimensional patterns," Physical Review A **63** (2001).

28. R. W. Boyd, and S. J. Bentley, "Recent progress in quantum and nonlinear optical lithography," Journal of Modern Optics **53**, 713-718 (2006).

29. O. Roslyak, C. A. Marx, and S. Mukamel, "Nonlinear spectroscopy with entangled photons: Manipulating quantum pathways of matter," Physical Review A **79** (2009).

30. B. E. A. Saleh, B. M. Jost, H. B. Fei, and M. C. Teich, "Entangled-photon virtual-state spectroscopy," Physical Review Letters **80**, 3483-3486 (1998).

31. J. Perina, B. E. A. Saleh, and M. C. Teich, "Multiphoton absorption cross section and virtual-state spectroscopy for the entangled n-photon state," Physical Review A **57**, 3972-3986 (1998).

32. J. Kojima, and Q. V. Nguyen, "Entangled biphoton virtual-state spectroscopy of the A(2)Sigma(+)-X-2 pi system of OH," Chemical Physics Letters **396**, 323-328 (2004).

33. O. Roslyak, and S. Mukamel, "Multidimensional pump-probe spectroscopy with entangled twin-photon states," Physical Review A **79** (2009).

34. P. P. Yupapin, "Fiber optic sensing applications using the entangled states walk-off compensations," Optik **120**, 265-267 (2009).

35. G. Gilbert, and Y. S. Weinstein, "Aspects of practical remote quantum sensing," Journal of Modern Optics **55**, 3283-3291 (2008).

36. J. Javanainen, and P. L. Gould, "Linear Intensity Dependence Of A 2-Photon Transition Rate," Physical Review A **41**, 5088-5091 (1990).

37. H. B. Fei, B. M. Jost, S. Popescu, B. E. A. Saleh, and M. C. Teich, "Entanglement-induced two-photon transparency," Physical Review Letters **78**, 1679-1682 (1997).

38. D. I. Lee, and T. Goodson, "Entangled photon absorption in an organic porphyrin dendrimer," Journal of Physical Chemistry B **110**, 25582-25585 (2006).

39. D. I. Lee, and T. Goodson, "Entangled and correlated two-photon absorption effects of an organic material," 2007 Digest of the Leos Summer Topical Meetings, 219-220 (2007).

40. D. I. Lee, and T. Goodson, "Quantum spectroscopy of an organic material utilizing entangled and correlated photon pairs - art. no. 66530V," Linear and Nonlinear Optics of Organic Materials Vii **6653**, V6530-V6530 (2007).

41. M. R. Harpham, O. Suzer, C.-Q. Ma, P. Bauerle, and T. Goodson, "Thiophene dendrimers as entangled photon sensor materials," J Am Chem Soc **131**, 973-979 (2009).

42. A. R. Guzman, M. R. Harpham, O. Suzer, M. M. Haley, and T. G. Goodson, "Spatial Control of Entangled Two-Photon Absorption with Organic Chromophores," Journal of the American Chemical Society **132**, 7840-+ (2010).

43. M. Minski, "Microscopy apparatus," U.S. Patent No. 3013467 (1961).

44. S. Inoue, "Foundations of confocal scanned imaging in light microscopy," Handbook of biological confocal microscopy, Second edition, 1-17 (1995).

45. J. B. Pawley, "Fundamental And Practical Limits In Confocal Light-Microscopy," Scanning **13**, 184-198 (1991).

46. W. Denk, and K. Svoboda, "Photon upmanship: Why multiphoton imaging is more than a gimmick," Neuron **18**, 351-357 (1997).

47. D. R. Sandison, R. M. Williams, K. S. Wells, J. Strickler, and W. W. Webb, "Quantitative fluorescence confocal laser scanning microscopy (CLSM)," Handbook of biological confocal microscopy, Second edition, 39-53 (1995).

48. C. J. R. Sheppard, and R. Kompfner, "Resonant Scanning Optical Microscope," Applied Optics **17**, 2879-2882 (1978).

49. W. Denk, J. H. Strickler, and W. W. Webb, "2-Photon Laser Scanning Fluorescence Microscopy," Science **248**, 73-76 (1990).

50. M. C. Teich, and B. E. A. Saleh, "Entangled-Photon Microscopy," *Ceskoslovensky casopis pro fyziku* **47**, 3-8 (1997).

51. M. Goppert-Mayer, "Elementary file with two quantum fissures," Annalen Der Physik **9**, 273-294 (1931).

52. W. Denk, D. W. Piston, and W. W. Webb, "Two-photon molecular excitation in laser-scanning microscopy," Handbook of biological confocal microscopy, Second edition, 445-458 (1995).

53. S. Lindek, E. H. K. Stelzer, and S. W. Hell, "Two new high-resolution confocal fluorescence microscopies (4Pi, Theta) with one- and two-photon excitation," Handbook of biological confocal microscopy, Second edition, 417-430 (1995).

54. M. C. Teich, and B. E. A. Saleh, "Entangled-photon microscopy, spectroscopy, and display," U.S. Patent No. 5796477 (1998)

55. H. Birk, R. Storz, and J. Engelhardt, "Entangled-photon microscopes," U.S. Patent No. US2002/0018290A1 (2001)

56. Y. Shih, M. D'Angelo, and M. Chekhova, "Multiphoton imaging using entangled photons and quantum lithography," International Patent No. WO02/095353A2 (2002)

57. O. Varnavski, X. Z. Yan, O. Mongin, M. Blanchard-Desce, and T. Goodson, "Strongly interacting organic conjugated dendrimers with enhanced two-photon absorption," Journal of Physical Chemistry C **111**, 149-162 (2007).

58. Michael R. Harpham, Özgün Süzer, Alica R. Guzman, Theodore Goodson III, “Virtual states, Entangled Photons, and Organic Nonlinear Optical Sensors,” Science (submitted, 2010)

CHAPTER VII

Summary and Conclusions

In this dissertation, I have focused on the practical application of quantum entanglement which, as a novel non-classical resource, has already had significant impact on a variety of avenues of research ranging from fundamental investigations of the foundations of quantum mechanics to the very practical novel techniques of optical materials characterization. I have concentrated my efforts on application of quantum entanglement to fundamental spectroscopy, experimentally investigating the interesting non-classical manner in which entangled pairs of photons interact with matter. Specifically, the two-photon absorption (TPA) of entangled pairs of photons that are generated by the process of spontaneous parametric down-conversion in organic dendritic molecules has been the primary subject matter of our experimental efforts. The question of what precise mechanism of interaction is responsible for the entangled two-photon response in materials is one that remains unanswered to date. However, the findings of our experimental investigations have contributed significantly to building a complete understanding of this scarcely researched phenomenon, while expanding on the well-established knowledgebase on the techniques of entangled photon-pair generation. Our group has pioneered the research of the entangled two-photon absorption (ETPA) phenomenon, opening up brand new venues of research into quantum optical

spectroscopy applications, and enabling an exciting new branch of quantum optical microscopy by demonstrating fluorescence emission subsequent to entangled photon-pair excitation in an organic dendrimer.

The research of fundamental quantum mechanical correlations between entangled pairs of photons is already a well-established field, where the general theoretical aspects and practical operational consideration of entangled photon pair sources, such as spontaneous parametric down-conversion (SPDC), are thoroughly studied. Despite the profuse collection of research that was already available in this field, in our efforts to obtain the optimum flux of entangled photon pairs for use in spectroscopy applications, I was able to identify a partial deficiency in the understanding of the behavior of the spontaneous parametric down-conversion process under focused pumping conditions. I was able to show that a pump beam that is focused into higher intensities under constant divergence can enhance the down-conversion efficiency and brightness of the SPDC entangled photon source utilized in our experiments. Although our results were in conflict with previous theoretical investigations that reported unchanged or reduced efficiency under such pumping conditions, by adopting a spherical-like description for the pump field, I was able to develop a theoretical model to help explain the discrepancy between the well-established theoretical predictions and our experimental results. Accordingly, the entangled photon source that is utilized in our experiments is capable of generating $\sim 10^7$ entangled photon pairs/sec, which is among the highest brightness sources reported in literature.

Furthermore, by systematically investigating a series of generations of a thiophene dendrimer, I was able to establish organic dendritic systems as viable and affective

sensors of entangled photons, which have applications in imaging of biological systems and remote sensing. A linear dependence of the absorption rate on excitation flux, which is a signature of the ETPA phenomenon, was demonstrated with every generation of thiophene dendrimers that was investigated in this study for samples that were prepared both in solution and as a thin film, with measured ETPA cross-sections on the order of 10^{-9}-10^{-7} cm^2 $molecule^{-1}$. Moreover, I was able to show that trends in the non-linear absorption cross-sections measured by the well-established two-photon excited fluorescence (TPEF) technique were matched by those measured by ETPA, despite the fact that approximately ten orders of magnitude fewer photons were required in the entangled measurements.

Expanding on the demonstrations of ETPA in various organic systems, I also in investigated mechanisms to control the ETPA process through control of the quantum entangled state in which the entangled excitation photons are emitted from the source. By selecting a set of distinct phase-matching conditions, through which I can control the spatio-temporal characteristics of the SPDC emission, I demonstrated that the patterns in which entangled photon pairs are emitted from the SPDC source offer a method to either enhance or limit the degree of entangled photon absorption in an organic material, where one of the investigated conditions behaved in a manner unlike the others. In trying to determine the source of this dissimilarity, I found that the widely-accepted benchmarks of entanglement quality for entangled photon sources such as polarization visibilities, entanglement time, and entanglement area did not vary significantly with the SPDC phase-matching conditions that I studied. As a result, I have suggested that the ETPA process in organic dendritic systems is sensitive to various entanglement parameters, and

entanglement time and area alone, which make up the parameters that are traditionally considered to be the sole parameters of importance, are insufficient in determining the character of a material. I observed that the ETPA cross-section of the organic conjugated Annulene systems that were investigated in this study decreased as the overlap of the signal and idler photons decreased, with an absence of absorption in the case where there is no spatial overlap. These results suggested the possibility of "tuning" the absorption response of these organic materials for utilization in quantum optical applications.

Moreover, in an attempt to better understand the material considerations that affect ETPA in organic systems, I investigated the ETPA response of a wide range of organic dendritic materials with known, and large, classical TPA response, but of differing geometry, donor-acceptor strength, and charge-transfer character. Our investigation found that materials with classical TPA cross-sections attributed to virtual transitions involving an intermediate state exhibited measurable and large ETPA responses, but materials whose classical TPA cross-section is attributed to a dipole transition, without involvement of an intermediate state, were nearly transparent to entangled photons. From these results, I suggested that entangled photons are sensitive to the intermediate states of a nonlinear optical material.

Finally, I was able to accomplish the first ever demonstration of entangled two-photon excited fluorescence (ETPEF) emission from an organic dendrimer by utilizing a high geometric efficiency optical fluorescence collection system that was specifically designed for the task. Upon elimination of processes that could generate false detections, I was able to show that the collected ETPEF rate exhibited a similar dependence on the excitation flux as the ETPA rate in the dendrimer material. Furthermore, an empirical

value for the fluorescence quantum yield of the dendrimer that was extracted from ETPEF and ETPA measurements was found to agree with the value reported in literature, despite the fact that the ETPEF experiments were carried out at extremely low excitation fluxes, on the order of 10^{12} photons cm^{-2}.

The ability to do spectroscopy at low excitation flux levels is an important development in the area of spectroscopy, materials, and sensing. This, combined with the ability to characterize fluorescence from an organic chromophore at such low light levels while utilizing a two-photon process has significant impact in various fields where photobleaching in and photodamage to a specimen is a concern, such as microscopy. The demonstration of ETPEF and ETPA organic materials is an enabling discovery for quantum microscopy applications.

APPENDIX A

Probability of Entangled Pair Creation in the Process of SPDC

We begin by considering a crystal in the form of M regularly arranged, fixed, non-interacting molecules. It is assumed that the size of each molecule is considerably smaller than the wavelength, such that a dipole approximation is applicable for interactions between molecules and electromagnetic fields.

In order to utilize Fermi's golden rule to describe the rate of biphoton creation, we shall define the initial $|i\rangle$ and final $|f\rangle$ states of the system as such:

Let all molecules be in the ground state $|a\rangle_j$ and the field contain N_s, N_i, N_p photons in the modes k_s, k_i, k_p at the initial time

$$|i\rangle = |a, N_s, N_i, N_p\rangle \equiv |a\rangle|i'\rangle . \tag{A.1}$$

Accordingly, the final state of the parametric system is

$$|f\rangle = |a, N_s + 1, N_i + 1, N_p - 1\rangle \equiv |a\rangle|f'\rangle . \tag{A.2}$$

Note that the transition results in the crystal returning to its initial state and only the field undergoes change because this process is parametric (a coherent transition).

According to Fermi's golden rule, the rate of transition per unit time is

$$W_{fi} = \frac{2\pi}{\hbar}|T_{fi}|^2 \delta(\varepsilon_f - \varepsilon_i), \tag{A.3}$$

where

$$T_{fi} = \sum_{v_1, v_2} \frac{\langle f | \mathcal{V} | v_2 \rangle \langle v_2 | \mathcal{V} | v_1 \rangle \langle v_1 | \mathrm{V} | i \rangle}{\left(\varepsilon_f - \varepsilon_{v_2}\right)\left(\varepsilon_i - \varepsilon_{v_1}\right)}, \tag{A.4}$$

and the summation over the intermediate virtual states v_1 and v_2 includes all possible transition "paths." It is assumed that no intermediate resonances take place, so the denominator of the above transition matrix is free of imaginary terms.

It is now necessary to consider various transition paths. For instance, the j th molecule may first emit a photon into the k_s mode and cross into the excited state $|b\rangle_j$. This process would be described by the matrix element

$$\langle v_1 | \mathrm{V} | i \rangle = -\langle N_s + 1, b_j | \mathbf{d}_j \cdot \mathbf{E}_j | N_s, a_j \rangle = -\langle v_1' | \mathbf{d}_{jba} \cdot \mathbf{E}_{js}^{(-)} | i' \rangle, \tag{A.5}$$

where $\mathbf{E}_{js}^{(-)}$ refers to the negative-frequency part of the unperturbed analytical field, which contains only creation operators $\mathbf{a}_s^{\dagger}$. Since the convolution of crystal and field states can be separated without loss of generality, the transition dipole matrix element $\mathbf{d}_{jba} = \langle b | \mathbf{d}_j | a \rangle$ has absorbed initial and intermediate crystal states and the primed indices of the states refer to states of the field only. Thus, the first step of the path under consideration gives the factor

$$-\langle v_1' | \frac{\mathbf{d}_{jba} \cdot \mathbf{E}_{js}^{(-)}}{\hbar\left(\omega_{\mathrm{ab}} - \omega_s\right)} | i' \rangle, \tag{A.6}$$

where $|v_1'\rangle = |N_s + 1, \mathrm{N_i}, N_p\rangle$, and $\varepsilon_i - \varepsilon_{v_1} = \hbar\left(\omega_{ab} - \omega_s\right)$. At the second step, the same molecule may cross into state $|c\rangle_j$, emitting a second photon, k_i. Similar to the first, the factor for this step would be written as

$$- \left\langle v_2' \right| \frac{\mathbf{d}_{jcb} \cdot \mathbf{E}_{ji}^{(-)}}{\hbar(\omega_{bc} - \omega_i)} \left| v_1' \right\rangle, \tag{A.7}$$

where $\left| v_2' \right\rangle = \left| N_s + 1, N_i + 1, N_p \right\rangle$. Because the whole path has to describe a parametric process, and energy conservation is enforced by the delta-function in Eq. 3, the molecule needs to return to its initial ground state $|i\rangle$ in the final step, absorbing a photon from the pump field, k_p, with energy $\omega_p = \omega_s + \omega_i$. The factor for this step is

$$- \left\langle f' \left| \mathbf{d}_{jac} \cdot \mathbf{E}_{jp}^{(+)} \right| v_2' \right\rangle, \tag{A.8}$$

and $\mathbf{E}_{jp}^{(+)}$ describes the annihilation of a pump photon. Finally, the path considered above yields the transition amplitude

$$T_{pis}^{(j)} = -\left\langle f' \left| \sum_{b,c} \frac{\left(\mathbf{d}_{jac} \cdot \mathbf{E}_{jp}^{(+)}\right)\left(\mathbf{d}_{jcb} \cdot \mathbf{E}_{ji}^{(-)}\right)\left(\mathbf{d}_{jba} \cdot \mathbf{E}_{js}^{(-)}\right)}{\hbar^2(\omega_{ac} - \omega_p)(\omega_{ab} - \omega_s)} \right| i' \right\rangle, \tag{A.9}$$

where the summation over states b and c accounts for all virtual states of the molecule, and subscripts p, i, s simply denote the sequence of photon radiation and absorption chosen here. In reality, there are $3! = 6$ possible sequences, so the full scattering amplitude on the j th molecule is given by the sum of permutations of indices p, s, i:

$$T^{(j)} = T_{pis}^{(j)} + T_{psi}^{(j)} + T_{sip}^{(j)} + \ldots = \sum_{(p,i,s)}^{6} T_{pis}^{(j)} \tag{A.10}$$

The tensor of the quadratic hyperpolarizability of the molecule is given by

$$\beta_{nml}^{p\bar{s}\bar{i}} = \sum_{(pn,im,sl)}^{6} \sum_{bc} \frac{\left(\mathbf{d}_{ac}\right)_n \left(\mathbf{d}_{cb}\right)_m \left(\mathbf{d}_{ba}\right)_l}{\hbar^2(\omega_{ac} - \omega_p)(\omega_{ab} - \omega_s)}, \tag{A.11}$$

where l, m, n denote Cartesian indices for coordinates in the x-, y-, and z-axes. At this point, it is necessary to take advantage of several simplifications on the 27 components of Eq. 11. For example, because of the presence of the sum of permutations, the one-time

non-cyclic permutations of the frequency and Cartesian indices ($\beta^{123}_{xyz} = \beta^{213}_{yxz} = ...$) are invariant. Further, considering a molecule of class C_{3v} symmetry further reduces this number. Combining Eq. 11 and Eq. 9, we can now write Eq. 10 as

$$T^{(j)} = -\langle f' | \beta_j \vdots \mathbf{E}^{(-)}_{js}\, \mathbf{E}^{(-)}_{ji}\, \mathbf{E}^{(+)}_{jp} | i' \rangle \equiv \langle f' | \mathcal{V}_{eff} | i' \rangle , \tag{A.12}$$

which effectively reduces the perturbation from third to first order, i.e. we take the effective energy to be of the form $-\beta \vdots \mathbf{E}^3$ instead of the perturbing energy $-\mathbf{d}\cdot\mathbf{E}$. At this point, the amplitude $T^{(j)}$ describes scattering by a single molecule. Expansion to the whole of the crystal introduces the macroscopic susceptibility of a unit of crystal volume, $\chi = \beta\, M/V$, and the effective perturbation energy is written as

$$\mathcal{V}_{eff} = -\chi \vdots \int_V \mathrm{d}\mathbf{r} \left(\mathbf{E}^{(-)}_s\, \mathbf{E}^{(-)}_i\, \mathbf{E}^{(+)}_p + \mathbf{E}^{(-)}_p\, \mathbf{E}^{(+)}_i\, \mathbf{E}^{(+)}_s \right), \tag{A.13}$$

where the second term of the integrand that describes the reverse process in which signal and idler modes are annihilated and a pump photon is created, is included to preserve hermiticity. This effective interaction results in a rate of creation of photon pairs given by

$$W_{fi} = \frac{2\pi}{\hbar^2} \left| \langle f' | \mathcal{V}_{eff} | i' \rangle \right|^2 \delta\left(\omega_s + \omega_i - \omega_p \right), \tag{A.14}$$

with matrix elements of the field defined as

$$\langle N_k - 1 | \mathbf{E}^{(+)}(\mathbf{r}) | N_k \rangle = \ell\, \mathbf{c}_k \sqrt{N_k}\, e^{\ell \mathbf{k}\cdot\mathbf{r}} \tag{A.15.1}$$

$$\langle N_k + 1 | \mathbf{E}^{(-)}(\mathbf{r}) | N_k \rangle = -\ell\, \mathbf{c}_k \sqrt{N_k + 1}\, e^{-\ell \mathbf{k}\cdot\mathbf{r}} \tag{A.15.2}$$

where $k = p, s, i$, and $\mathbf{e}_k$ are unit vectors of polarization, and the proportionality constant $\mathbf{c}_k \equiv \mathbf{e}_k \left(\hbar\, \omega_k\, u_k\, v / 4\pi^2 c\, n_k \cos\rho_k \right)^{1/2}$.

Substituting Eq. 15 and Eq. 13 into Eq. 14 gives the transition rate of $|i\rangle \to |f\rangle$, which is proportional to $(N_s+1)(N_i+1)N_p$. Similarly, the transition rate from $|i\rangle$ to $|N_s-1, N_i-1, N_p+1\rangle$ is proportional to $N_s\, N_i\,(N_p+1)$, with the same weight of proportionality. As a result, the rate of appearance (or disappearance) of photon pairs in modes k_s and k_i will be equal to

$$W = \frac{2\pi}{\hbar^2}\delta(\omega_s+\omega_i-\omega_p)\left[(N_s+N_i+1)N_p - N_s\,N_i\right]\left|\chi\vdots \mathbf{c}_s\mathbf{c}_i\mathbf{c}_p\right|^2 f(\Delta k), \quad \text{(A.16)}$$

where $f(\Delta k)\equiv\left|\int_V \mathrm{d}\mathbf{r}\, e^{\ell\,\Delta k\cdot\mathbf{r}}\right|^2$, and $\Delta\mathrm{k} = \mathrm{k}_s + \mathrm{k}_i - \mathrm{k}_p$.

For the case of spontaneous parametric down-conversion, by definition, there are initially no photons in the signal and idler fields, $N_{s,i} = 0$. Thus, the rate of biphoton generation is directly proportional to N_p.

It only remains to express N_p in terms of the flux of pump photons entering the quantization box L^3 and interacting in volume V (L^3 contains V) per unit time. The flux density is equal to the photon concentration N_p/L^3 multiplied by the group velocity vector. Thus, the full flux entering through a face with surface area A is equal to

$$\frac{N_p}{L^3}\,A\,u_{p_z} = \frac{c\,A\,n_p\cos\theta_p\cos\rho_p}{2\pi\,\hbar\omega_p}\left|\left\langle N_p-1\left|E_p^{(+)}\right|N_p\right\rangle\right|^2, \quad \text{(A.17)}$$

where $u_{p_z} = u_p\cos\theta_p$ is the projection of the group velocity on the axis perpendicular to A (z-axis), and Eq. 15 has been used to express N_p in terms of E_p. The probability of biphoton creation is thus given by

$$\wp = \frac{(2\pi\, c_s\, c_i\, \chi)^2\, A}{\hbar\, c\, \bar{n}_p}\,\delta(\omega_s+\omega_i-\omega_p)f(\Delta k)\left|\left\langle N_p-1\left|E_p^{(+)}\right|N_p\right\rangle\right|^2, \quad \text{(A.18)}$$

with trigonometric factors absorbed into $\bar{n}_p$, and $\chi \equiv \boldsymbol{\chi} \vdots \mathbf{e}_s\, \mathbf{e}_i\, \mathbf{e}_p$.

It is extremely important here to note that in the case of the classical approximation of the pump field, we can replace the matrix element in Eq. 18 with the pump field magnitude, E_p, which gives

$$\wp = \frac{(2\pi\, c_s\, c_i\, \chi)^2\, A}{\hbar\, c\, \bar{n}_p}\, \delta(\omega_s + \omega_i - \omega_p) f(\Delta k) \left| E_p \right|^2 . \tag{A.19}$$

Now, observe that the pump intensity, $\left| E_p \right|^2$, multiplied by the cross sectional area A of the interaction volume is equivalent to the average power of the pump field, P_p.

Thus, we observe that biphoton creation probability in the process of spontaneous parametric down-conversion does not depend on pump intensity, but rather on the average number of pump photons incident on the interaction volume, described by pump power in the classical field approximation.

APPENDIX B

Technical Drawings of the Optical Collection Assembly

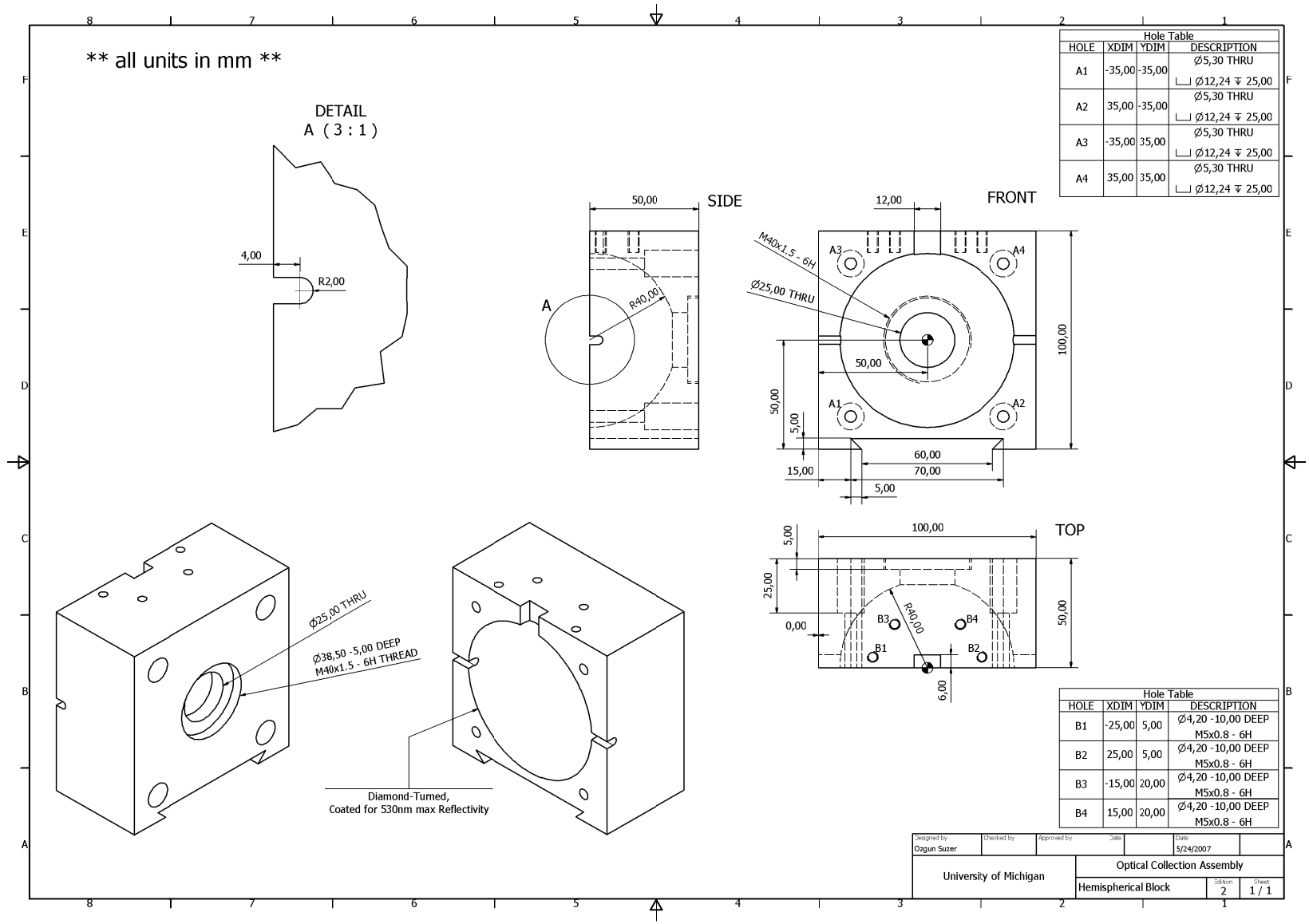
** all units in mm **
DETAIL
A (3 : 1)
4,00
R2,00
SIDE
50,00
A
R40,00
FRONT
12,00
M40x1.5 - 6H
Ø25,00 THRU
A3
A4
A1
A2
100,00
50,00
50,00
5,00
60,00
70,00
15,00
5,00
TOP
100,00
5,00
25,00
0,00
R40,00
B3
B4
B1
B2
50,00
6,00
Ø25,00 THRU
Ø38,50 -5,00 DEEP
M40x1.5 - 6H THREAD
Diamond-Turned,
Coated for 530nm max Reflectivity
Hole Table
HOLE | XDIM | YDIM | DESCRIPTION
A1 | -35,00 | -35,00 | Ø5,30 THRU ⌴ Ø12,24 ↧ 25,00
A2 | 35,00 | -35,00 | Ø5,30 THRU ⌴ Ø12,24 ↧ 25,00
A3 | -35,00 | 35,00 | Ø5,30 THRU ⌴ Ø12,24 ↧ 25,00
A4 | 35,00 | 35,00 | Ø5,30 THRU ⌴ Ø12,24 ↧ 25,00
Hole Table
HOLE | XDIM | YDIM | DESCRIPTION
B1 | -25,00 | 5,00 | Ø4,20 -10,00 DEEP M5x0.8 - 6H
B2 | 25,00 | 5,00 | Ø4,20 -10,00 DEEP M5x0.8 - 6H
B3 | -15,00 | 20,00 | Ø4,20 -10,00 DEEP M5x0.8 - 6H
B4 | 15,00 | 20,00 | Ø4,20 -10,00 DEEP M5x0.8 - 6H
Designed by
Ozgun Suzer
Checked by
Approved by
Date
5/24/2007
University of Michigan
Optical Collection Assembly
Hemispherical Block
Edition
2
Sheet
1 / 1

** all units in mm **

Hole Table			
HOLE	XDIM	YDIM	DESCRIPTION
A1	-35,00	-35,00	Ø4,20 THRU M5x0.8 - 6H TAPPED
A2	35,00	-35,00	Ø4,20 THRU M5x0.8 - 6H TAPPED
A3	-35,00	35,00	Ø4,20 THRU M5x0.8 - 6H TAPPED
A4	35,00	35,00	Ø4,20 THRU M5x0.8 - 6H TAPPED

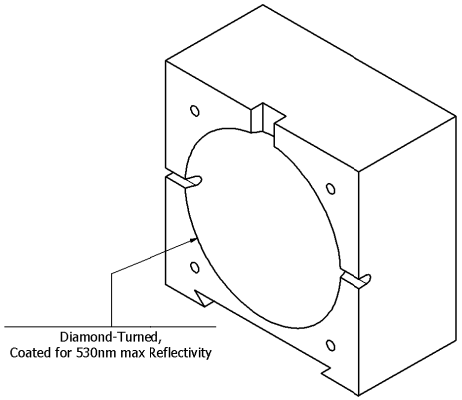

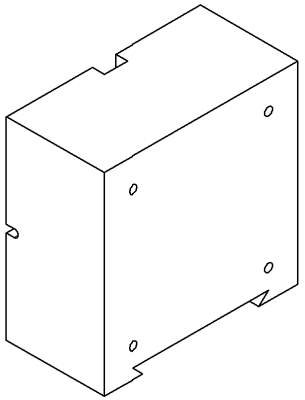

SIDE

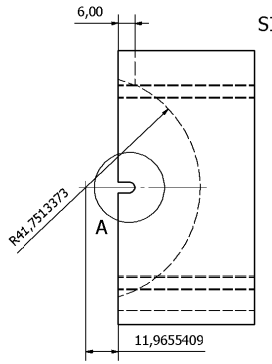

DETAIL
A (3 : 1)

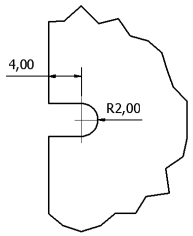

FRONT

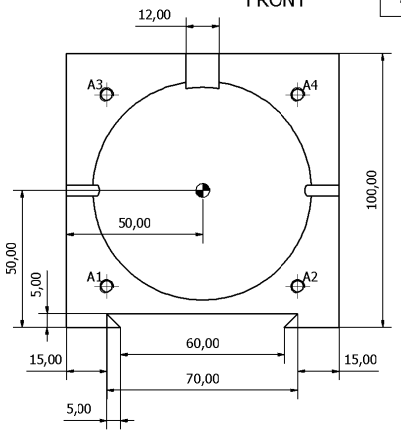

TOP

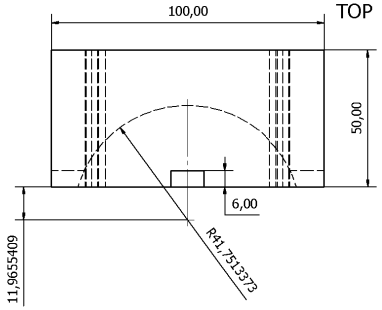

Designed by: Ozgun Suzer	Checked by	Approved by	Date		Date: 5/24/2007	
University of Michigan			Optical Collection Assembly			
			Spherical Cap Block	Edition: 2	Sheet: 1 / 1	